

UNCLASSIFIED

AD NUMBER

AD862107

LIMITATION CHANGES

TO:

Approved for public release; distribution is unlimited.

FROM:

Distribution authorized to U.S. Gov't. agencies and their contractors; Critical Technology; SEP 1969. Other requests shall be referred to Air Force Materials Laboratory, Wright-Patterson AFB, OH 45433. This document contains export-controlled technical data.

AUTHORITY

AFML ltr, 7 Dec 1972

THIS PAGE IS UNCLASSIFIED

AFML-TR-66-310
PART IV
VOLUME I

AD 862107

INTEGRATED RESEARCH ON CARBON COMPOSITE MATERIALS

VOLUME I MATERIALS RESEARCH

UNION CARBIDE CORPORATION
CARBON PRODUCTS DIVISION
- IN ASSOCIATION WITH -
CASE WESTERN RESERVE UNIVERSITY
BELL AEROSYSTEMS COMPANY, A TEXTRON COMPANY

PROGRAM SUPERVISORS

H.F. VOLK
H.R. NARA
D.P. HANLEY

TECHNICAL REPORT AFML-TR-66-310, PART IV, VOLUME I
SEPTEMBER 1969

AIR FORCE MATERIALS LABORATORY
AIR FORCE SYSTEMS COMMAND
WRIGHT-PATTERSON AIR FORCE BASE, OHIO

THIS DOCUMENT IS SUBJECT TO SPECIAL EXPORT CONTROLS AND
EACH TRANSMITTAL TO FOREIGN GOVERNMENTS OR FOREIGN
NATIONALS MAY BE MADE ONLY WITH PRIOR APPROVAL OF THE
NONMETALLIC MATERIALS DIVISION, MAN, AIR FORCE MATERIALS
LABORATORY, WRIGHT-PATTERSON AIR FORCE BASE, OHIO 45433

NOTICES

When Government drawings, specifications, or other data are used for any purpose other than in connection with a definitely related Government procurement operation, the United States Government thereby incurs no responsibility nor any obligation whatsoever; and the fact that the Government may have formulated, furnished, or in any way supplied the said drawings, specifications or other data, is not to be regarded by implication or otherwise as in any manner licensed the holder or any other person or corporation, or conveying any rights or permission to manufacture, use, or sell any patented invention that may in any way be related thereto.

This document is subject to special export controls and each transmittal to foreign Governments or foreign Nationals may be made only with prior approval of the Nonmetallic Materials Division, MAN, Air Force Materials Laboratory, Wright Patterson Air Force Base, Ohio 45433.

Copies of this report should not be returned unless return is required by security considerations, contractual obligations or notice on a specific document.

INTEGRATED RESEARCH ON
CARBON COMPOSITE MATERIALS

Summary Technical Report
AFML-TR-66-310, Part IV
Volume I
Materials Research

Program Supervisors

H. F. Volk
H. R. Nara
D. P. Hanley

September 1969

This document is subject to special export controls and each transmittal to foreign Governments or foreign Nationals may be made only with prior approval of the Nonmetallic Materials Division, MAN, Air Force Materials Laboratory, Wright-Patterson Air Force Base, Ohio 45433.

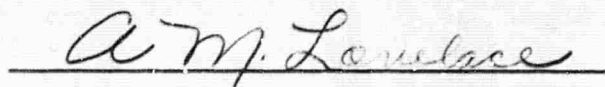
FOREWORD

The work reported herein was performed under the sponsorship of the Advanced Research Projects Agency, Department of Defense, through a contract with the Air Force Materials Laboratory, MAN, AFSC, Wright-Patterson Air Force Base, Ohio, Contract No. AF 33(615)-3110, ARPA Order No. 719, Program Code No. 6D10. Mr. H. S. Schwartz, MAN, is the Air Force Program Manager.

The prime contractor is Union Carbide Corporation, Carbon Products Division; the subcontractors are Case Western Reserve University and Bell Aerosystems Company, a Textron Company. At the beginning of this reporting period, the program was administered by a committee composed of: J. C. Bowman (Chairman) and G. B. Spence (Program Supervisor) from Union Carbide; R. H. Thomas and L. A. Schmit (Program Supervisor) from Case Western Reserve University; and W. H. Dukes and F. M. Anthony (Program Supervisor) from Bell Aerosystems Company. During this reporting period, the Program Supervisors were changed to H. F. Volk (Union Carbide); H. R. Nara and T. P. Kicher, Associate Program Supervisor (Case Western Reserve University); and D. P. Hanley (Bell Aerosystems Company). Technical personnel participating in the program are indicated as authors of their portions of the report. The manuscript was released by the authors August 1969 for publication.

This report covers work performed from July 1968 to June 1969 and is issued in three volumes. Volume I covers materials research; Volume II, structural mechanics; and Volume III, structural component development.

This technical report has been reviewed and is approved.



A. M. Lovelace
Director
Air Force Materials Laboratory

BLANK PAGE

ABSTRACT

The surface characteristics of various carbon and graphite fibers and the interfacial region between fibers and resin in composites were investigated by using electron microscopy, electron diffraction and Raman spectroscopy. The latter technique permits differentiation between graphite fibers of different origin. Graphite fiber composites were prepared by *in situ* polymerization on nylon 6. This technique improves the wetting of the fibers and yields void-free composites. Oriented crystallization of the monomers of nylon 6 and nylon 66 on graphite fibers and subsequent solid state reaction yielded dimers and trimers, respectively, instead of the usual polymers, thus showing a strong and specific effect of surface interactions. Sophisticated vacuum microbalance equipment has been constructed to study the surface characteristics of graphite fibers by gas adsorption. Work on graphite-fiber, nickel-matrix composites was concerned with improvements in the electrodeposition process, the fabrication of larger test specimens, the fabrication of thin tape which can be further processed into samples of more complicated configurations, and the evaluation of composite properties. The latter included measurements of the elastic properties, stress-strain curves and composite thermal expansion.

This abstract is subject to special export controls and each transmittal to foreign governments or foreign nationals may be made only with prior approval of the Nonmetallic Materials Division, MAN, Air Force Materials Laboratory, Wright-Patterson Air Force Base, Ohio 45433.

TABLE OF CONTENTS

<u>Section</u>	<u>Page</u>
I INTRODUCTION.	1
II SUMMARY	5
III RESEARCH ON GRAPHITE-FIBER, RESIN-MATRIX COMPOSITES . .	16
A. New Physical Techniques to Elucidate the Structure of the Fiber-Resin Interface (Professors Baer and Koenig and Dr. F. Tuinstra, Case)	16
B. Graphite Fiber - Polymer Matrix Composites (Professor Litt and Dr. J. B. Shortall, Case)	25
C. Crystallization and Reaction on Graphite-Like Fiber Surfaces (Professor Lande and Mr. P. D. Frayer, Case)	37
IV ADSORPTION, WETTABILITY, AND ADHESION IN FIBER REINFORCED COMPOSITES (Professor Fort, Dr. R. J. Nash, and Mr. S. C. Sharma, Case)	49
A. Gas Adsorption Studies.	49
B. Solution Adsorption Studies	50
V RESEARCH ON GRAPHITE-FIBER, METAL-MATRIX COMPOSITES (R. V. Sara, Union Carbide)	54
A. Electrodeposition of Nickel on Graphite Yarn.	54
B. Fabrication of Test Specimens	55
C. Elastic Properties of Unidirectional Graphite- Fiber, Nickel-Matrix Composite.	55
D. Composite Stress-Strain Behavior.	64
E. Thermal Expansion of Graphite-Fiber, Nickel-Matrix Composite	77
F. Fabrication and Properties of Uniaxial and Orthogonal Plates	82

TABLE OF CONTENTS, (Cont'd.)

<u>Section</u>	<u>Page</u>
G. Fabrication Studies and Tensile Testing of Unidirectional Composite.	91
REFERENCES.	97

LIST OF ILLUSTRATIONS

<u>Figure</u>		<u>Page</u>
1	Surface Replica of a "Thornel" 50 Fiber	18
2	Electron Micrograph of a Graphite Crystal Surface on which an Oriented Layer of Polyethylene is Deposited.	20
3	Microsampling Cell for Composite Studies	23
4	Raman Spectra of Some Graphite and Other Carbon Samples.	24
5a	Preparation of a Composite Using Nylon 6	26
5b	Preparation of a Composite Using a Polyurethane Matrix	27
6	Relative Induction Periods for Polymerization of ϵ -Caprolactam.	29
7	Induction Periods for Anionic Polymerization of ϵ -Caprolactam Using Diethyl Carbonate as the Latent Catalyst	33
8	X-ray Pattern of a Bundle of "Thornel" 40 Carbon Fibers	39
9	X-ray Pattern of HMDA Epitaxially Crystallized on the Carbon Fibers.	40
10	The ab-Plane Projection of the HMDA Molecules.	41
11	X-ray Pattern of the HMDA Reacted in the Solid State at 75°C with HCl Catalyst to Form Cyclic Dimer	42
12	X-ray Pattern of ACA Epitaxially Crystallized on the Carbon Fibers.	44
13	X-ray Pattern of ACA Reacted in the Solid State at 53°C with HCl Catalyst to Form Cyclic Trimer	45
14a	IR Spectra of the Cyclic Dimer Isolated from the Polymer by Extraction.	47
14b	IR Spectra of the Cyclic Dimer Prepared in the Solid State (Reacted Crystals Removed with Tweezers)	47
15	Gravimetric Gas Adsorption Apparatus	52

LIST OF ILLUSTRATIONS (Cont'd.)

<u>Figure</u>		<u>Page</u>
16	Liquid Chromatograph	53
17	Experimental and Predicted Variations in Young's Modulus with Test Angle for a Uniaxial Composite . . .	61
18	Experimental and Predicted Variations in Shear Modulus with Test Angle for a Uniaxial Composite	62
19	Experimental and Predicted Variations in Poisson's Ratio with Test Angle for a Uniaxial Composite	63
20	Stress-Strain Behavior of Unidirectional Composites. . .	66
21	Stress-Strain Curves of Unidirectional Off-Axis Test Specimens.	67
22	Effect of Specimen Gauge Width on Stress-Strain Behavior of 90° Specimens.	68
23	Relationship Between Young's Modulus of Graphite-Fibers and Applied Stress.	69
24	Compression Specimen and Test Fixture.	70
25	Stress-Strain Behavior of Nickel and Graphite-Fiber, Nickel-Matrix Composite in Compression	72
26	Stress-Strain Curves for Unidirectional Composite. . .	73
27	Cyclic Behavior of Constituents and Composite.	74
28	Tension-Compression "Breakaway" Points in Unidirectional Composite	76
29	Linear Thermal Expansion of Nickel and of Graphite-Fiber, Nickel-Matrix Composite	78
30	Effect of Thermal Cycling on Longitudinal Expansion of Graphite-Fiber, Nickel-Matrix Composite	80
31	Temperature and Cyclic Dependence of Composite Longitudinal Thermal Expansion Coefficient and of Axial Thermal Expansion Coefficient of "Thornel" Graphite Fibers.	81

LIST OF ILLUSTRATIONS (Cont'd.)

<u>Figure</u>		<u>Page</u>
32	Variation in Tensile Strength of Uniaxial and Orthogonal Composites with Test Angle.	84
33	Normalized Ultimate Tensile Strengths versus Number of Plies for Orthogonal Laminates	85
34	Variation in Young's Modulus of Uniaxial and Orthogonal Composites with Test Angle	87
35	Normalized Young's Modulus Versus Number of Plies for Orthogonal Laminates.	88
36	Stress-Strain Curves for 5-Ply Orthogonal Specimens with Different Orientations.	90
37	Microstructure of Graphite-Fiber, Nickel-Matrix Composite Fabricated at 1250°C. Magnification 750X .	92
38	Fracture Edge of Graphite-Fiber, Nickel-Matrix Composite Tensile Specimen. Magnification 750X . . .	93
39	Fracture Edge of Graphite-Fiber, Nickel-Matrix Composite with Transverse Fiber Orientation	94
40	Fiber-Matrix Debonding in a Tensile Specimen with Transverse Fiber Orientation.	95
41	Tensile Specimen Configurations	96

LIST OF TABLES

<u>TABLE</u>		<u>Page</u>
I	EXPERIMENTS USING LATENT CATALYST.	32
II	ELASTIC STIFFNESS CONSTANTS OBTAINED FOR GRAPHITE- FIBER, NICKEL-MATRIX COMPOSITES BY ULTRASONIC VELOCITY MEASUREMENTS	57
III	COMPARISON BETWEEN SONIC AND STATIC YOUNG'S MODULUS IN UNIDIRECTIONAL COMPOSITES HAVING DIFFERENT FIBER ORIENTATIONS	59
IV	FIBER AND MATRIX PROPERTIES USED IN ANALYTICAL PREDICTIONS.	60

BLANK PAGE

SECTION I

INTRODUCTION

This report covers the fourth year's work of a program which represents a novel approach designed to fulfill three different, but clearly interdependent, needs of the Department of Defense: a materials need, a structural design capability need, and a need for more scientists and engineers trained in applied materials problems and advanced design methods. The Carbon Products Division of Union Carbide Corporation, Case Western Reserve University, and Bell Aerosystems Company have formed an Association to meet these needs.

The Association has formulated a broad program which includes the development of new materials, generation of advanced analyses and design methods, and education of graduate students. In brief, the major objectives are (1) to develop high modulus graphite fiber composites, (2) to extend the methods of structural mechanics, (3) to identify DOD applications toward which the program efforts should be directed, (4) to educate engineers capable of developing and using modern materials, and (5) to integrate materials research with the needs of the designer by extending the technique of structural synthesis to include material variables.

The primary responsibilities of Union Carbide Corporation, Carbon Products Division, are the development and production of composite materials and the measurement of those mechanical and thermal properties needed for the structural design work within the Association. The technical program at Union Carbide consists of: (1) materials research, a basic research program to develop new, improved composites of high modulus graphite fibers in both resin and metal matrices; (2) materials fabrication, an applied research program to produce materials for the joint research programs of the Association and to seek new ways of fabricating components which better utilize the superior properties of composite materials; (3) properties evaluation, the measurement of the mechanical

and thermal properties of certain composites to provide data for the joint research programs of the Association; and (4) failure criteria, a basic research program to determine experimentally adequate failure criteria for anisotropic materials under multi-axial stress states and to find ways of representing the failure surface which can be used by the designer in practical calculation.

The work at Case Western Reserve University has two major objectives. The first objective is to advance the basic structural mechanics technology required for rational design with composite materials. Composite materials offer the structural design engineer the prospect of being able ultimately to carry on simultaneously the design of the structural configuration and the material. Achieving this capability will require fundamental advances in structural synthesis as well as a substantially improved understanding of the behavior of composite materials. The goals of the structural mechanics research program at Case are (1) the quantitative formulation and efficient solution of the structural synthesis problem, including material variables, for elementary, but representative components fabricated from composite materials; (2) experimental stress analysis studies and theoretical investigations in micromechanics with the objective of improving the measurement and calculation of stiffness properties and failure mode criteria for composite materials; and (3) the development of improved analysis methods for anisotropic, nonlinear, and nonconservative materials. The second objective of the work at Case Western Reserve University is to develop new or improved graphite fiber-resin composites through materials research. At present, the knowledge of fiber surface morphology and the relation between fiber surface characteristics and interfacial adhesion to the resin system(s) is incomplete. A better understanding of these interfacial interactions will lead to improvements in presently used fiber resin composites and will ultimately permit the judicious selection of new resins and new fabrication methods, thus leading

to a second generation of advanced composites. The materials research work at Case Western Reserve University has been initiated during the second half of the report period. The present report covers the program plans and some initial results.

The primary purposes of Bell Aerosystems Company's participation in this program are to interject user requirements into the applied materials research efforts; to apply, at the prototype design level, the advanced analytical procedures and improved understanding of material behavior which will result from the research; and to establish application-related property specifications for materials research activities. To attain these objectives, a six-part technical program is being performed by Bell: (1) application selection, the objective of which is to define representative configurations and environmental conditions which reflect DOD requirements; (2) recognition of failure modes, a task which involves the overall structural behavior such as elastic instability, deformation limits, and fracture and the material failure modes; (3) determination of the nature of and methods for the application of analytical tools needed to cope with the anisotropic, anelastic, and nonconservative material property behavior and the multiaxial stress distributions anticipated in structural configurations associated with the use of the subject materials; (4) structural synthesis, a task which involves the application of structural synthesis techniques at the practical level to define the most desirable material compositions within a particular class of composites; (5) study of creative design concepts which will be required because of the complex material behavior of composites; (6) testing to verify the value of analysis procedures used to design composite materials and the components made from composite materials.

In contrast to the previous three Annual Reports,^(1,2,3) which consisted of single volumes, the present report has been divided into three volumes. Volume I covers the effort on materials research; Volume II covers the work on structural mechanics,

analysis, and optimization; and Volume III covers the design, fabrication, and testing of a representative subscale fuselage component. This division was made because particular projects might be of interest to a particular audience; this arrangement also made possible the reduction of the physical size of each volume. However, this introduction and the following Summary (Section II) are common to each volume.

SECTION II

SUMMARY

The activities of the Association formed by Union Carbide Corporation, Case Western Reserve University, and Bell Aerocsystems Company are directed toward designing, fabricating, and evaluating a representative composite fuselage component; investigating selected critical problem areas in advanced composite technology; and involving students in an important new technology. The component activity serves as a hardware performance demonstration and also serves to reveal new, or to emphasize suspected, technological shortcomings. Investigations of these shortcomings and of other problems which clearly must be solved for the next generation of advanced composite applications form the basic, long range studies. Through knowledge of the total program and by participation in specific projects, the graduate students gain skill in advanced composite technology and become better informed concerning the nature of industrial research and development.

The experimental and theoretical work presented in this report covers materials research in the following areas: graphite fiber reinforced resin-matrix and metal-matrix composites, physical properties and design data studies of fiber composites, the mechanics of fiber composites, advanced analysis and synthesis, and fabrication and testing of a representative fuselage component. Although these projects are clearly related in their common objective of advancing the state of the art of composite materials, the diversity and physical volume of this work made it desirable to present the report in three volumes. Volume I covers materials research on graphite fiber, resin-matrix and metal-matrix composites; Volume II is concerned with the structural mechanics of composite materials; and Volume III covers the structural development of a representative, subscale fuselage component. The following paragraphs summarize the contents of each of the three volumes.

Volume I: Materials Research

Techniques were developed to study the interfacial region between fiber and resin in composite materials. The tools used were electron microscopy, electron diffraction, and laser excited Raman spectroscopy. The electron microscope was used in the study of epitaxial growth of polyethylene on graphite fiber surfaces (cleaned with boiling water) and on the 001 planes of graphite single crystallites. Electron diffraction results indicate that the crystals grown on the graphite single crystal surfaces are oriented so that the molecules stand upright on the substrate. A microsampling technique was developed for the Raman spectroscopy studies. By this technique, spectra of graphite fibers and graphite single crystals could be obtained and compared. The spectra show bands at 1580 cm^{-1} and 1355 cm^{-1} . The relative intensity of the two bands is different for the various graphite samples, allowing differentiation among fibers of different origin. The spectra can be correlated with the presence of more or less graphitized surfaces.

Graphite-fiber, resin-matrix composites were prepared by *in situ* polymerization of ϵ -caprolactam (the monomer of nylon 6) on "Thornel" 25 fibers (cleaned with boiling water). The kinetics of this anionic polymerization of caprolactam, in which various latent catalysts were used, were investigated. With a number of catalysts, the presence or absence of water in the monomer was found to affect the catalysis of polymerization. However, since diethyl carbonate was found to catalyze the polymerization under both wet and dry conditions, this latent catalyst was used for the preparation of composites. These composites were examined by X-ray diffraction and electron microscopy. The examination showed the complete absence of voids and confirmed the original hypothesis that *in situ* polymerization would lead to greater wetting of the fibers by the polymer than that which resulted from using conventional methods and would therefore yield void-free composites.

The oriented crystallization and subsequent oriented solid state reaction of the monomers of nylon 66 (hexamethylene-diammonium adipate) and nylon 6 (6-aminocaproic acid) on "Thorne1" 40 carbon fibers have been investigated. The reaction of these monomers, epitaxially crystallized on the carbon fiber substrate, yields cyclic dimer and cyclic trimer, respectively, whereas reaction in the absence of substrate under otherwise identical conditions yields the respective polymers. The strong and specific effect of surface interactions on these solid state reactions is clearly demonstrated. *In situ* polymerization of these cyclic materials and other monomers is being investigated.

Sophisticated equipment has been constructed to characterize the graphite fiber surfaces by measurements of adsorption from the gas phase and from solution. A highly sensitive balance capable of detecting a weight change of 1×10^{-6} grams in a 1-gram sample was designed and constructed for use in this study.

Graphite-fiber, nickel-matrix composites were fabricated by electrodepositing nickel uniformly around each filament and hot-pressing the precoated, prealigned filaments into fully densified composites. Previously, fabrication of large test specimens was limited by the relatively slow electrodeposition process. This problem was partially rectified by construction of equipment which can electrodeposit nickel continuously on two untwisted plies of "Thorne1" yarn. Higher deposition rates were also obtained by applying current simultaneously to both ends of the yarn as it enters and leaves the plating bath, but the nickel distribution was not uniform. The most uniform deposition of nickel around the filaments is achieved if cathodic contact is employed only at the entrance roller. The fabrication of larger specimens was extended to include uniaxial test bars up to three inches long and orthogonal plates up to three inches square. Short sections of tape approximately 0.010 inch thick were also prepared and will be used for further fabrication into laminates of complex geometry and configuration. A problem of adherence between the graphite mold surface

and the tape after hot-pressing was overcome by using boron nitride at the interface. Three-inch square tape prepared by this process showed minor delaminations parallel to the fibers. Studies of the influence of fabrication variables (pressure, temperature, and time) on properties of the composite were extended to include 1250°C as a fabrication temperature. The average tensile strength (89,400 psi) and Young's modulus (33.6×10^6 psi) are consistent with previously established trends. The fiber morphology showed only slight change.

The elastic properties of unidirectional graphite-fiber, nickel-matrix composites were obtained by static, sonic, and ultrasonic methods. The values derived from each of these methods are in reasonable agreement. Experimental values of Young's modulus, shear modulus, and Poisson's ratio were correlated with predictions based on Whitney's micromechanics model for orthotropic filaments. All measured elastic properties, with the exception of the transverse modulus, can be reconciled with predicted values based on fiber and matrix properties. Stress-strain data were obtained on unidirectional specimens with fibers oriented at various angles to the tensile axis. Strain at failure when the fibers are parallel to the test axis is 0.4 percent. Deformation is considerably greater at slight angles ($\sim 15^\circ$) and much less at the highest test angles ($>45^\circ$). Composites with 45 percent fibers are characterized by a sharply defined yield point at 12,000 psi and a secondary modulus. The secondary modulus is stress dependent. If the matrix contribution to the secondary modulus is assumed to be zero, the fiber modulus corresponds to 36.5×10^6 psi at low stresses, a value which gradually increases to 45×10^6 psi at 160,000 psi stress. The composite modulus in compression is 28.7×10^6 psi, appreciably less than the tensile modulus of 32.2×10^6 psi. Failure in compression occurs at 96,000 psi. The constituent behavior during a strain cycle experiment was analyzed from the known tensile and compression stress-strain curves. The linear thermal expansion was measured

between room temperature and 1000°C and found to be $0.5 \times 10^6/^\circ\text{C}$ and $20 \times 10^6/^\circ\text{C}$ in the longitudinal and transverse directions, respectively. The composite is highly anisotropic and the thermal expansion is controlled by the thermal behavior of the graphite fiber. Cyclic behavior and plastic deformation of the matrix were also studied. Orthogonal laminates with 3-, 5-, and 7-ply configurations with orientations of 0°, 45°, and 90° were tested in tension to obtain the static modulus, stress-strain behavior, and ultimate tensile strength. These properties correlated well with predictions based on uniaxial properties. This correlation indicates that, to a first approximation, microcracks caused by thermal expansion differences of the laminate layers do not decrease the composite strength and modulus properties. Attempts were made to correlate the tensile strength values obtained on three-inch long test specimens with data measured previously on one-inch bars. The three-inch specimens, either dog-boned or of the IITRI type, failed outside the gage section.

Volume II. Structural Mechanics

A finite element displacement analysis computer capability for the microstress analysis of fibrous composites has been developed. A specialized finite element containing a circular fiber in a finite elastic matrix is used as the basic analysis block. Several test cases have been examined to assess the accuracy of the capability.

The investigation of stress and strain concentration factors due to inclusions of various shapes in a physically nonlinear matrix has been continued. Emphasis was placed on developing a method, that may be extended to nonlinear solids, for solving linearly elastic inclusion problems. Some success has been achieved in this respect. The general solution of the elastic curvilinear inclusion problem has been found in the case of antiplane, or transverse, shear deformation. In the case of plane deformation, only the general functional form of solution for rigid curvilinear inclusion and cavity has been found.

The experimental methods and techniques necessary to study the plane strain fracture toughness of fiber composites as related to the void content have been developed. The effect of the width of the specimen on the fracture toughness has been determined. Work was also done in studying microscopically the effect of voids on the fracture of composites.

Examination of the fracture surfaces of cross-plyed "Thornel" fiber tensile specimens provided indications for the fracture mechanism, which also accounts for the effect of specimen width on the tensile strength. Results of creep studies on unidirectional composites indicated that the matrix was in the plastic region for a significant period of time before failure.

The stress-strain behavior and fracture strength under uniaxial, torsional, and combined stresses have been determined for "Thornel" 50 graphite fiber, epoxy-matrix composites. The combined-stress tests were conducted on four-ply (orthogonal) hollow cylinders. Torsional properties were measured on both orthogonal and on uniaxial (hoop-wound) cylinders. Uniaxial tensile and compressive strengths were determined on orthogonal plates. The experimental fracture strength was found to be lower than that predicted by several theories of fracture. This result is attributed mainly to a non-homogeneous structure of the test specimens and in some cases, to premature buckling failure.

Test techniques have been devised for adapting the scattered light method of photoelastic stress analysis to multilayered fiber composites. A special polariscope has been designed and built to obtain the data from multilayered composite photoelastic models. A computation scheme employing numerical methods has been devised to obtain the full stress tensor from the photoelastic data and the stress relations of elasticity. The experimental and computational techniques have been tested by application to a homogeneous model: a sphere in compression under two self-equilibrating concentrated loads while imposing the constraints of

the multilayered composite. The results obtained were compared with those obtained by other investigators, and the agreement is considered good under the constraints imposed on the problem.

An experimental study of the vibrations of laminated orthotropic plates has been completed. The experimental results were correlated with classical homogeneous plate theory. For unbalanced plates, the reduced flexural stiffness yielded values which indicated good correlation between theoretical and experimental results.

A program for the prediction of post-buckling strengths of composite plates which would increase the utility of composites in aircraft construction has been formulated. Classical methods of post-buckling analysis for isotropic metallic plates have been surveyed for possible extension to anisotropic nonhomogeneous composites.

An approximate solution for the eigenvalue problem for simply supported anisotropic plates has been suggested. The buckling mode takes the form of a finite series which satisfies the buckling equation throughout the field and the boundary conditions at a finite number of points. Better approximations can be achieved by carrying more terms in the series to satisfy boundary conditions at more points. If an infinite number of terms were used, the exact solution could be obtained. The solution technique is applicable to any type of boundary conditions.

The analysis of unbalanced cross-plyed elliptic plates under uniform pressure has been extended to configurations where the principal axes of the material are skewed to the semi-major axis of the ellipse. The fully clamped boundary condition case has been solved in closed form.

A finite deflection discrete element analysis capability for predicting displacement and force distributions in sandwich plates and cylindrical structures with unbalanced laminated faces has been completed. Correlation of the results with published data and experiment results for "Inornel" fiber composites show excellent agreement.

Laminated fiber composite plate and shell configurations may be viewed as a collection of highly orthotropic lamina. If one assumes that the layup is not unidirectional, the lamina are highly heterogeneous through the thickness. An investigation has been initially aimed at critically assessing several basic assumptions upon which current laminated plate and shell theory rests.

A study of the accuracy of various shell theories when applied to anisotropic cylindrical shells is currently underway. Flugge's theory is accepted as a standard for comparison of several approximate theories. The range of validity of the various approximate theories will be determined.

A structural synthesis capability for stiffened fiber composite cylindrical shells has been developed. The design variables consist of both configuration and material parameters. The optimal design problem is formulated as a nonlinear mathematical programming problem. Numerical examples are discussed.

Volume III: Structural Component Development

The previous (third) annual report⁽³⁾ described work on the implementation of advanced structural analysis methods and the material and structural element evaluations leading to final design of a graphite-fiber, epoxy-resin composite fuselage section. Initial fabrication activities and a tentative test program plan for the fuselage component were also presented. Additional design work and analysis studies were completed during the present report period. A design solution was found for an interference fit problem concerned with insertion of the fiberglass block end buildups. The basic fuselage structure was analyzed by the discrete element method; stresses, displacements, and margin of safety predictions were obtained for four loading conditions. Influence of the stringer-ring-skin combination tie was studied with regard to the performance expected of the structure during test. Ring-to-skin bond loads due to Poisson effects were examined; these bond stresses should not cause problems during the fuselage component test.

Several treated "Thornel" 50 stiffened panel end attachment specimens were fabricated by using the final shell geometry and were tested. Ultimate strengths were 2710 and 3070 lb/in. in tension and compression, respectively; failures occurred in the gage sections. Effective elastic moduli of the specimens were 14.7 and 17.3×10^6 psi. The failure levels were well above design requirements and demonstrated stiffness and weight advantages over conventional metallic construction. Based on these design and analysis data and test results, fabrication of the fuselage component was begun.

The representative fuselage component was fabricated by using treated "Thornel" 50 graphite-fiber, ERL 2256 epoxy matrix composites. A tapered, cylindrical fuselage skin, 48 inches long with end diameters of 24 inches and 20 inches, was constructed by using a fiber lay-up orientation of $(90^\circ, \pm 15^\circ, 90^\circ)$. The 90° layers were wet-wound on a plaster mandrel, and the inner 15° layers were constructed by hand lay-up of prepregged sheet. Forty-five hat-shaped stringers, 50 to 52 inches long, were molded from prepregged sheet having a fiber orientation of $(+10^\circ, -10^\circ, -10^\circ, +10^\circ)$, and their properties were measured on coupons cut from each end of the stringers. Thirty-one of these stringers were bonded to the fuselage skin by an adhesive consisting of 70 weight percent Araldite 6005 epoxy resin and 30 weight percent ZZL-0325 hardener. Segmented ring stiffeners, consisting of a balsa wood core reinforced with "Thornel"-fiber, epoxy-resin panels of $(0^\circ, \pm 45^\circ)$ orientation, were fabricated and also bonded to the fuselage skin. The ends of the fuselage component were reinforced with a lay-up of fiberglass tape. Segmented aluminum rings, designed and fabricated at Bell Aerosystems, were bonded to the fiberglass laminate. The function of the fiberglass lay-up and aluminum rings is to permit attachment of the fuselage component to the test stand. A weight analysis of the representative fuselage component was also prepared.

Inspection of the finished fuselage component by visual and mechanical techniques revealed stringer debonding, minor ring debonding, and cracks in the shell skin and ring-stiffener shear panels. These defects were more thoroughly characterized by other inspection techniques such as helium leak detection, a contact ultrasonic technique and an acoustic impact bond inspection method. Correlations of data obtained from the various nondestructive inspections were made.

Potential causes of the damage in the fuselage component have been studied in both experimental and analytical investigations with emphasis on the problem of stringer-to-skin debonding. Experimental studies examined possibilities of surface contamination which may have affected the bond strength, bond line thickness effects, possibility of adhesive embrittlement due to post-cure, and other potential causes such as fixturing expansion during component cure and air bubble entrapment within the adhesive. It was concluded that thermal embrittlement of the adhesive and thermal stresses in the bond-line probably contributed most to the observed debonding, although the influence of the other factors cannot be completely discounted. Analytical studies were also made of thermal stresses due to elevated temperature exposures and of mechanical stresses due to radius of curvature mismatches between the stringers and shell skin. The thermal analysis suggests that stresses in the adhesive were sufficiently large and, in conjunction with end effects, peeling actions, and possible adhesive embrittlement, may have contributed significantly to the debonding. Predicted transverse stresses due to skin fabrication also appeared significant and may be related to the observed skin cracks. Peel loads due to the curvature mismatches between stringers and skin were found to be small and were not likely to have contributed to the stringer debonding.

Repair of the fuselage component was successfully accomplished. The stringers were rebonded to the skin using a room-temperature curing adhesive (Scotchweld 2216 clear). For this purpose, perforated polyethylene bladders were inserted into the stringers, filled with adhesive, and pressurized to force the adhesive to flow into the debonded areas. After the bonding was completed, the bladders were removed, thus minimizing the quantity of excess adhesive remaining in the stringer cavities. The ring stiffeners were rebonded to the skin by using an overlay of fiberglass tape prepregged with room-temperature-curing Scotchweld 2216 gray. The craze cracks in the skin were similarly repaired by patching with the same prepregged fiberglass tape. Prior to rebonding, both adhesive systems and the rebonding procedures were extensively evaluated by tensile, lap shear, and bond peel tests; compression tests on stringer stiffened plates were carried out, and practice bonding runs of full length stringers bonded to an aluminum mock-up of the component skin were made.

The shell loads for the component test evaluation have been revised to reflect the material change from untreated "Thornel" 40 to treated "Thornel" 50. The instrumentation plan for response and destructive testing of the component has been defined, and fixturing and test preparations have been made. Testing of the repaired component is expected to begin in the fall of 1969.

SECTION III
RESEARCH ON GRAPHITE-FIBER
RESIN-MATRIX COMPOSITES

A. New Physical Techniques To Elucidate the Structure of the Fiber-Resin Interface

(Professors Baer and Koenig and Dr. F. Tuinstra, Case)

For a given fiber-polymer system, the structure within the fiber-polymer interface region largely determines whether good or poor composite performance is achieved. Questions of fundamental and practical importance concern (1) the structure of the fiber surface compared with that of the bulk fiber, (2) the nature of the fiber-polymer bond, and (3) changes in the polymer morphology produced by the interfacial bond. Because of severe experimental difficulties, very little is known of these phenomena for any composite system. The objectives of this project are, first, to develop new tools or adapt old tools for studying the fiber-polymer interface region and, second, to apply these tools to study graphite fiber composites. Tools which may be investigated include X-ray diffraction, optical and electron microscopy, infrared spectroscopy, and laser-excited Raman spectroscopy.

Because of our special interest in surface and interfacial regions of less than 1 μm thick, the tools selected must be modified to allow microsampling. For this reason, we selected the electron microscope and the Raman-laser spectrometer as the most promising tools. The electron microscope will give us information on the morphology of the surface; the Raman-laser spectrometer will give us, together with the electron diffraction, structural information. The fibers used in this research were graphite fibers.

1. Electron microscopy

If we want to look at the surfaces of the graphite fibers, we have to use replication techniques because the fibers themselves are too thick to be translucent to the electron beam. As the fibers have a diameter of about 8 μm , replicas of single fiber surfaces are difficult to obtain.

Therefore we developed the following technique. Fibers are glued to a smooth surface (i.e. a glass slide) by a thin layer of glue. From the surface of the formed "composite" a replica is made. While applying this technique, we encountered some difficulties which are related to the main subject of our research, to wit the resin-fiber bond.

The major difficulty was the choice of the right glue. The glue chosen must have an affinity to the fiber surface such that when applied as a very thin layer it does not wet all the surface but, on the other hand, it must cover and wet a reasonable area of the surface such that the fiber is glued tightly to the underlying surface. Several types of glue were tried, among them commercial epoxy resins, solder, different polymer solutions, etc. In some cases we got a replica of the glue covering the fibers; in other cases the replica stuck to the fibers again showing just the glue; in a third case, the fibers came off with the replica. The only glues which gave occasional results were waterglass (however, these were difficult to reproduce) and Araldite (scientific grade), although gelatine may also be useful in some cases. With waterglass we were able to obtain some micrographs of the fiber surface, showing quite a lot of detail. In Figure 1 the high orientation of the surface layer can be visualized. The picture shows the undulating surface with microridges and grooves, both of which are highly oriented along the fiber axis. The picture shows clearly the troubles with the replication.

So that reproducible experiments could be achieved, we modified the above technique. After the glue has set in the above procedure, a top layer is scraped off from the "composite" with a knife. This procedure gives us a number of flat surfaces of fibrous graphite which now coincide with the surface of the bulk "composite". These freshly scraped surfaces allow easy replication. The micrographs show the same detailed structure of the fiber as shown by pictures of the original outer fiber surfaces.

With this reproducible replication technique we tried to study the crystal growth of polyethylene (P.E.) on these graphite surfaces. The freshly scraped surfaces were then immersed for a period of 30 minutes in a 0.1% solution of P.E. xylene at a temperature of 110°C. Deposits of

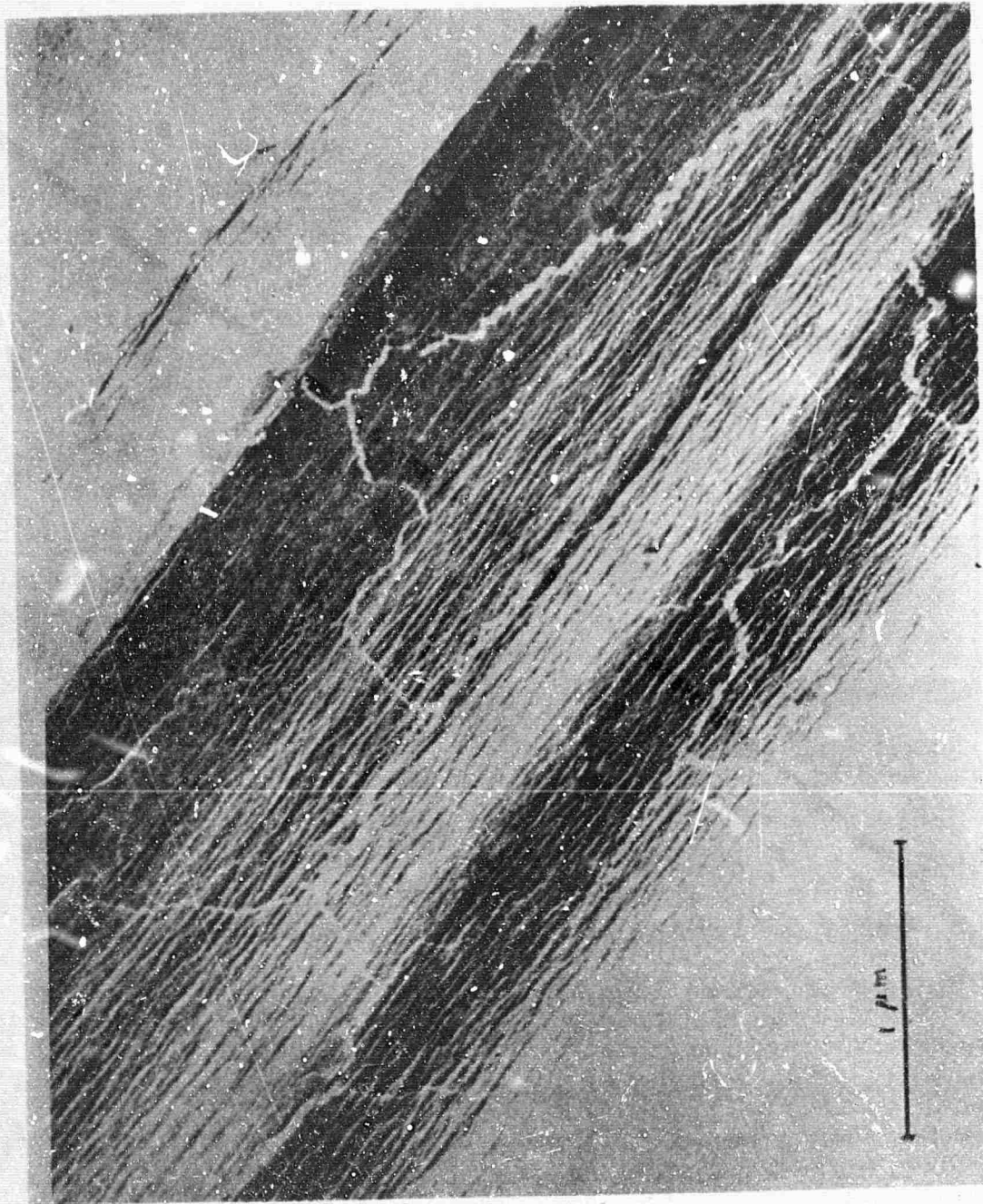


Figure 1. Surface Replica of a "Thornel" 50 Fiber.
N-22142

crystalline P.E. were observed; however, the orientation of the crystallites was not pronounced although a preference for perpendicular and parallel orientation to the fiber axis was present.

So that information about the crystal growth on the fibers could be obtained, crystal growth at surfaces of single crystalline platelets of natural graphite (Ticonderoga flakes) were observed. These platelets were furnished by Union Carbide Corporation. The platelets were put in a 0.1% solution of polyethylene in xylene and split in the solution to obtain fresh and clean cleavage planes. The crystals were kept for 10 to 45 minutes in a solution at temperatures ranging from 95°C up to as high as 115°C. The electron micrographs of replicas of the surface show a well-oriented network of rodlike crystallites. The three preferred directions are clearly inclined to each other at 60°, as shown in Figure 2. The shadowing gives good contrast, usually for just two of the preferred directions.

Two unusual observations should be noted. First, it has been reported⁽⁴⁾ that at a temperature of 115° in the xylene solvent no epitaxial crystallization of P.E. was observed using alkali halides as substrates. In order to exclude a possible deposition of P.E. from an evaporating droplet of the solution which clung to the surface while the sample was pulled out of the solution, a rinsing cycle was introduced. During the removal of the sample from the solvent, its surface was rinsed with pure solvent at the appropriate temperature. The difference between rinsed and unrinsed samples was negligible. This result suggests that deposition occurs during the exposure of the cleaved graphite surface to the solution. So that deposition was prevented until the sample reached the solution temperature, the graphite crystal was heated to the appropriate temperature before cleaving.

The second unusual behavior was found when we obtained electron diffraction patterns from the deposited layer. Most of the time a thin layer of graphite was sticking to the replica, as were the P.E. crystallites. The latter melt quickly if kept in the electron beam. We succeeded, however, in getting a diffraction pattern of the deposited P.E. layer. The diffraction pattern was a superposition of three P.E. diffraction patterns inclined to each other at 120°. This result shows that the morphological "hexagonal" orientation corresponds to a structural orientation of the crystallites of



N-22143

Figure 2. Electron Micrograph of a Graphite Crystal Surface on which an Oriented Layer of Polyethylene is Deposited.

P.E. However, the indexing of the reflections revealed that the crystallites are oriented with respect to the substrate such that the molecular axes of the P.E. are perpendicular to the substrate. In all the experiments reported on overgrowth of P.E. on alkali halides, however, the molecules are always oriented parallel to the substrate. We have to repeat this experiment so that new light might be shed on the graphite polymer bond.

2. Raman spectroscopy

Because of our interest in spectra obtained from very thin layers of material, it was to be expected that the usual bulk sampling techniques would fail here. Indeed with these methods we did get neither a spectrum of graphite fibers nor of single crystals. A possible reason was absorption of the signal (if any) by the highly absorbing graphite. But, of course, not only was the Raman signal absorbed, even the incident laser beam (500 m.w.) was absorbed. This effect caused great difficulties in attempts to observe the spectrum of a thin layer of a polymer on the graphite surface. The polymer layer was made thick enough to show a spectrum, but when placed on the graphite surface it failed to show a spectrum. Apparently the polymer was melting and evaporating on the hot graphite substrate, the latter being heated by the laser beam.

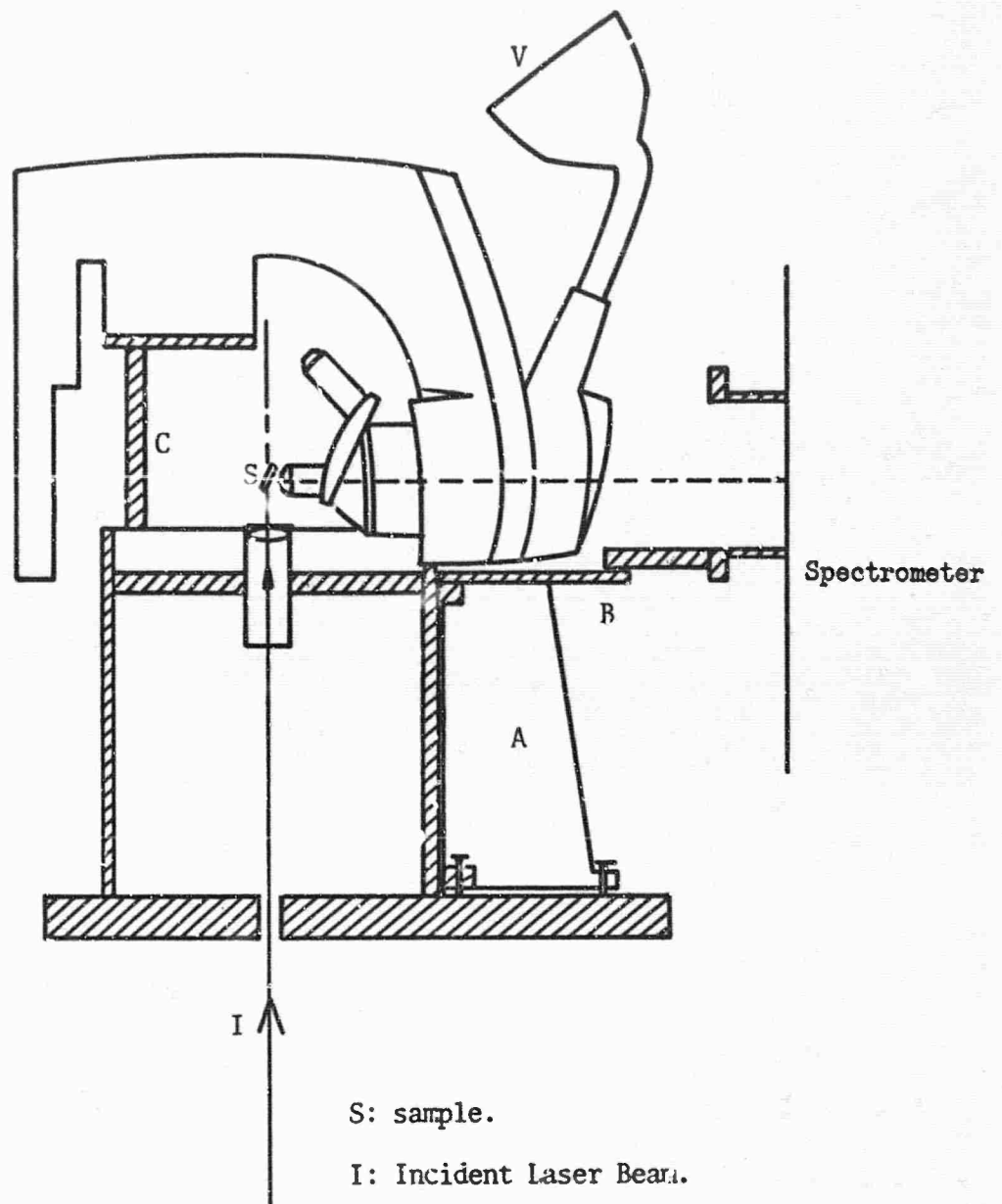
So that this "heating problem" could be avoided, we designed and built a cell in which the sample is suspended in a liquid to conduct away the excess heat. The cell was constructed so that the liquid can be kept at any temperature between 25°C and 140°C. The cell has been tested; spectra of good quality can be obtained with it and the temperature can be controlled within 0.5°C or less.

We first had to use microsampling techniques so that useful results could be obtained with the heating cell. Because the Raman signal increases with the intensity of the incident beam, it is worthwhile to increase the intensity by decreasing the illuminated spot. The laser beam has the advantageous feature of being coherent and linearly polarized. This feature allows us to focus the beam down to a very small spot of extremely high intensity. We designed a mount for a microscope on the spectrometer to aid us in focusing the beam. The microscope permits the sample to be seen at the

same angle as the spectrometer sees the sample. The sample is illuminated by the laser beam, and the image is projected through the microscope on a screen to avoid eye damage to the observer (Figure 3). In this way we were able to focus the laser beam onto the surface of the sample and illuminate an area of only 25 μm in diameter. After removal of the microscope the very bright spot is imaged on the entrance slit of the double-spectrometer. With this set-up, we repeated the initial attempts to obtain the spectra of crystalline graphite, which had first showed a spectrum consisting of several lines. All but one of these bands proved to be due to the vibrational and rotational spectra of N_2 and O_2 in the air surrounding the sample. After blowing helium gas against the sample, we got rid of these "impurities", and a single non-polarized band was left. This single band is located at 1580 cm^{-1} . After this test, many types of graphite and carbon samples were tried, such as many of the available types of graphite fibers, pyrolytic graphite, Madagascar flakes, activated charcoal, and lamp black.

All of these samples showed the band near 1580 cm^{-1} but, in addition to this band, another band at 1355 cm^{-1} appeared. The relative intensity of the two bands is different for all types of samples mentioned and is apparently characteristic of the fiber. Since the incident laser beam penetrates only slightly into these highly absorbing media (and the scattered Raman light escapes even from a thinner layer), the spectra will be characteristic of the surface layer of these samples. The differences in the spectra of graphite fibers obtained from different manufacturers show that this method is a promising tool for the characterization of graphite fibers.

A preliminary calculation of the normal vibrations of graphite shows that we could expect one doubly degenerate Raman active band, whereas none of the vibrational modes is infrared active. The single band is thus assigned to the graphite structure; the second band at 1355 cm^{-1} which is close to the diamond band of 1333 cm^{-1} is attributed to the vibrations of a diamond-like structure. Figure 4 shows a comparison on a relative scale of a number of the spectra obtained.



- S: sample.
- I: Incident Laser Beam.
- A. B. C: Microscope Supports.
- V: Viewing Screen.

Figure 3. Microsampling Cell for Composite Studies.

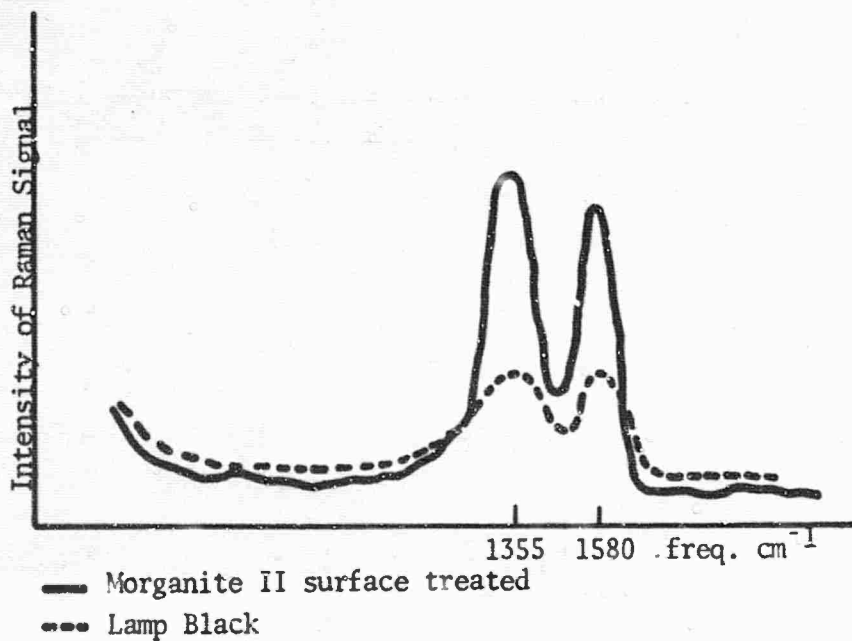
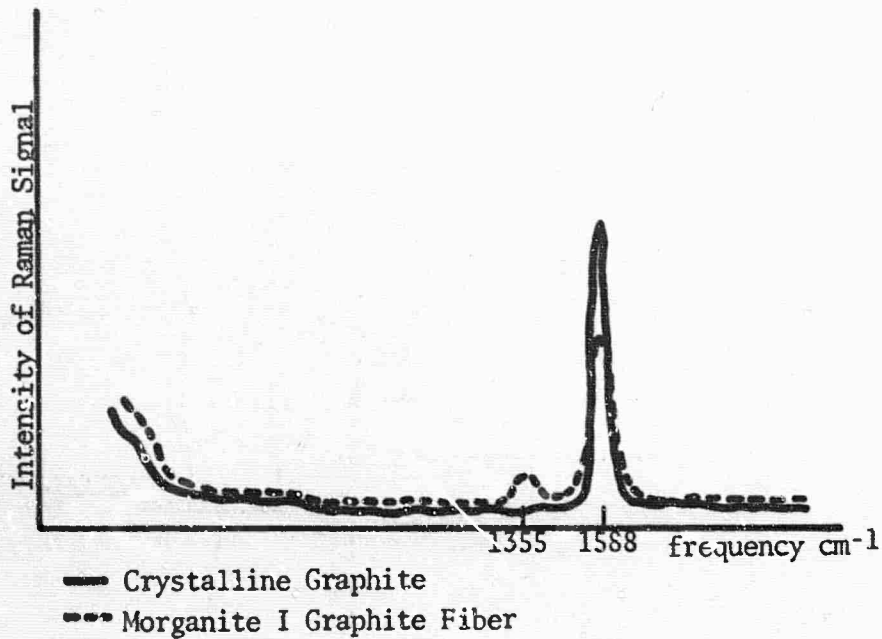


Figure 4. Raman Spectra of Some Graphite and Other Carbon Samples.

B. Graphite Fiber - Polymer Matrix Composites
(Professor Litt and Dr. J.B. Shortall, Case)

1. Introduction

The purpose of this program was to study the viability of using polymer systems such as polyamides and polyurethanes as the matrix element in graphite fiber composites, a special aspect of the work being the incorporation of the fibers in the polymer by "in situ" polymerization on the fibers. It was anticipated that this method would lead to greater wetting of the fibers by the polymer than would more conventional methods and would also lead to the formation of void-free composites.

A further aspect of the work was to use as the graphite reinforcement in the composite not only graphite fibers but also graphite papers of known alignment.

The graphite fibers which have been used so far are "Thornel"^{*} 25, but the more recent "Thornel"⁷⁵ will be used as well as the various Morganite^{**} fibers and, it is hoped, graphite fibers produced by Rolls Royce Ltd.

The polyamide used so far is Nylon 6; polyurethanes used will be based on polyfunctional ethers and aromatic diisocyanates. A block diagram of the steps involved in the preparation of a composite using a nylon matrix and graphite fibers is shown in Figure 5a. A block diagram of the steps involved in the preparation of a composite using a polyurethane matrix and graphite fibers is shown in Figure 5b.

* Thornel is a registered trademark of Union Carbide Corporation

** Product of Morgan Crucible Company Ltd.

NYLON 6/CARBON FIBER COMPOSITE

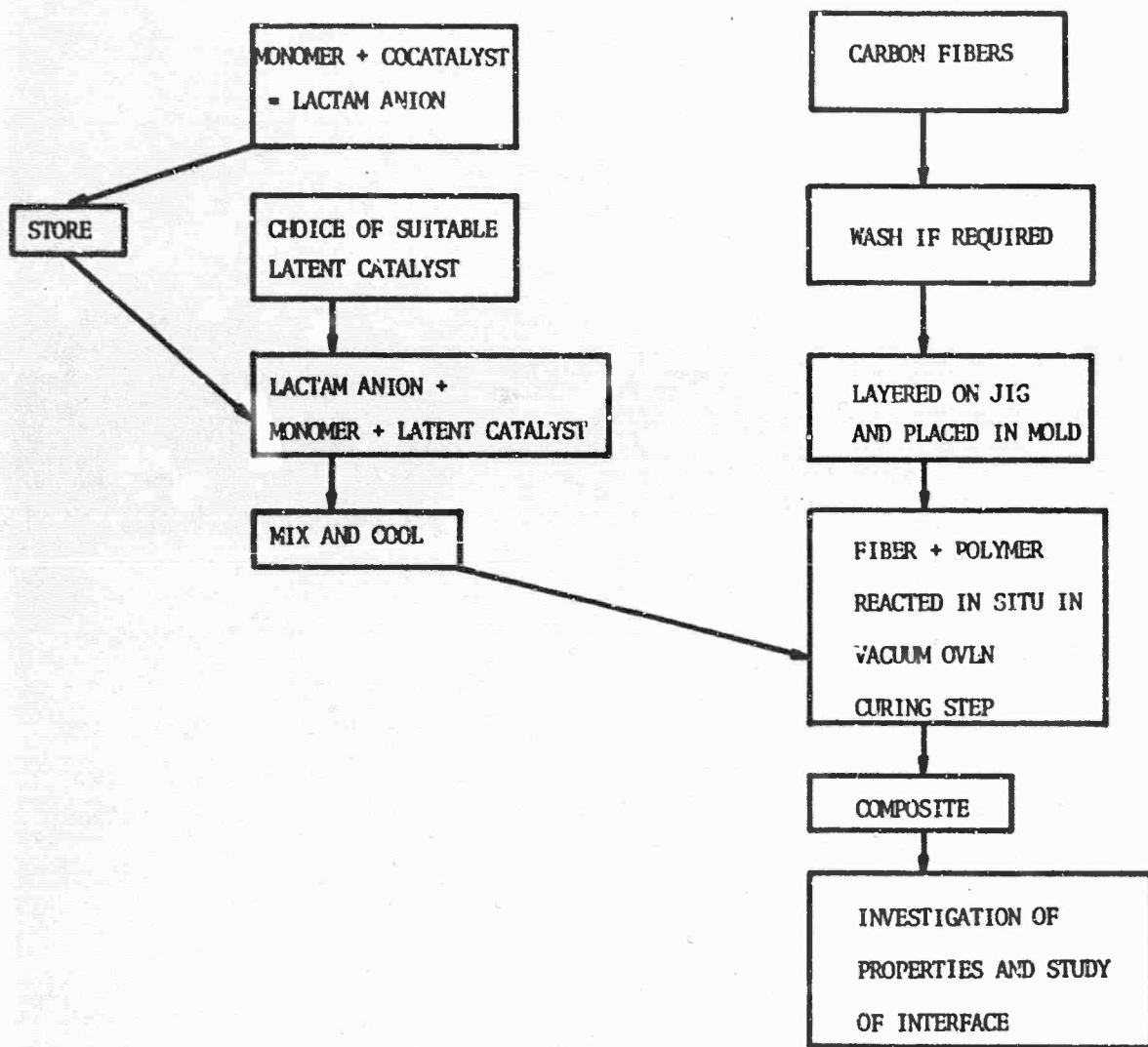


Figure 5a. Preparation of a Composite Using Nylon 6.

POLYURETHANE/CARBON FIBER COMPOSITE

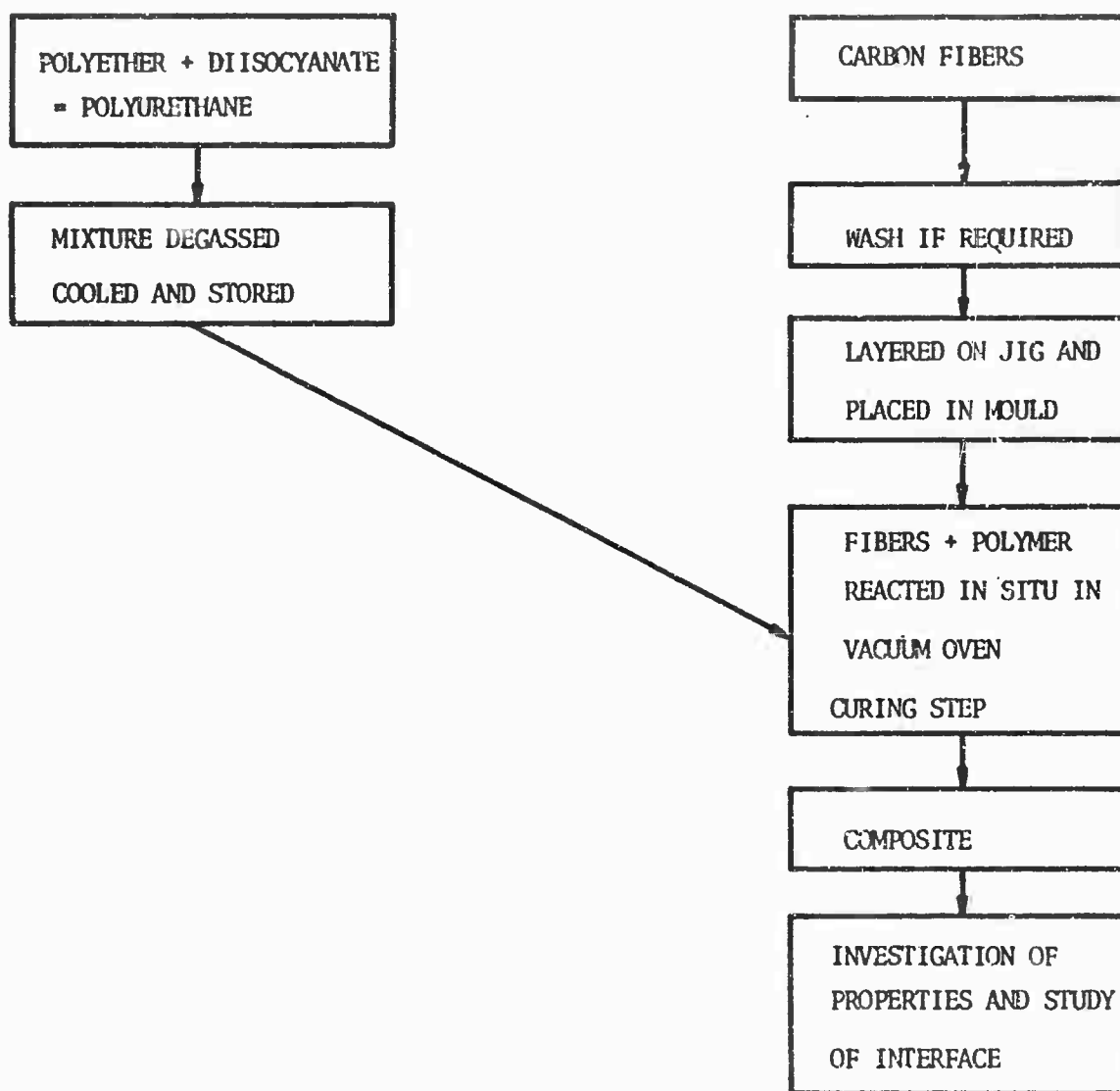


Figure 5b. Preparation of a Composite Using a Polyurethane Matrix.

2. Polymerization of ϵ -Caprolactam to Nylon 6.

This polymerization is normally carried out by heating the sodium salt of ϵ -caprolactam at temperatures above the melting point of the nylon. In this case the induction period, before any polymer is formed, can be several hours. If large quantities of sodium caprolactam are used, at temperatures of about 270°C to 280°C, there is no induction period (Figure 6).

Neither of these alternatives is suitable for the method of polymerization *in situ* in which an induction period of 10 to 20 minutes is slow enough to give control over reaction conditions but sufficiently fast to be a viable method.

To achieve such induction periods latent catalysts must be used in the polymerization, and experiments have been carried out to study the kinetics of the polymerization using such latent catalysts.

A true co-catalyst may be defined as a catalyst which rapidly forms acyl caprolactam which then catalyses the polymerization, whereas a latent catalyst is a material which will transform slowly to acyllactam relative to the rate of polymerization.

A comprehensive literature search has revealed that many such catalysts are available. Generally acylating agents, such as acid chlorides and anhydrides, may be classed as co-catalysts. Other such catalysts are nitrogen containing compounds in which the nitrogen atom is directly attached to at least two radicals selected from the group consisting of carbonyl, thio carbonyl, sulfonyl and nitroso radicals. Latent catalysts which have been reported are carbon disulfide, carbon monoxide, isocyanates, carbodiimides, cyanimides, nitriles, esters, carbonates, urea and thiourea derivatives and perhalogenated ketones.

The catalyst itself in the polymerization reaction may be an alkali or alkaline earth metal, e.g. sodium, potassium or lithium, either in metallic form or as the hydrides, borohydride, oxide, hydroxide or carbonate.

Many of these latent catalysts could be disregarded without further consideration mainly because the polymerization takes place without the

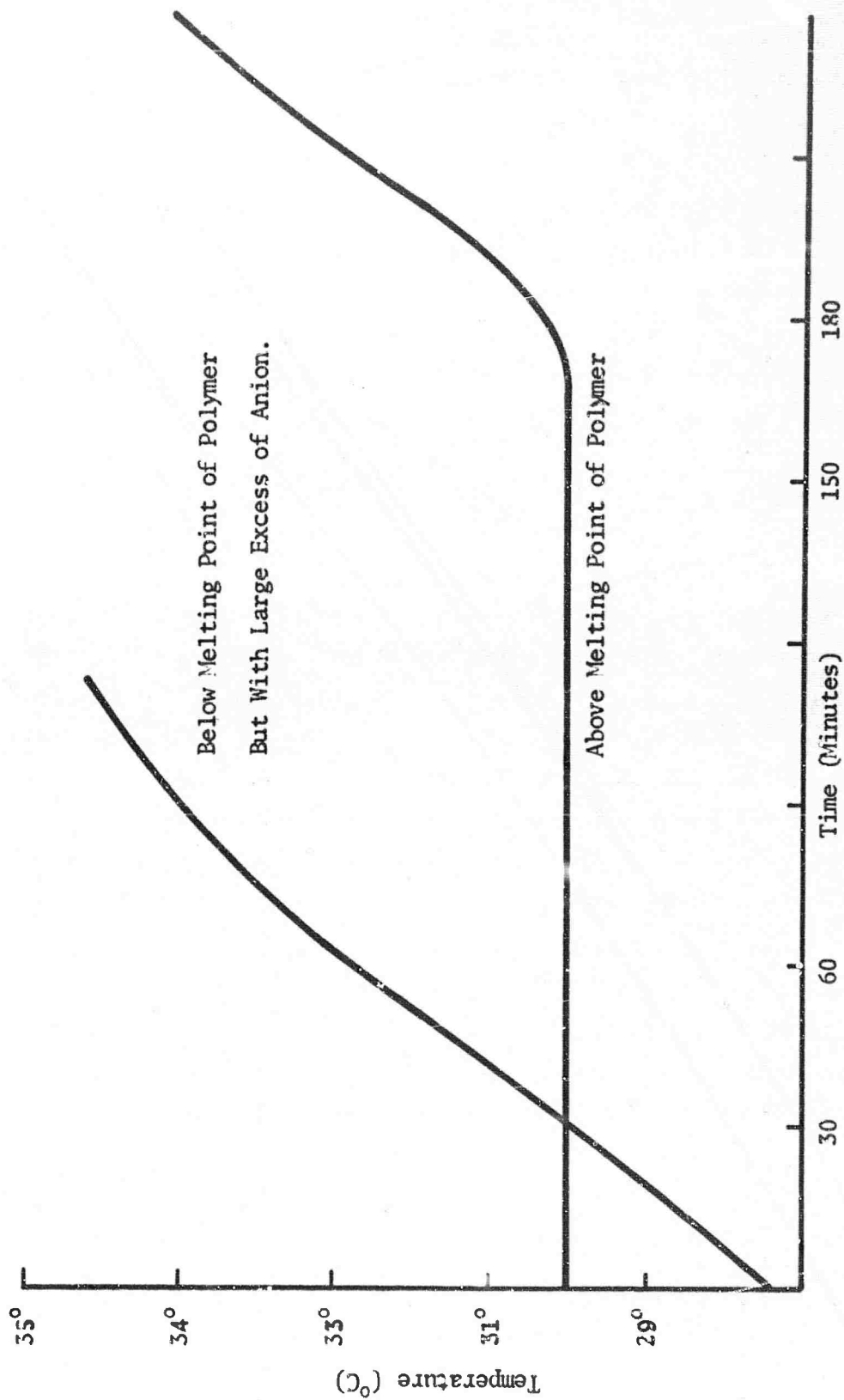


FIGURE 6. Relative Induction Periods for Polymerization of ϵ -Caprolactam

necessary induction period although polymerization is catalysed well below the melting point of the polymer. Among these latent catalysts are the isocyanates, carbon disulphide, carbon monoxide, perhalogenated ketones and nitriles.

The latent catalysts which have been evaluated or are in the process of being evaluated are: dimethyl urea, ethylene urea, methyl benzoate, N, N-dimethyleacetemide, diphenyl thiourea, γ -butrolactone, diethyl carbonate, ethyl pivalate, ethyl isobutyrate and diphenyl carbazole. Propylene carbonate was also evaluated but found to liberate carbon dioxide at the reaction temperature.

3. Results and Discussion

The apparatus for the experiments consisted of an oil filled heating bath on a hot plate equipped with a magnetic stirrer. Four large test tubes were suspended in the heating bath and contained glass wool as insulating material. Smaller test tubes containing the lactam anion - ϵ -caprolactam mixtures were fitted into the glass wool. These inner test tubes were fitted with a cork through which passed a nitrogen inlet tube, a thermocouple and a stirrer. When the temperature of the mixture reached the temperature of the heating bath, the latent catalyst was added and temperature measurements commenced.

Initial experiments suggested that water had an effect on the reactivity of some of the latent catalysts tried. To overcome this effect the ϵ -caprolactam was purified by distillation under reduced pressure until the water content was reduced to 50-60 ppm. The water content estimation was carried out by the Karl Fischer method. This method is based essentially on the reduction of iodine by sulphur dioxide in the presence of water. The reaction is quantitative when pyridine and methanol are present to react with the sulphuric acid and hydroiodic acid formed.

When examination of the latent catalysts was conducted using impure lactam it was found that methyl benzoate, N,N-dimethyl acetamide, γ -butyrolactone and diphenyl thiourea did not catalyse polymerization with water present. Dimethyl urea, ethylene urea, and diethyl carbonate did catalyse

polymerization when water was present. In the absence of water, dimethyl urea and diphenyl thiourea did not catalyse polymerization while diethyl carbonate did. Ethylene urea, methyl benzoate, N, N-dimethyl acetamide, γ butrolactone ethyl pivalate, ethyl isobutyrate and diphenyl carbazole are to be examined as possible latent catalysts in the absence of water. The results of the experiments so far are given in Table I. Experiments have been carried out to determine the viability of diethyl carbonate as a latent catalyst for water free materials.

These experiments were conducted at 180°C in anhydrous conditions and under an atmosphere of nitrogen. The concentration of lactam anion was 1/40 mole per 1 mole of ϵ -caprolactam. In experiments incorporating graphite fibers, the fibers used were "Thornel" 25 which had been washed in boiling water.

Mixtures containing 1/200 M and 1/400 M ratio of diethyl carbonate to caprolactam polymerized after about 6 and 9 minutes respectively (Figure 7). These conditions are ideal for polymerization *in situ* on the fibers.

However, a mixture containing a 1/400 M ratio of diethyl carbonate and with a small amount of unwashed graphite fibers (graphite fibers coated with polyvinyl alcohol) immersed in it, did not polymerize at 180°C.

When unwashed graphite fibers were immersed in a mixture containing a 1/200 M ratio of diethylcarbonate polymerization still did not occur.

A mixture containing a 1/400 M ratio of diethyl carbonate and with washed graphite fibers (washed by boiling in water followed by oven drying at 120°C) immersed in it also did not polymerize. The addition of a 1/400 M ratio of diethyl carbonate to this mixture after 90 minutes still did not catalyse polymerization. This result could suggest that lactam anion is adsorbed on the graphite fibers and that any polymerization occurring is with the the remaining unadsorbed anion.

However, when washed graphite fibers were immersed in a mixture containing a 1/200 M ratio of diethyl carbonate, polymerization occurred after about 10 minutes. By increasing the ratio of lactam anion to 1/30 M and using a 1/200 M ratio of diethyl carbonate with washed graphite fibers immersed in the mixture, polymerization occurred after about 6 minutes.

TABLE I

EXPERIMENTS USING LATENT CATALYST

LATENT CATALYST	RESULTS OF EVALUATION	TO BE EVALUATED IN ABSENCE OF WATER
Isocyanates	Too fast	
Carbon disulphide	Too fast	
Carbon monoxide	Too fast	
Perhalogenated ketones	Too fast	
Nitriles	Too fast	
Dimethyl urea	Only reacts in presence of water	
Diphenylthio urea	No reaction in presence or absence of water	
Ethylene urea	Reacts in presence of water	✓
Methyl benzoate	No reaction in presence of water	✓
N, N dimethylacetamide	No reaction in presence of water	✓
γ butyro lactone	No reaction in presence of water	✓
Diethyl carbonate	Reacts in both wet and dry conditions	
Ethyl pivalate	Not yet evaluated	✓
Ethyl isobutyrate	Not yet evaluated	✓
Diphenyl carbazole	Not yet evaluated	✓
Propylene carbonate	Liberates CO ₂ at reaction temperature	

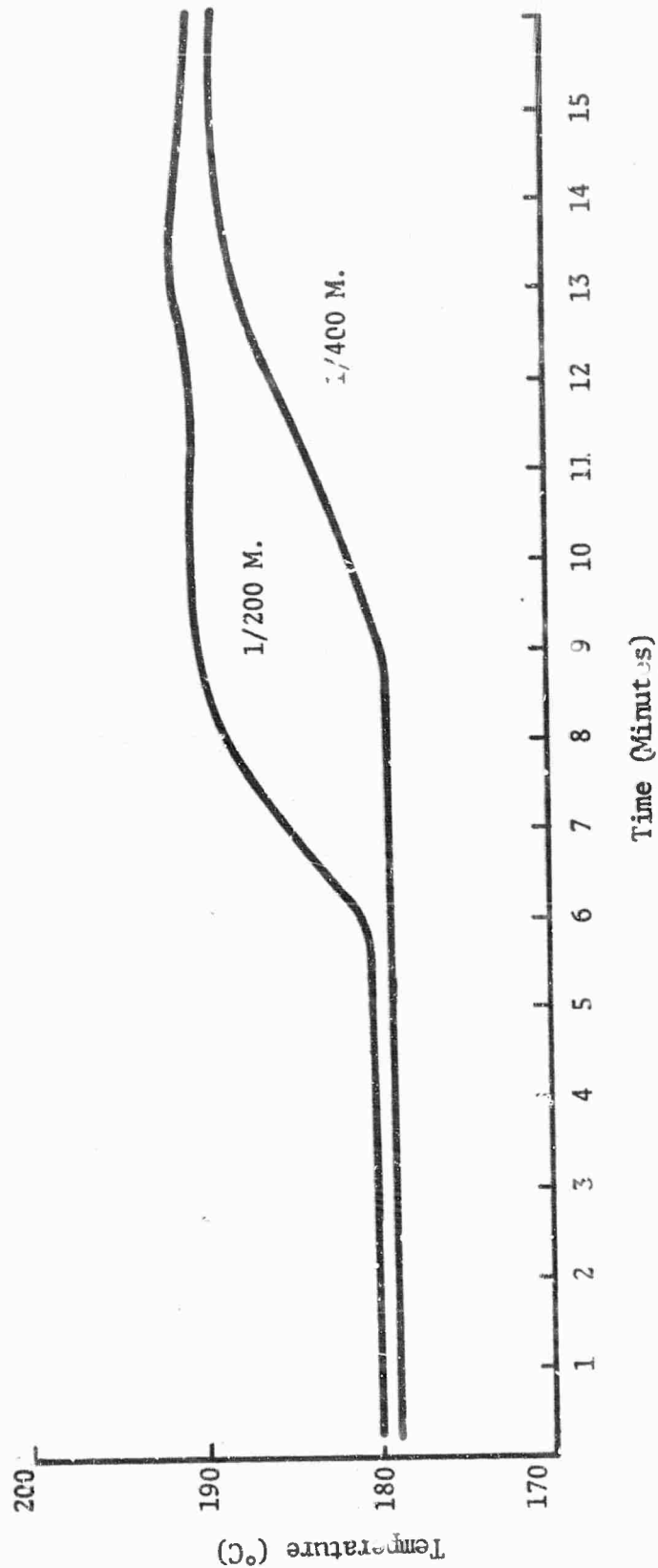


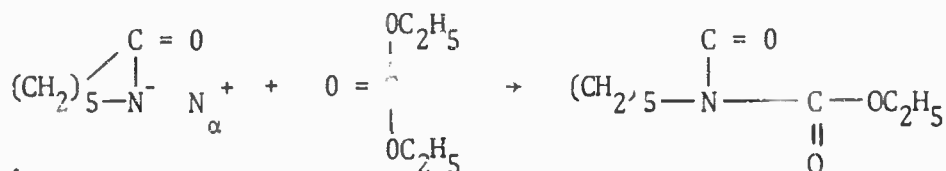
FIGURE 7. Induction Periods For Anionic Polymerization of ϵ -Caprolactam Using Di Ethyl Carbonate as the Latent Catalyst

The anionic polymerization of ϵ -caprolactam to nylon 6 using diethyl carbonate latent catalyst is shown by the following equations.

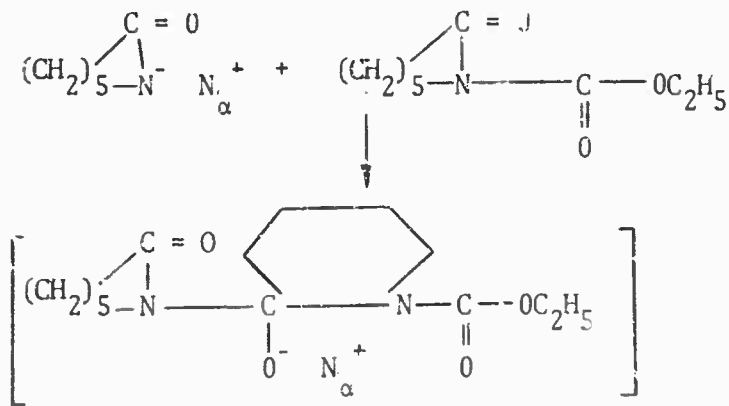
Initiation:



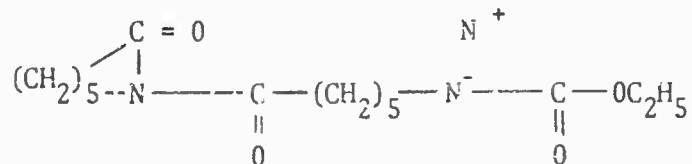
The lactam anion acts as a catalyst for the anionic polymerization of caprolactam. It can be assumed that the latent catalyst reacts with the lactam anion to give an acyl lactam (the reactive carbonyl group of the diethyl carbonate is attacked by a lactam anion). This acyl lactam now reacts further with the ϵ -caprolactam, forming further lactam anion and acyl lactam:



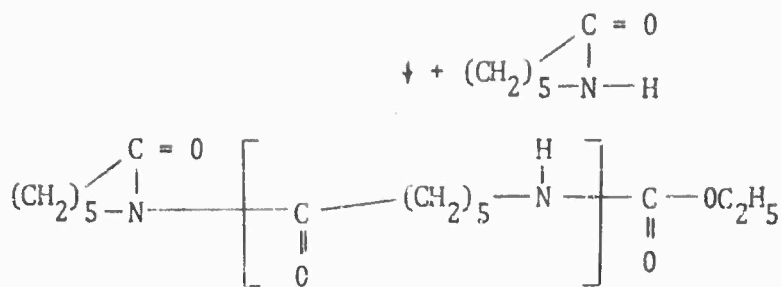
The lactam anion now acts as the primary catalyst for the anionic polymerization of this lactam by attacking the reactive carbonyl group.



This reaction is followed by ring opening and formation of a new acyl lactam:



The propagation to polymer proceeds by step-wise addition of caprolactam and lactam anion:



The rate of polymerization is proportional to $[L^-]^2 [\epsilon c] [t]$

where L^- is lactam anion
 ϵc is latent catalyst
 t is time

Therefore conversion is proportional to L^2 which means that at the beginning of the reaction there is very little production of polymer and therefore very little viscosity increase, allowing easy manipulation of the solution.

Using this method of polymerization, a composite has been prepared in situ in the following way. The requisite quantities of lactam anion and ϵ -caprolactam were melted under vacuum in an oven maintained at 170°C ; melting under these conditions helped to degas the mixture. When the materials had melted, at about 70°C , the diethyl carbonate was added so that the proportions of lactam anion to ϵ -caprolactam to diethyl carbonate were in the molar ratios 1/40 to 1 to 1/200.

After mixing well, the monomer solution was poured onto the graphite fibers (which were oriented in one direction) contained in a heat sink. The heat sink consisted of a stainless steel beaker filled with sand on which rests an aluminum petri-dish containing the fibers. The oven was again evacuated for about three minutes; the vacuum was removed, and an inert atmosphere of nitrogen passed into the oven. At 170°C polymerization did not occur even after four hours. However, on increasing the oven temperature to 200°C , polymerization occurred within one hour and the polymer crystallized out. Raising the temperature probably melted low molecular weight polymer which had formed and allowed complete polymerization to occur.

The composite is now in the process of being studied by electron microscopy and x-ray diffraction techniques. Slices less than 1000 Å thick have been microtomed prior to examination. Preliminary inspection of the slices using an optical microscope shows the complete absence of voids, thus confirming our initial hypothesis.

As a next stage in this work, composites will be made using other latent catalysts which may prove suitable and which have a higher fiber content than the approximate 20% fiber content obtained in the first composite.

C. Crystallization and Reaction on Graphite-Like Fiber Surfaces
(Professor Lando and Mr. P. D. Frayer, Case)

1. Introduction

Many reactions in the solid state have been shown to proceed by a topotactic mechanism (5-8), i.e., the molecular orientation of the product can be correlated with the molecular orientations in the reactant crystal. Epitaxial or oriented crystallization of a material on a crystalline substrate has also been demonstrated many times (9-11). In this phenomenon the crystallography of the two substances can be correlated by lattice matching (12); however, oriented crystallization of organic materials can occur on crystalline substrates without this matching (11, 13). In our work the possible correlation of topotaxy with epitaxy was investigated. We have studied the deposition of crystalline monomers on graphite-like fiber surfaces ("Thornel" 40 fibers) followed by reaction on the solid state. The specific interaction of the carbon fiber substrate with the deposited crystalline monomers was found to affect the solid state reaction, determining not only the reaction products but also their conformation. This investigation has given information about the carbon fiber surface which is in agreement with recent studies on graphitic materials. The ultimate aim of this work is to make unique polymer-carbon fiber composites.

2. Results

The deposition and reaction of two crystalline monomers will be discussed in detail. The two monomers are hexamethylenediammonium adipate (HMDA) ($T_m=197^\circ\text{C}.$) and 6-aminocaproic acid (ACA) ($T_m=210^\circ\text{C}.$) which are the monomers of nylon 66 and nylon 6, respectively. The substrate on which the monomers are crystallized is "Thornel" 40 graphite fibers which had been washed in boiling water. Materials were crystallized from methanol and water solutions. The deposited monomers were reacted at temperatures from 50°C to 100°C with HCl gas as a catalyst and above 100°C without a catalyst.

The following tools were used to study the deposition and the subsequent solid state reaction: wide angle x-ray (Debye-Scherrer powder camera using Cr K_α radiation and Weissenberg camera using Cu K_α radiation),

infrared spectroscopy (Perkin-Elmer model 521 Infrared Spectrophotometer), and differential thermal analysis (Du Pont model 900 Differential Thermal Analyzer).

Figure 8 shows an x-ray pattern of a bundle of "Thornel" graphite fibers. The graphite-like crystal planes and the edges of these planes are aligned along the carbon fiber axis. HMDA was found to crystallize epitaxially (i.e. oriented) on the graphite fiber as shown in the x-ray pattern on Figure 9. The HMDA was crystallized from methanol solution at room temperature. The (201) reciprocal lattice direction of HMDA is aligned along the carbon fiber axis. The \bar{b} -axis of HMDA is perpendicular to the carbon fiber axis. Weissenberg photographs have shown the \bar{b} -axis of HMDA to be randomly oriented around the carbon fiber (which is cylindrically symmetric). Figure 10 gives the projection of the HMDA molecules onto the ab-plane from the crystal structure determination of Brown (14).

The solid state polymerization of HMDA has been studied in detail (15). It was found that complete conversion to polymer could be obtained by heating single crystals of HMDA at 160°C for 24 hours, but there was no observed preferred direction of polymerization. For reaction temperatures below 145°C the reaction yielded partially oriented polymer. No reaction occurred below 120°C unless a catalyst was used. HMDA crystals in an HCl gas atmosphere reacted by a topotactic mechanism at temperatures as low as 70°C. The material obtained was found to be polymer (nylon 66) and some linear oligomer. Kinetic studies showed the reaction to be surface nucleated (15).

The solid state reaction at 75°C in HCl gas of HMDA which is crystallized on the carbon fibers is topotactic as shown in the x-ray pattern of Figure 11. However, the reaction does not yield either polymer or linear oligomer, as it would in the absence of the substrate, but does yield a cyclic dimer of HMDA. The polymerization reaction rate (absence of substrate) is much slower than the dimer reaction rate (presence of substrate). Thus, the cyclic dimer is also obtained at higher reaction temperatures (100-110°C) without HCl gas. Presumably, the surface interaction between the substrate and the epitaxially crystallized monomer must be strong enough to control the topotactic reaction. Since we are only now in the process of determining

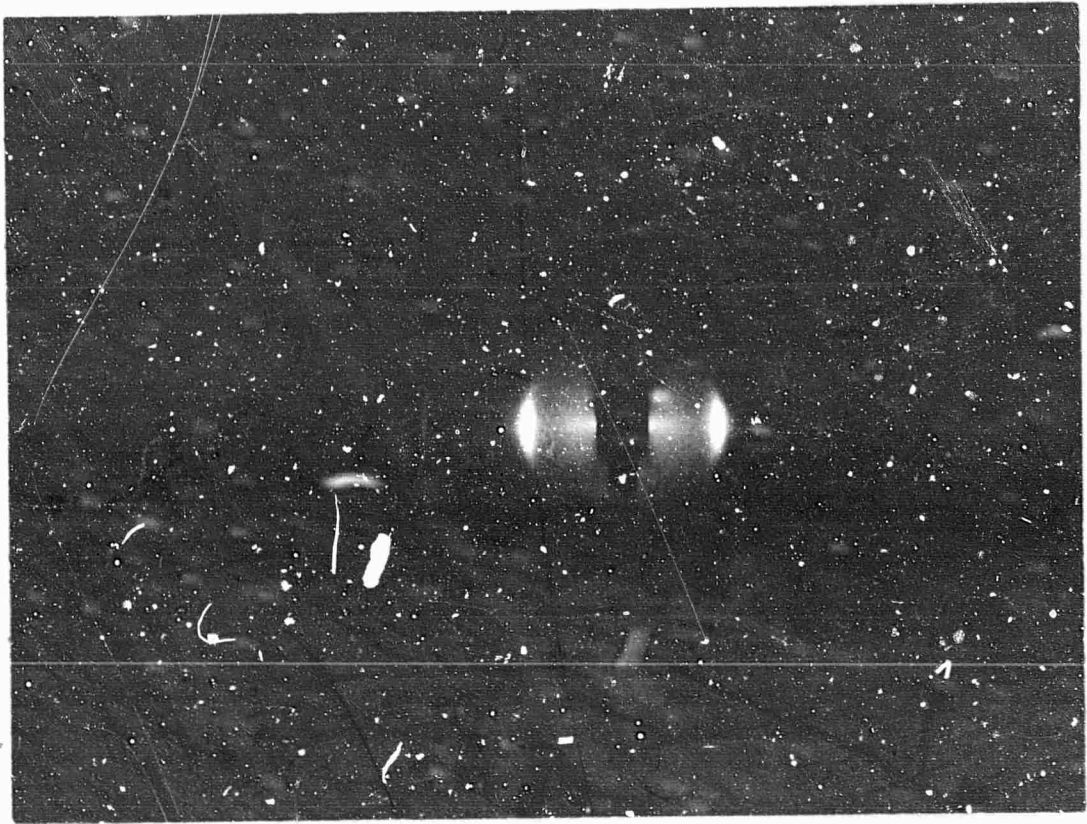


Figure 8. X-ray Pattern of a Bundle of "Thornel" 40 Carbon Fibers.

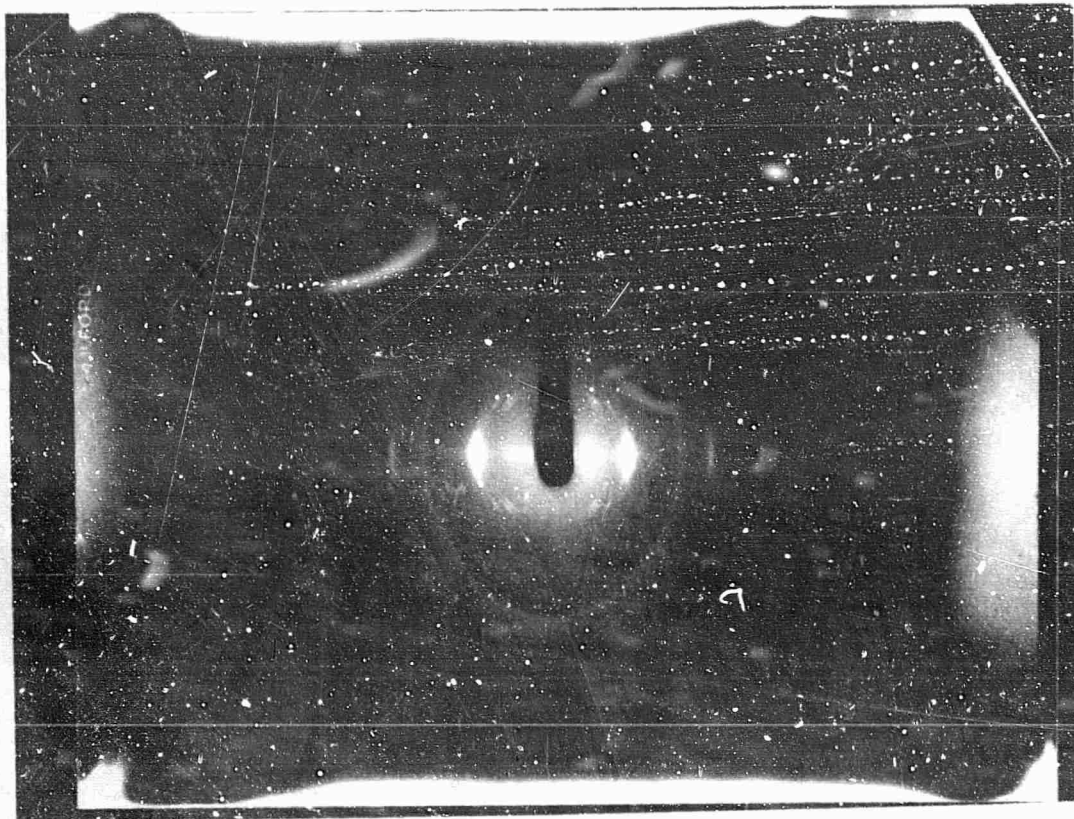


Figure 9. X-ray Pattern of HMDA Epitaxially Crystallized on the Carbon Fibers.

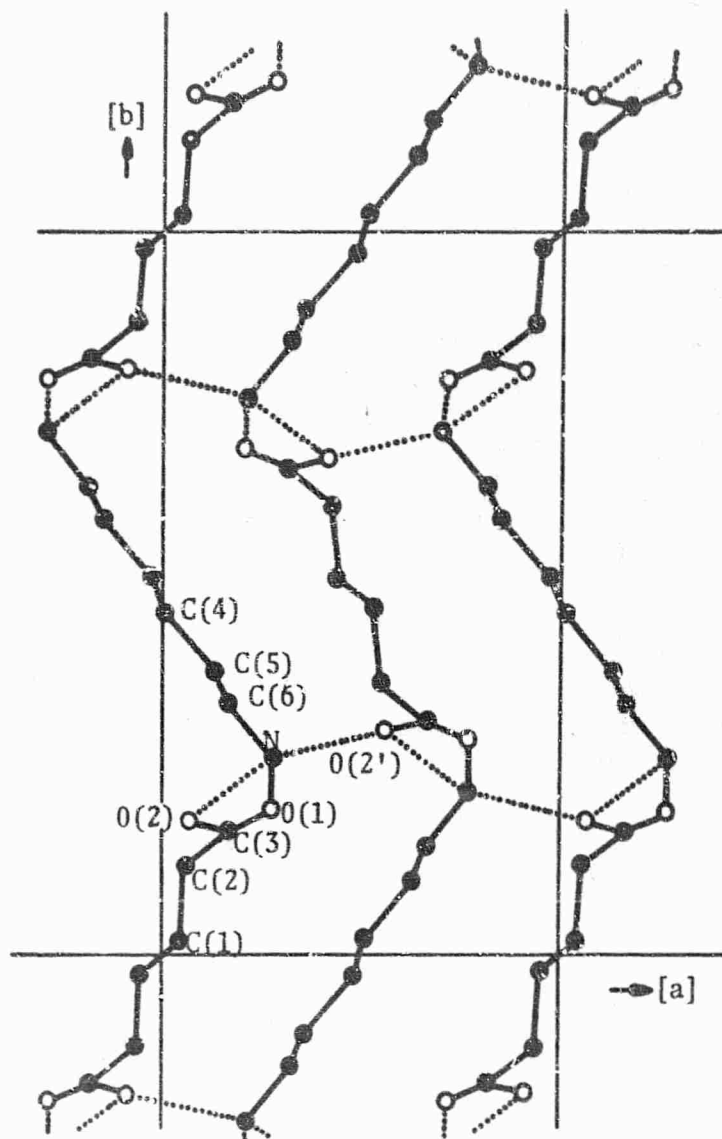


FIGURE 10. The ab -Plane Projection of the HMDA Molecules (Brown(8)).

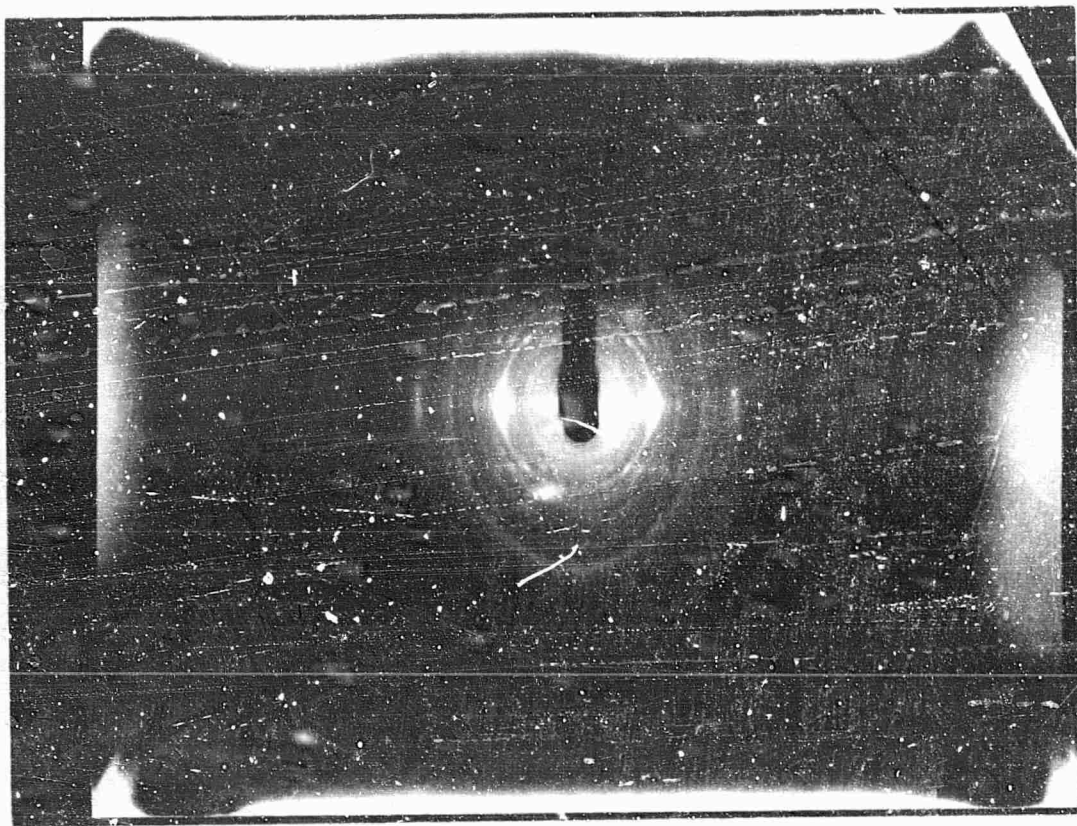


Figure 11. X-ray Pattern of the HMDA Reacted in the Solid State at 75°C with HCl Catalyst to Form Cyclic Dimer.

crystal structure of the cyclic dimer, the correlation of the monomer molecular orientation with that of the cyclic dimer has not been determined unequivocally. Zahn *et al.* (16) have reported that the cyclic dimer has a monoclinic unit cell $a=10.78$ A, $b=25.12$ A, $c=9.67$ A, and $\beta=92^{\circ}22'$. Based upon these data it was determined that the (201) reciprocal lattice direction of the cyclic dimer is aligned along the carbon fiber axis. When the dimer was deposited on the carbon fibers from methanol solution, it crystallized epitaxially with the same preferred orientation as the dimer formed in the solid state reaction on the carbon fiber surface. Therefore, the surface interaction between the substrate and the dimer must be specific and strong.

Figure 12 shows an x-ray pattern of monoclinic 6-aminocaproic acid (ACA) which has been crystallized epitaxially on the "Thornel"40 fibers. The crystal structure has been reported (17), and the topotactic polymerization to nylon 6 has been described (8). This reaction may also be surface nucleated. It was found that the (103) reciprocal lattice direction of ACA crystallizes with a preferred orientation along the fiber axis. The \bar{b} -axis of ACA is found to be perpendicular to and randomly oriented around the carbon fiber axis. The ACA was crystallized from water at room temperature by evaporation.

The solid state reaction is again topotactic and does not yield either polymer or linear oligomer, but does yield a cyclic trimer of ACA. The x-ray data obtained from the solid state prepared trimer on the carbon fibers (53°C and HCl catalyst), shown in Figure 13, was found to match the Debye-Scherrer data of Hermanns (18). Hermanns' original paper called this material a " β -cyclic dimer," but Rothe *et al.* (19) corrected the molecular weight determination and found it to be a cyclic trimer. Again one must postulate a strong surface interaction to explain these results.

The IR spectra of the cyclic materials were compared with the spectra of their corresponding polymers. Many similarities were observed. The spectra of the cyclic dimer of IMDA contains bands found in nylon 66 which have been assigned to the conformation of the fold in that polymer (20). These bands are absent in the linear oligomers of nylon 66. The cyclic dimer can be isolated from the commercial polymer by extraction (21). This extracted dimer has been found to be of a different form than the solid state

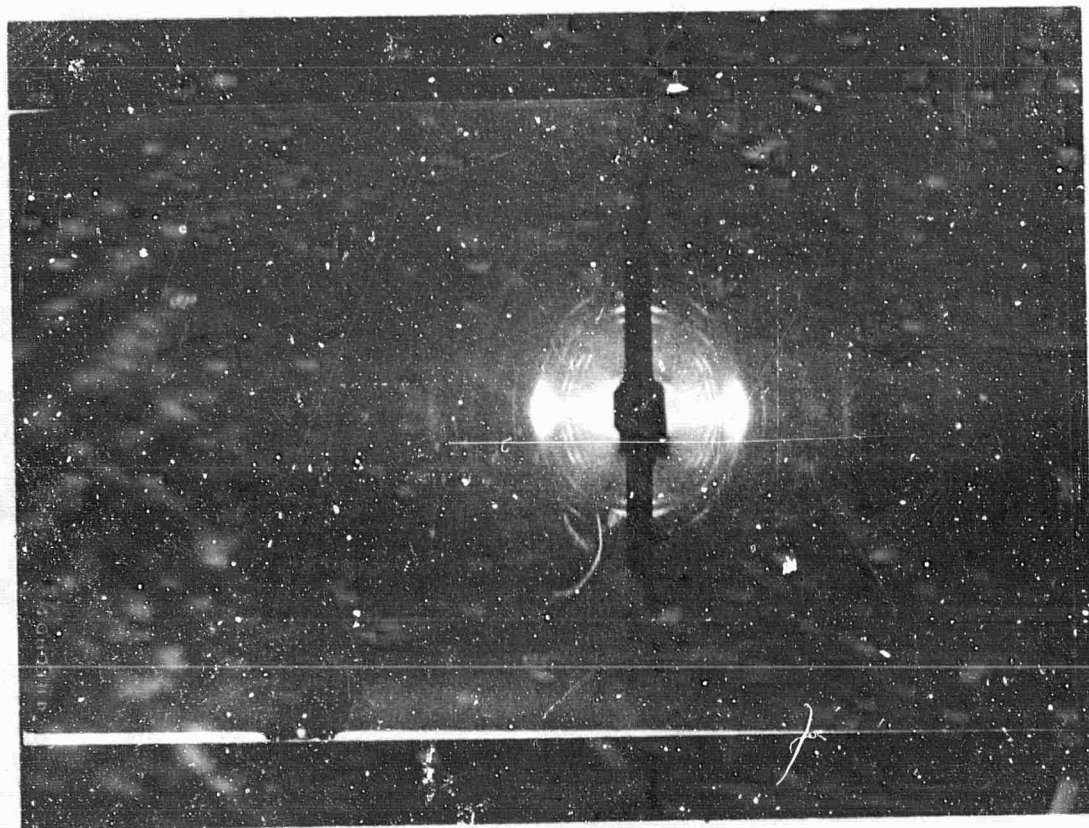


Figure 12. X-ray Pattern of ACA Epitaxially Crystallized on the Carbon Fibers.

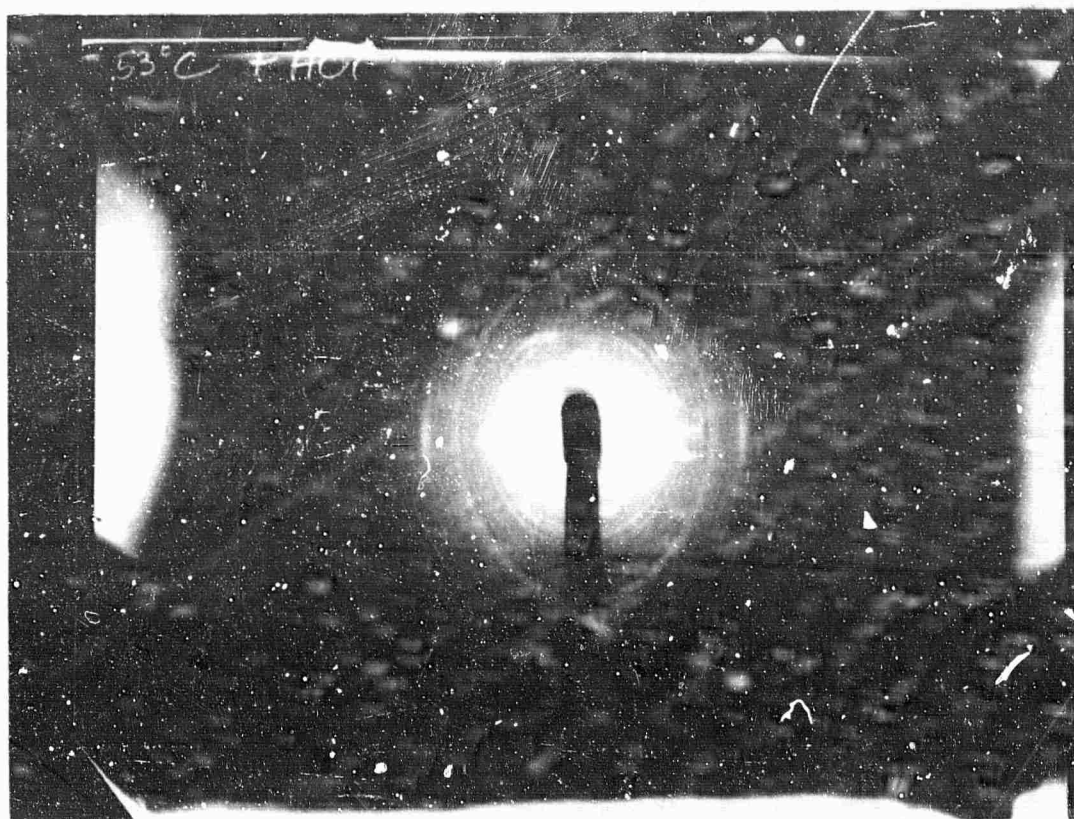


Figure 13. X-ray Pattern of ACA Reacted in the Solid State at 53°C with HCl Catalyst to Form Cyclic Trimer.

prepared cyclic dimer as observed by IR and DTA. Figure 14 shows the IR spectra of the cyclic dimer isolated by extraction (A) and prepared in the solid state on the carbon fiber surface, (B). The extracted dimer is seen to have the 1224 cm^{-1} band whereas the solid state prepared dimer does not. When the solid state dimer was dissolved and recrystallized from water under the same conditions as the extracted dimer was crystallized, the IR spectra were identical. Thus, a conformational difference involving a centrosymmetric and concentrosymmetric dimer has been proposed (22). The carbon fiber surface not only controls the nature of the product and its orientation in the solid state reaction of IMDA but also the conformation of the resulting dimer.

The carbon fibers have been found to affect both the crystallization and the reaction of two monomers. The oriented crystallization suggests some interesting features about the carbon fiber surface which are in complete agreement with recent studies on graphitic materials. Coughlin *et al.* (23) and other researchers in the field of absorption from solution onto various carbons have shown that the "free valences" at the edges of the graphite planes are reactive and form surface compounds or functional groups, while foreign atoms or molecules are only weakly absorbed on the basal planes. Ruland *et al.* (24) have studied the interstitial compounds of potassium with "Thornel" carbon fibers, and also electron diffraction by these fibers (25). Their work indicates that the graphite-like layers stack in groups of about ten. A cross-sectional view of a carbon fiber would reveal these stacks of layers to be randomly arranged with respect to one another; however, the edges of the layers are preferentially aligned along the axis of the carbon fiber. This morphology is apparent from Figure 8 which shows that only (00 λ) planes of graphite are oriented. The present work suggests further that the monomers are attracted to various functional groups on these layer edges of the graphite-like planes, crystallizing with a preferred orientation along the carbon fiber axis in order to maximize the monomer-substrate interaction. If crystallization occurred on the basal faces of single crystals, one would expect three preferred directions of growth due to the hexagonal symmetry. If crystallization occurred on the basal faces of the carbon fibers, one would expect no preferred directions of growth because these faces are randomly oriented. Tuinstra (26) in our

FIGURE 14A IR Spectra of the Cyclic Dimer Isolated from the Polymer by Extraction

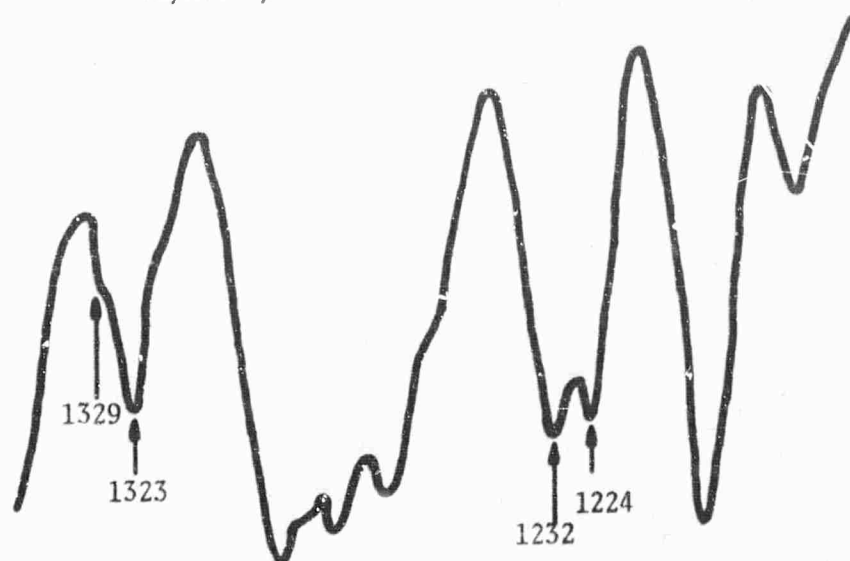
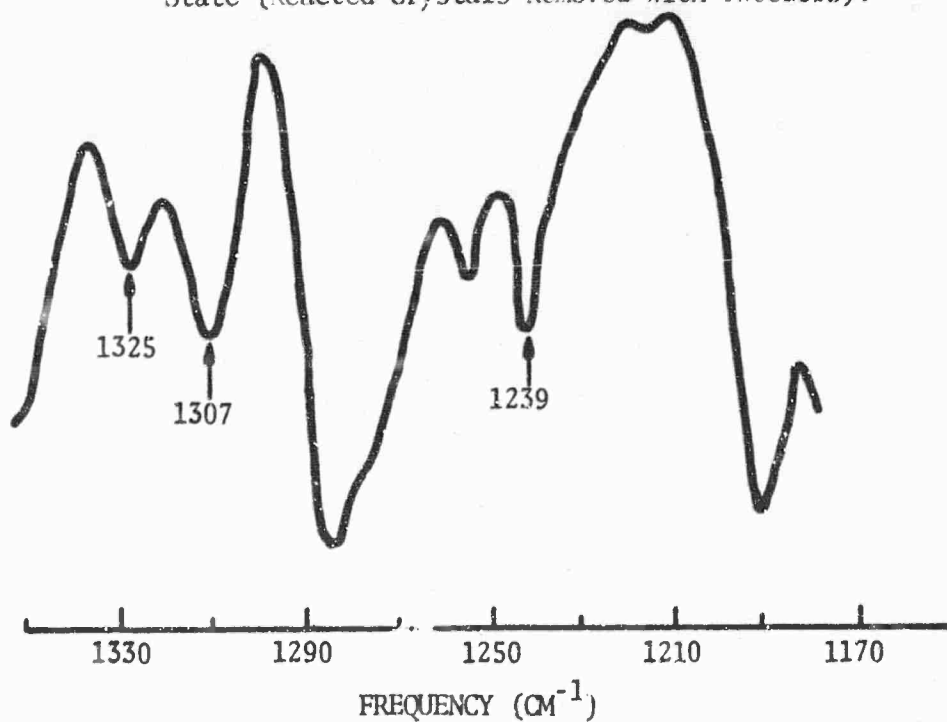


FIGURE 14B IR Spectra of the Cyclic Dimer Prepared in the Solid State (Reacted Crystals Removed with Tweezers).



laboratories has, as expected, obtained three preferred directions of crystallization of polyethylene on the basal faces of graphite single crystals.

The results obtained on the crystallization and reaction of HMDA and ACA strongly suggest that a relationship exists between epitaxial crystallization and topotactic reaction. The substrate influence on the reaction can be explained by assuming that part of the driving force of a topotactic reaction is the oriented crystallization of the product on remaining reactant. In the case of a surface nucleated reaction, the crystallization of the product on the substrate provides part of the driving force. Thereafter, crystallization of the dimer on itself provides the reason for continued reaction to the dimer.

3. Future Plans

Evidence in the literature suggests that the cyclic oligomers of nylons can be reacted to form high polymer although the process may be an equilibrium reaction (27). This polymerization is being investigated. In particular, the effects of temperature, hydrogen bonding vapors, and decreased pressure will be investigated.

In addition to the two monomers which have been described in detail, other monomers are being studied. One is 4-aminobutyric acid, the precursor to forming nylon 4, another aliphatic polyamide. Three other monomers which can form polyamides with exceptional thermal properties are p-aminobenzoic acid (PABA), hexamethylenediammonium terephthalate (HMDT), and 1,4-aminomethylcyclohexanecarboxylic acid. Successful epitaxial deposition has been obtained for PABA and HMDT. The solid state reactions have not been investigated previously, and we are now studying these reactions. Because the aromatic molecules are stiffer, it is proposed that these monomers may polymerize rather than cyclize on the carbon fiber surface.

SECTION IV
ADSORPTION, WETTABILITY, AND ADHESION IN
FIBER REINFORCED COMPOSITES

Professor Fort, Dr. R. J. Nash, and Mr. S. C. Sharma, Case

The weakest part of most fiber reinforced composite structures is the interface between the fiber and the polymer matrix which surrounds it. Maximum (theoretical) joint strength is seldom, if ever, achieved. Reasons for failure may be poor contact of one phase with another (poor wetting), weak boundary layers, stresses set up on solidification of the adhesive, or poor attraction of adhesive to adherend. All these failure mechanisms are controlled by the surface character of the materials in contact. Knowledge of this surface character is necessary for systematic optimization of fiber-polymer matrix adhesion and composite strength.

The objectives of this research are to: (1) characterize the surface area, surface chemistry and surface roughness of selected, high strength, thermally stable fibers; (2) relate these surface properties to fiber wettability, bulk morphology, and adhesion; (3) optimize fiber reinforced composite performance through use of the information obtained. Present work is concerned with fiber surface characterization through measurements of adsorption from the gas phase and from solution.

A. Gas Adsorption Studies

A well-established method for determining surface properties is to study the interaction of the surface with various gases. A solid sample, when weighed in a gaseous atmosphere at various pressures, will increase in weight as the gas pressure is increased. The weight increase is caused by the adsorption of gas molecules onto the surface of the sample. Knowing the weight of one molecule, the number of adsorbed molecules can be calculated. The relationship between the number of gas molecules adsorbed and the gas pressure, at various temperatures, yields information about the nature and energetics of the surface; e.g., whether the surface is porous or nonporous, and whether it is energetically uniform or contains areas of high and low energy.

It is planned to use gravimetric gas adsorption measurements to characterize the surface properties of carbon fibers. A system is being constructed which will allow these measurements to be carried out. Carbon fibers have a small surface area and, consequently, adsorb only small quantities of gas molecules. To measure the small weight increase produced by such limited adsorption it is necessary to employ a highly sensitive balance. Our design incorporates a Cahn Electrobalance which is capable of detecting a weight change of 1×10^{-6} grams in a 1-gram sample.

To make meaningful measurements it is necessary to install the balance in a system free from contaminating vapors. These vapors include those from the grease used to lubricate conventional vacuum valves, the oil used in vacuum pumps, and the mercury used in manometers and diffusion pumps. Our design is completely free of these contaminants. A Vac Sorb pump evacuates the system to 10^{-3} torr by adsorbing gas molecules onto molecular sieve at -196°C . A Vac Ion pump removes gas molecules from the system by burying them under evaporated layers of titanium. The vacuum taps are of all metal construction. The apparatus is made of stainless steel and Pyrex glass and can be baked out to 250°C during initial evacuation.

A mercury manometer, read by a cathetometer, is the most accurate pressure measuring device for the pressure range to be used in the present study. A spiral gauge will be used to keep the system free of mercury vapor. A specially designed cryostat will be used to maintain the carbon filament sample at constant temperature.

B. Solution Adsorption Studies

The interactions at the interface in a fiber-reinforced composite may be closely modeled by the interactions between a fiber surface and a molecule adsorbed from solution in a nonreactive solvent. Solution adsorption studies are, therefore, a useful way of characterizing a fiber surface. A difficulty is that, because of the low (ca. $1 \text{ m}^2/\text{g}$.) specific surface of the fibers, classical techniques cannot be used to develop adsorption isotherms.

However, our preliminary experiments indicate that frontal analysis liquid chromatography can give reliable quantitative information about adsorption on fiber surfaces. Using this technique, the amount adsorbed can be calculated from a knowledge of the dead space volume, the retention volume, and the concentration of the solution stream contacting the fibers which act as the adsorbing surface in the chromatograph.

Figure 16 shows a flow diagram of a liquid chromatographic apparatus now under construction. The system may be operated isothermally over a range of temperatures and pressures. It may also be heated and evacuated for cleaning purposes between experiments.

The chromatographic column contains graphite fibers wound in a spiral fashion around a glass or metal rod. This method of packing should result in a uniform and reproducible column. Application of pressure may be necessary to avoid unduly long solution retention times. Dead volume will be determined by using radioactively labelled solvent. Composition of the effluent stream will be monitored with a continuous recording differential refractometer.

First experiments will involve adsorption of long chain fatty acids from their solutions in hydrocarbon solvents. The purpose is both to obtain data and to test the new chromatographic system. Fatty acid adsorption onto carbon powders has been previously studied, and the known adsorption isotherms will serve as a reference point for this work. Investigation of the adsorption of low molecular weight polymers which closely model polymer matrices used in fiber reinforced composites will then be initiated. Measurements will be made at different temperatures using solutions of varying composition. From the resulting data, the nature and distribution of active sites on the fiber surfaces will be determined.

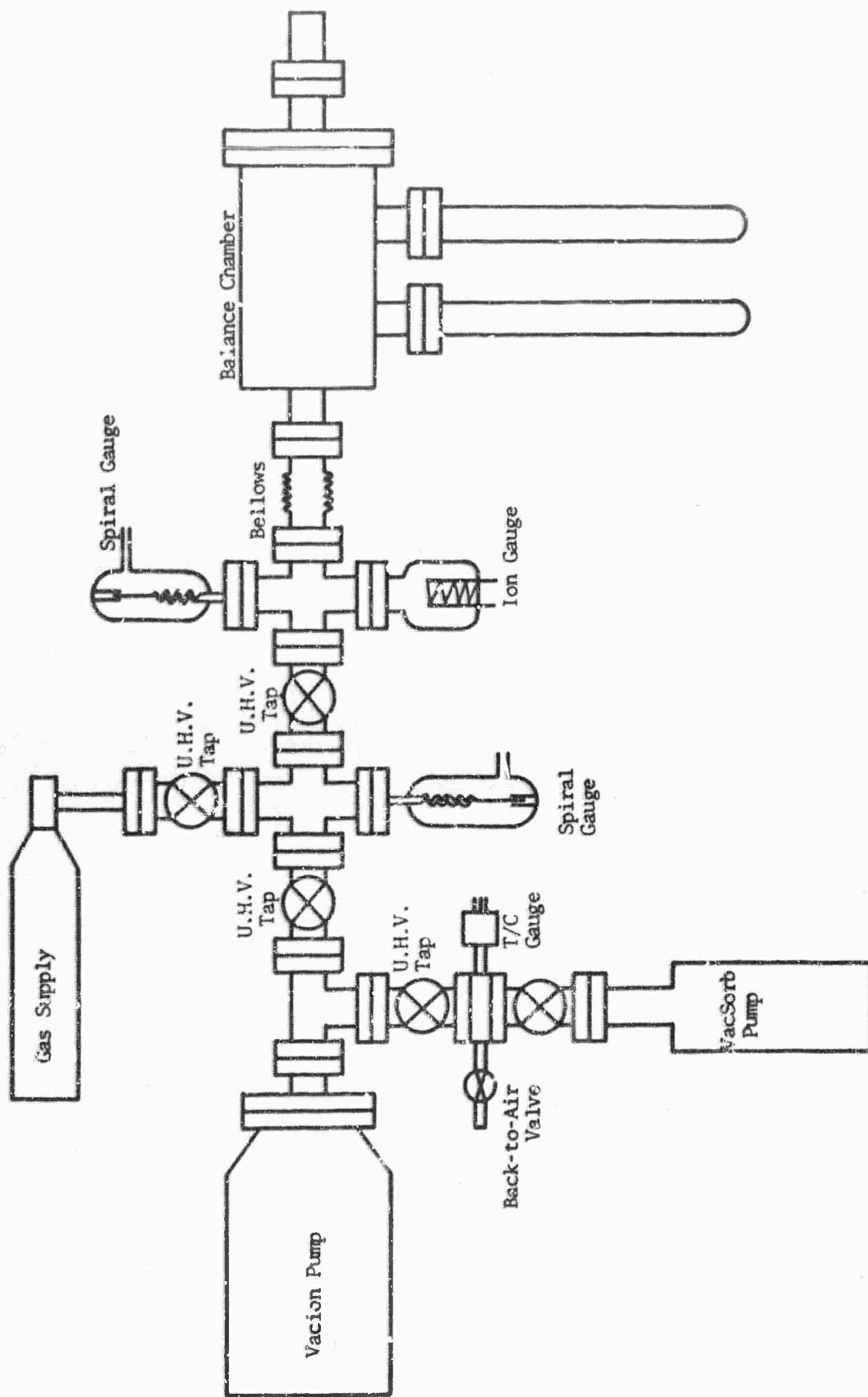


Figure 15. Gravimetric Gas Adsorption Apparatus.

LEGEND

- 1 Solvent reservoir
- 2 Solution reservoir
- 3.4 Positive displacement pumps
- 5.6 Debubblers
- 7.8 Pulse dampers
- 9.10 Heat exchangers
- 11.12 Pressure gauges
- 13 Chromatographic column
- 14 Flow meter
- 15 Detector (LDC refractometer)
- 16 Recorder

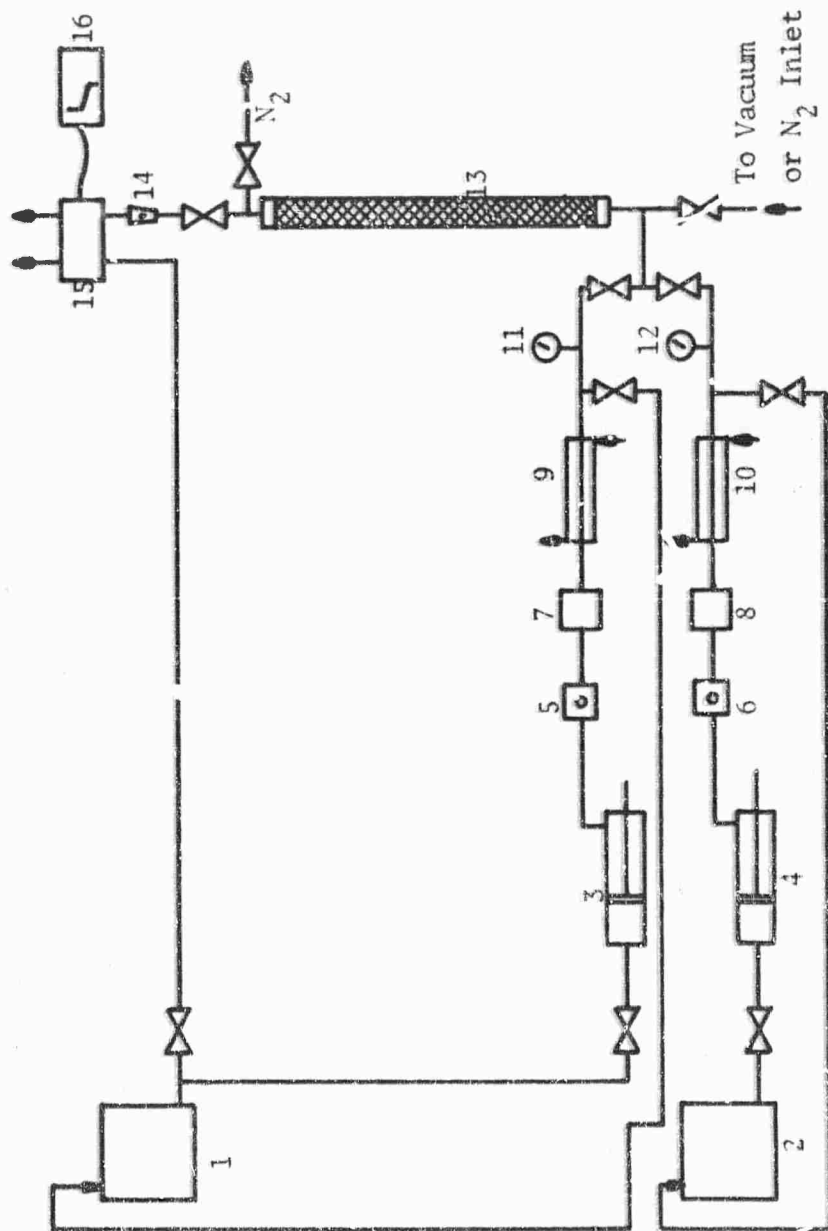


FIGURE 16. Liquid Chromatograph

SECTION V

RESEARCH ON GRAPHITE-FIBER, METAL-MATRIX COMPOSITES

R. V. Sara, Union Carbide

A. Electrodeposition of Nickel on Graphite Yarn

The system for the continuous electrodeposition of nickel on "Thornel" graphite yarn has been described in Section III of the Third Annual Report,⁽³⁾ together with certain problems which prevented the output of large quantities of plated yarn. Several changes were made in that process for the specific purposes of increasing the production rate of plated yarn and for curtailing fiber breakage. The latter could not be related specifically to the plating process because broken filaments were also detected in the uncoated yarn. As a precaution, however, all guidance devices for the yarn with small radii of curvature were replaced with large radii configurations.

Attempts were made to increase the nickel deposition rate by increasing the plating current; this was done by applying the current simultaneously to both ends of yarn. This procedure resulted in improved deposition rates but photomicrographs showed some inhomogeneity in the nickel distribution. A more uniform deposition of nickel around the filaments is achieved if cathodic contact is employed only at the first feed roller over the plating bath, a result that confirms earlier observations.

The production rate of plated yarn was increased two-fold by doubling the number of plies which are processed simultaneously. This arrangement required that the yarn be untwisted prior to storing on the feed spools, a slight modification from earlier procedures. Suitable guides were designed to keep the strands in close proximity to each other without overlapping. The four-ply plated yarn is a coherent, ribbon-like product similar to, but approximately twice as wide, as the previous two-ply plated yarn. Approximately 1500 feet of four-ply yarn have been

plated with this revised process for subsequent use in fabrication of test plates. The yarn used throughout these metal-matrix studies was "Thornel" 50 graphite yarn. The volume content of nickel electrodeposited on the yarn corresponded to 43-46 percent.

B. Fabrication of Test Specimens

Several varieties of plate-like shapes were prepared for test purposes but in each instance hot pressing was employed to compress the nickel-coated yarns into dense composites. All specimens measuring more than one inch in length were prepared in a furnace having good (10^{-5} torr) vacuum capability whereas the one-inch specimens were pressed in a vacuum of approximately 20 micron pressure. Virtually all hot pressing was done at a temperature of 1050°C for one hour, except for one series of one-inch specimens. The latter were prepared at 1250°C as part of the fabrication studies program. The pressures employed varied from 2000 to 3500 psi. The lower range of pressures was used to press $1/16 \times 1/2 \times 3$ inch bars; all others were pressed at 3000 to 3500 psi.

C. Elastic Properties of Unidirectional Graphite-Fiber, Nickel-Matrix Composite

Previous studies of the elastic properties of graphite-fiber, nickel-matrix were concerned primarily with sonic measurements of the Young's modulus. This property was studied in conjunction with fabrication processing variables. In addition, the measured Young's modulus in composites with varying fiber contents was correlated with rule-of-mixture predictions. The sonic procedure for determining modulus was also adapted to off-axis specimens. A significant factor which emerged from these evaluations is that the measured modulus of elasticity was significantly lower from values predicted at all test angles. For example, 39×10^6 psi was calculated for E in a 45 v/o fiber composite. The measured values, however, invariably fall within the limits of $32 - 35 \times 10^6$ psi.

A similar difference was observed in off-axis specimens. In an effort to rationalize these differences, the elastic measurements and related experiments which are presented in subsequent sections were conducted with this problem in mind.

1. Elastic Stiffnesses of Graphite-Fiber,
Nickel-Matrix Composite

A unidirectional block measuring 0.066 x 0.562 x 0.835 inch was fabricated for measurement of stiffness constants by ultrasonic methods. The test specimen was prepared by hot-pressing six 1/16-inch thick uniaxial plates stacked together. The composite was theoretically dense and contained 44 v/o "Thornel" graphite fibers having a 50×10^6 psi modulus of elasticity. The procedure adopted for determining elastic constants by velocity measurements was described previously in Section III of the Third Annual Report.⁽³⁾ A larger specimen was employed at this time in order that the scope and accuracy of these measurements could be increased.

The elastic stiffness matrix for an orthotropic material is the following:

$$c_{ij} = \begin{vmatrix} c_{11} & c_{12} & c_{13} & 0 & 0 & 0 \\ & c_{22} & c_{23} & 0 & 0 & 0 \\ & & c_{33} & 0 & 0 & 0 \\ & & & c_{44} & 0 & 0 \\ & & & & c_{55} & 0 \\ & & & & & c_{66} \end{vmatrix}$$

The lower half of the matrices is not indicated since c_{ij} is symmetric. The subscript 1 corresponds to the fiber direction.

Values obtained experimentally for a number of the matrix components are shown in Table II.

The similarities between c_{22} and c_{33} and between c_{55} and c_{66} indicate that the 2-3 plane is isotropic; the stiffness matrix becomes

$$c_{ij} = \begin{array}{cccccc} c_{11} & c_{12} & c_{12} & 0 & 0 & 0 \\ & c_{22} & c_{23} & 0 & 0 & 0 \\ & & c_{22} & 0 & 0 & 0 \\ & & (c_{22}-c_{23})/2 & 0 & 0 & 0 \\ & & & & c_{55} & 0 \\ & & & & & c_{55} \end{array}$$

It is evident from Table II and the preceding matrix that three of the five independent stiffness constants have been determined. In order to determine values for c_{12} and c_{23} , ultrasonic velocities must be measured at 45° to the fiber direction. An attempt will be made to measure these velocities after appropriate changes have been made in the specimen geometry.

TABLE II
ELASTIC STIFFNESS CONSTANTS OBTAINED FOR GRAPHITE-FIBER,
NICKEL-MATRIX COMPOSITES BY ULTRASONIC VELOCITY MEASUREMENTS

c_{ij}	10^6 psi
c_{11}	34.1
c_{22}	8.19
c_{33}	8.20
c_{44}	2.17
c_{55}	5.05
c_{66}	5.01

The c_{ij} 's shown in Table II are not in complete agreement with earlier data. In particular, c_{22} is significantly larger and c_{55} is smaller than previously determined values. As a result of these changes, the latter is in better agreement with 4.5×10^6 psi determined for $1/s_{55}$ by sonic methods. Although the relation between c_{22} and $1/s_{22}$ is complicated by a coupling term involving the three Poisson's ratios, the stiffness constant c_{22} is generally only slightly greater than $1/s_{22}$. The status at present is that $c_{22} = 8.20 \times 10^6$ psi and $1/s_{22} = 5.0 \times 10^6$ psi.

Similarly, c_{11} cannot be equated directly to $1/s_{11}$, but the two values in this instance compare favorably: 34.1×10^6 psi and 33.4×10^6 psi for c_{11} and $1/s_{11}$, respectively.

2. Young's Modulus Determined by Static Methods

The principal Young's moduli (engineering constants E_1 and E_2) are equivalent to the reciprocals of the compliances s_{11} and s_{22} , respectively. Representative values for these two moduli, on the basis of sonic measurements, were cited above. The elastic stiffnesses c_{11} and c_{22} define upper limits for E_1 and E_2 if the Poisson ratios are zero. These limiting values are still significantly smaller than moduli predicted for this composite system.⁽³⁾ As a final confirmation of the sonic and ultrasonic elastic measurements, it seemed advisable that E_1 , E_2 and the modulus of select off-axis specimens be determined by static methods. This procedure seemed necessary even though comparative tests made on graphite-fiber, resin matrix composites under this contract established that statically and dynamically measured moduli are similar.

The data shown in Table III are averaged results for Young's moduli measured by the sonic method and with strain gages. Two strain gages were mounted on either side of the specimen and connected in series to cancel bending moments. The minimum number of specimens, representing an average sonic value in Table III, is five and the maximum is seven. The results of five 0° specimens are averaged for the static case, three for 90° specimens, and one each with 15° and 45° fiber orientations.

The Young's modulus values obtained by sonic and static procedures are very similar as evidenced by the results in Table III. This agreement indicates that the discrepancy which exists between measured and predicted values is real and unrelated to test methods.

TABLE III
COMPARISON BETWEEN SONIC AND STATIC YOUNG'S MODULUS
IN UNIDIRECTIONAL COMPOSITES HAVING DIFFERENT FIBER ORIENTATIONS

Fiber Direction (deg)	Young's Modulus Sonic (10 ⁶ psi)	Young's Modulus Static (10 ⁶ psi)
0	32.9	33.1
15	24.2	25.5
45	10.3	9.3
90	5.0	6.0

3. Analytical Prediction of Elastic Constants

Additional consideration was given to correlating the Young's modulus of off-axis test specimens with values predicted on the basis of Whitney's model for orthotropic filaments.^(2,3) In earlier work,⁽³⁾ consideration was given principally to the effect of longitudinal, E_L , and transverse, E_T , fiber modulus on the predicted off-axis properties. Other fiber and matrix properties used in those calculations are shown in Table IV. Values of 30×10^6 psi and 0.01×10^6 psi were used for E_L and E_T in addition to other properties cited in the Table IV. In the present study, the effect of Poisson ratio, ν_{TT} (0.05 and 0.95), was found to have only minor influence on the modulus at high angles. A change in the matrix modulus, E_M , effects the composite modulus at all angles. As shown in Figure 17, agreement with composite test data is improved significantly if the matrix modulus is reduced from the accepted value of 30×10^6 psi to 17×10^6 psi. The most obvious factor which could lower the matrix modulus to this extent is porosity, a supposition which is inconsistent with metallographic observations.

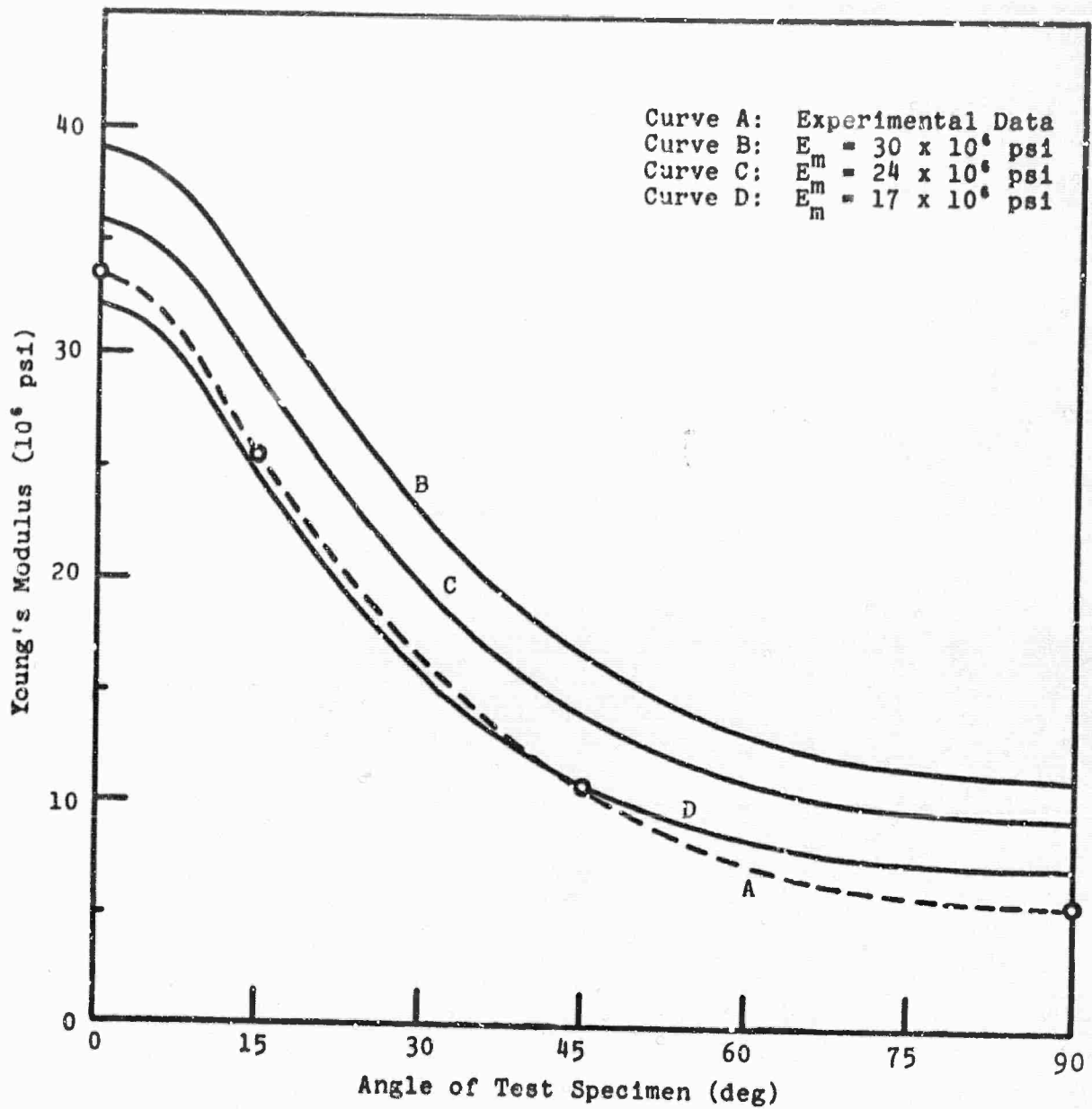
TABLE IV
FIBER AND MATRIX PROPERTIES
USED IN ANALYTICAL PREDICTIONS

Property	Matrix	"Thornel" 50
E_L	30	50
E_T		1
G_{LT}	11.5	1
ν_{LT}	.301	.25
ν_{TT}		.25

Unit: Moduli - 10^6 psi

The status of correlating the experimental Young's modulus with predicted values is that satisfactory agreement has been reached at all orientations only when a lower matrix modulus is assumed. For calculating the longitudinal modulus E_L , the "rule-of-mixtures" relationship is a good approximation. Thus, it is possible to establish agreement by reducing the fiber modulus instead of the matrix. However, when this approach is taken, the transverse Young's modulus cannot be reconciled with experimental data even though most orthotropic properties of the filament were evaluated. The exception was ν_{LT} . It is questionable that fiber parameters of reasonable magnitude exist which might improve the correlation of calculated values with experimental data.

The expression for calculating the shear modulus according to Whitney⁽²⁸⁾ is exactly the same expression as that obtained by Hashin and Rosen⁽²⁹⁾ even though orthotropic filaments were assumed. For the case of G_F and G_M equal to 1×10^8 psi and 11.5×10^6 psi respectively, analytical results are shown in Figure 18. The average experimental shear modulus, 5.2×10^6 psi, which is based on numerous sonic measurements, is in good agreement with the predicted value at 0° or 90° . The c_{55} value of 5.05×10^6 psi indicated in Table II also concurs with these results.



N-21838

Figure 17. Experimental and Predicted Variations in Young's Modulus with Test Angle for a Uniaxial Composite.

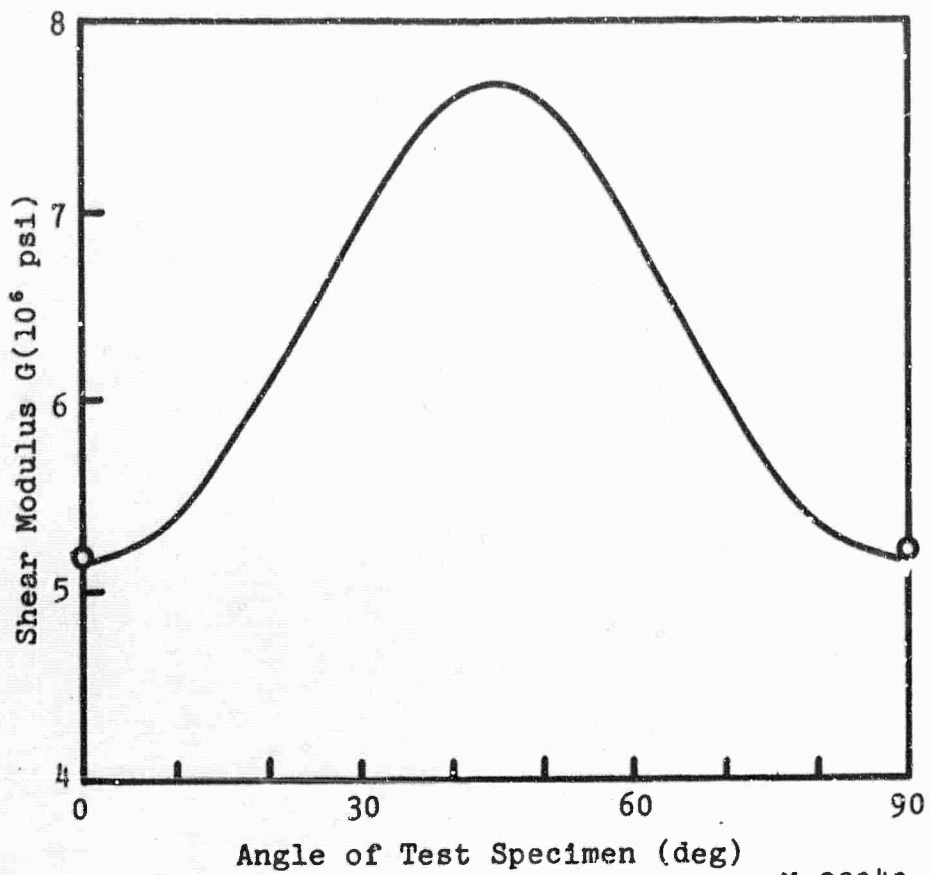


Figure 18. Experimental and Predicted Variations in Shear Modulus with Test Angle for a Uniaxial Composite.

If the matrix modulus is in fact 17×10^6 psi, according to "best fit" criteria, the shear modulus for this constituent is 6.5×10^6 psi according to the equation

$$G = \frac{E}{2(1+\nu)}$$

Accordingly, the composite shear modulus is 3.25×10^6 psi for specimen test angles of 0° or 90° . This value is significantly less than the measured 5.2×10^6 psi indicated in Figure 18. Thus, a low matrix modulus improves the agreement between calculated and experimental Young's moduli but not for the shear modulus.

The variation of Poisson's ratio, ν , with test angle is shown in Figure 19. The results are based on Whitney's expression which closely resembles a "rule-of-mixtures" relationship. Standard transformation formula was also employed. Experimental results are shown only for test angles of 0° and 90° .

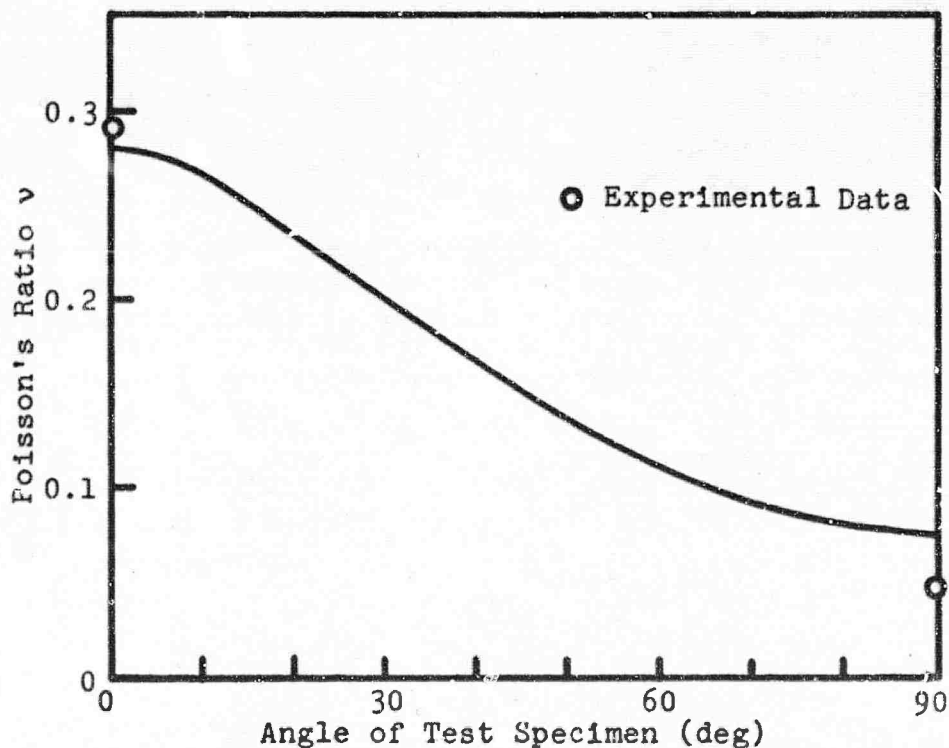


Figure 19. Experimental and Predicted Variations in Poisson's Ratio with Test Angle for a Uniaxial Composite.

N-22039

D. Composite Stress-Strain Behavior

1. Tensile Stress-Strain Behavior of Unidirectional Composites

Stress-strain data were obtained on unidirectional specimens with fiber orientations of 0°, 15°, 45° and 90° to the tensile axis. Two strain gages, one on each side of the specimen, were connected in series to cancel bending moments. The two strain gages also expedited alignment of the specimen in the Instron test instrument. Occasionally the two gages were monitored separately through the test cycle.

Stress-strain curves from two "dog-boned" specimens are shown in Figure 20. The differences are significant and reflect variations in microstructure, principally fiber alignment. Curve A is representative of early specimens which had numerous misaligned filaments whereas curve B is typical for composites currently being fabricated with untwisted yarn. It is evident from curve B that a yield point is more sharply defined and the tangent modulus of the recent composites does not decrease at the highest stress. The change in slope at 12,000 psi is associated with the elastic-plastic transition or yield point of nickel. Lower yield strengths (~6000 psi) were observed in straight-sided IITRI-type specimens. The stress-strain behavior of off-axis specimens is shown in Figure 21. The 15° specimen is capable of being deformed to an exceptional degree before failure occurs. Strain at failure for the 90° specimen is dependent on the specimen gage width to a certain extent as shown in Figure 22. Specimens with gauge sections less than 1/4 inch x 1/16 inch fail at lower stresses and appear to have slightly lower modulus of elasticity.

The 0° and 15° specimens have a secondary modulus when the yield strength of nickel is exceeded. The expression applicable to this situation is:

$$E_s = V_f E_f + (1 - V_f) \left(\frac{d\sigma_m}{d\epsilon_m} \right)$$

The term $\left(\frac{d\sigma_m}{d\epsilon_m}\right)$ applies to plastically deforming nickel but is essentially zero. Consequently, the secondary modulus expression reduces to:

$$E_s = V_f E_f.$$

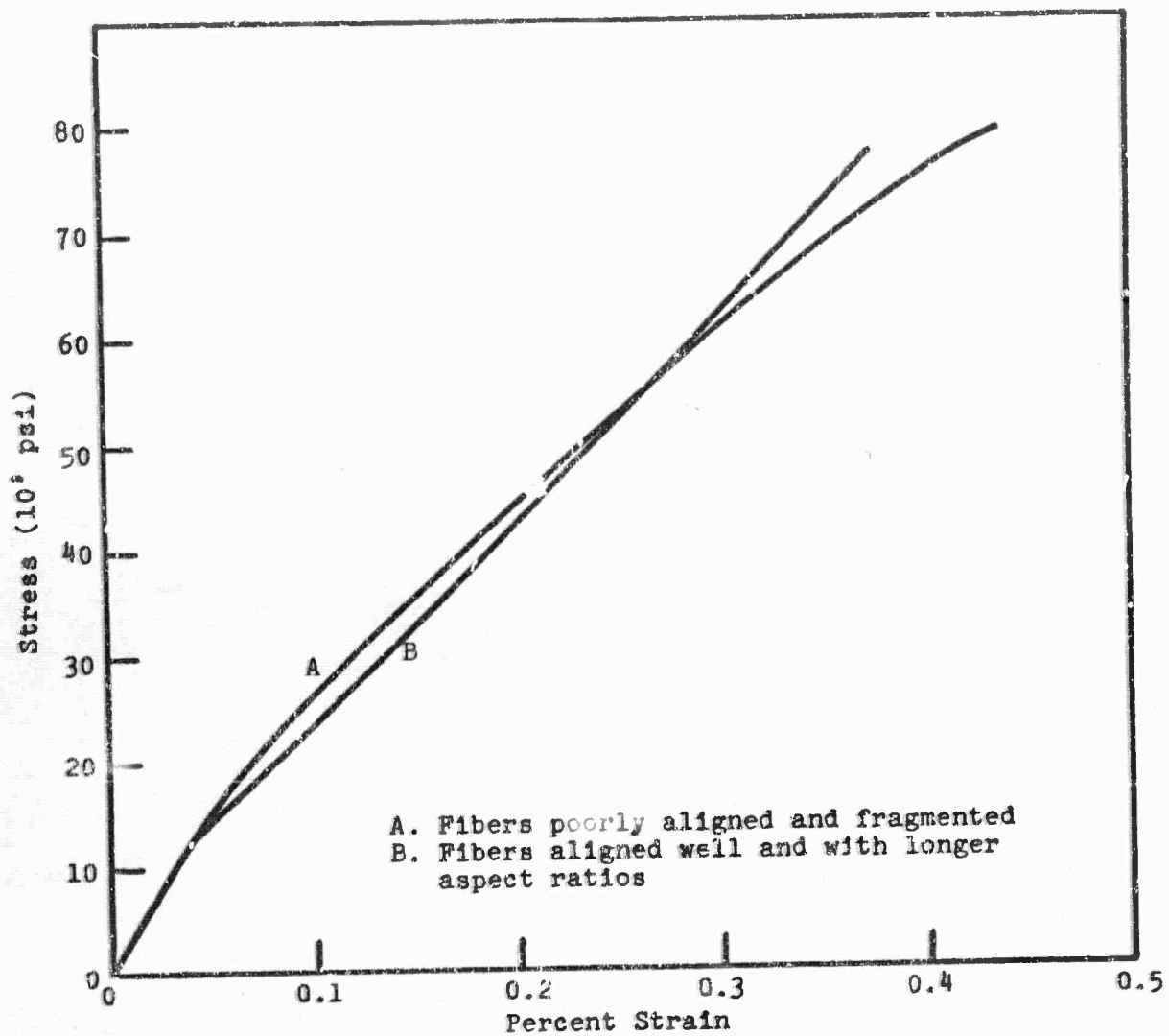
An approximate value for E_s in 0° specimens is 19×10^6 psi.

A close examination of the experimental results has shown a dependency of secondary modulus on stress. Figure 20 shows that, as stress is increased, according to curve B, the tangent modulus also increases. This non-linear behavior might be related to the unique "non-Hookean" effect observed in graphite fibers by workers at Harwell, England (³⁰). If the matrix contribution $\left(\frac{d\sigma_m}{d\epsilon_m}\right)$ to the secondary modulus is assumed to be zero,

a relationship between fiber modulus and stress exists as shown by curve A in Figure 23. The fiber modulus at lowest stress levels was calculated by rule-of-mixtures considerations by using static and dynamic composite modulus values. The results show that, at zero stress, the fiber modulus is 36.5×10^6 psi; at 160,000 psi, the fiber modulus has increased to 45.0×10^6 psi. The linear portion of the curve represents a least squares fit to the data. Curve B represents the dependency of graphite fiber modulus on applied stress as indicated by ultrasonic measurements on individual fibers.⁽³⁰⁾ The two curves show considerable parallelism and conceivably could be relating a common phenomenon. An explanation which has been advanced is that longitudinal tensile stresses increase crystallite alignment in the fibers.

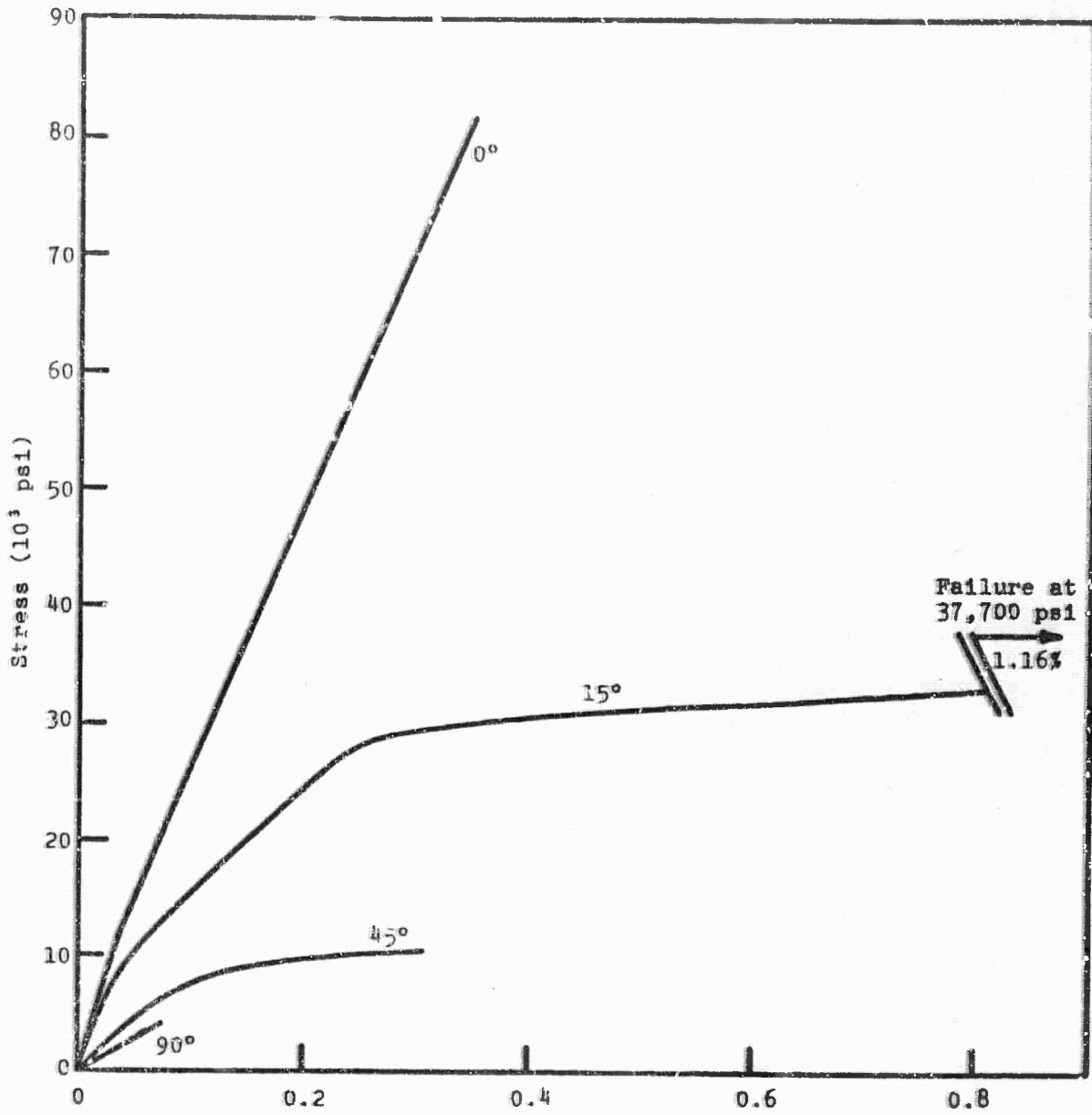
Graphite fibers having a Young's modulus of 50×10^6 psi were employed to fabricate the composites characterized by Curve A in Figure 23. According to data presented above, post fabrication measurements indicate that this property has been reduced to 36.5×10^6 psi. The decrease might be associated with a relaxation of the crystallite alignments, perhaps promoted by compressive

action of the matrix on the fiber axis during cooling from the fabrication temperature. However, indications are that a substantial portion of the modulus is recovered as the stress applied to the composite is increased.



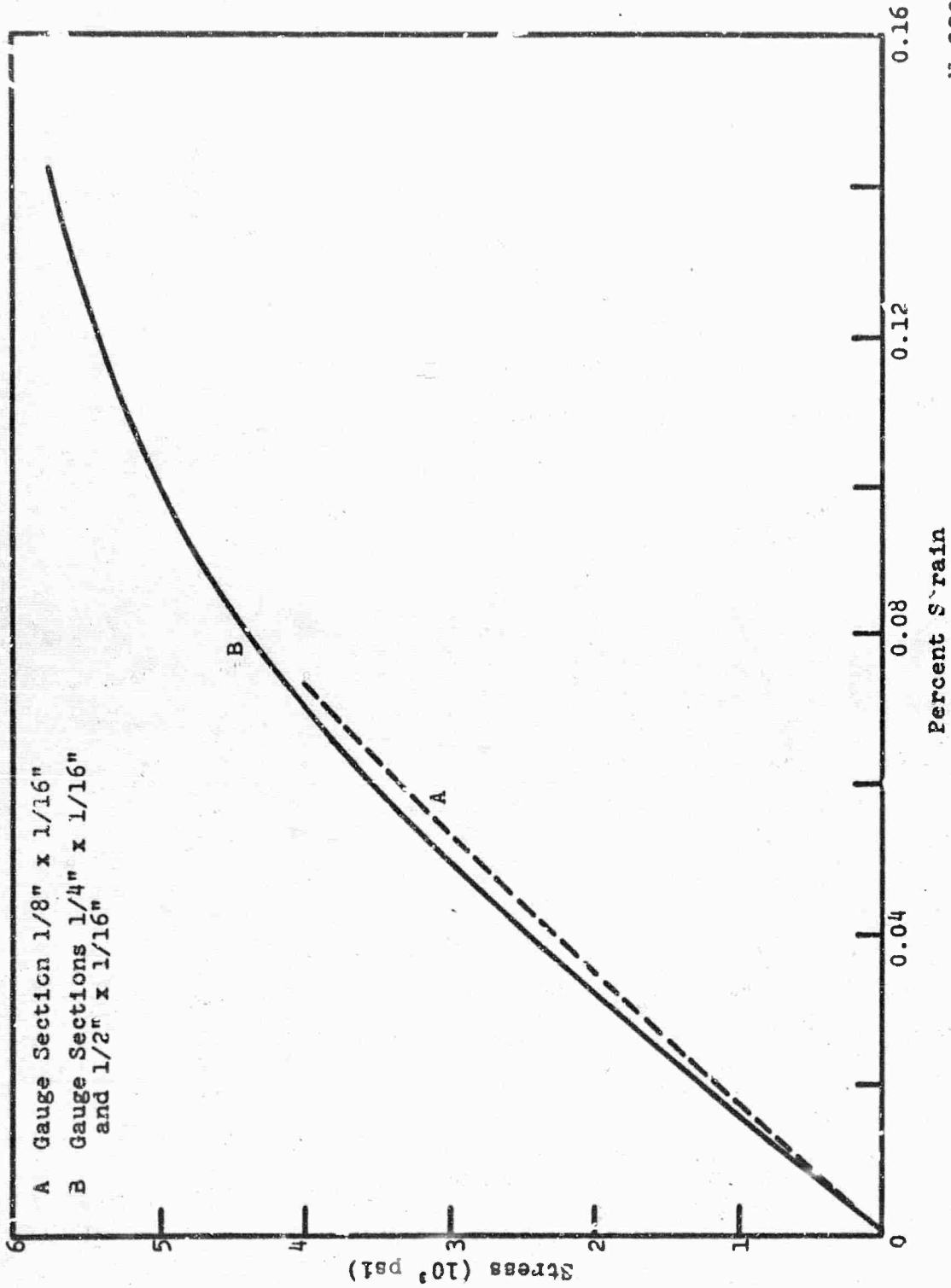
N-21834

Figure 20. Stress-Strain Behavior of Unidirectional Composites.



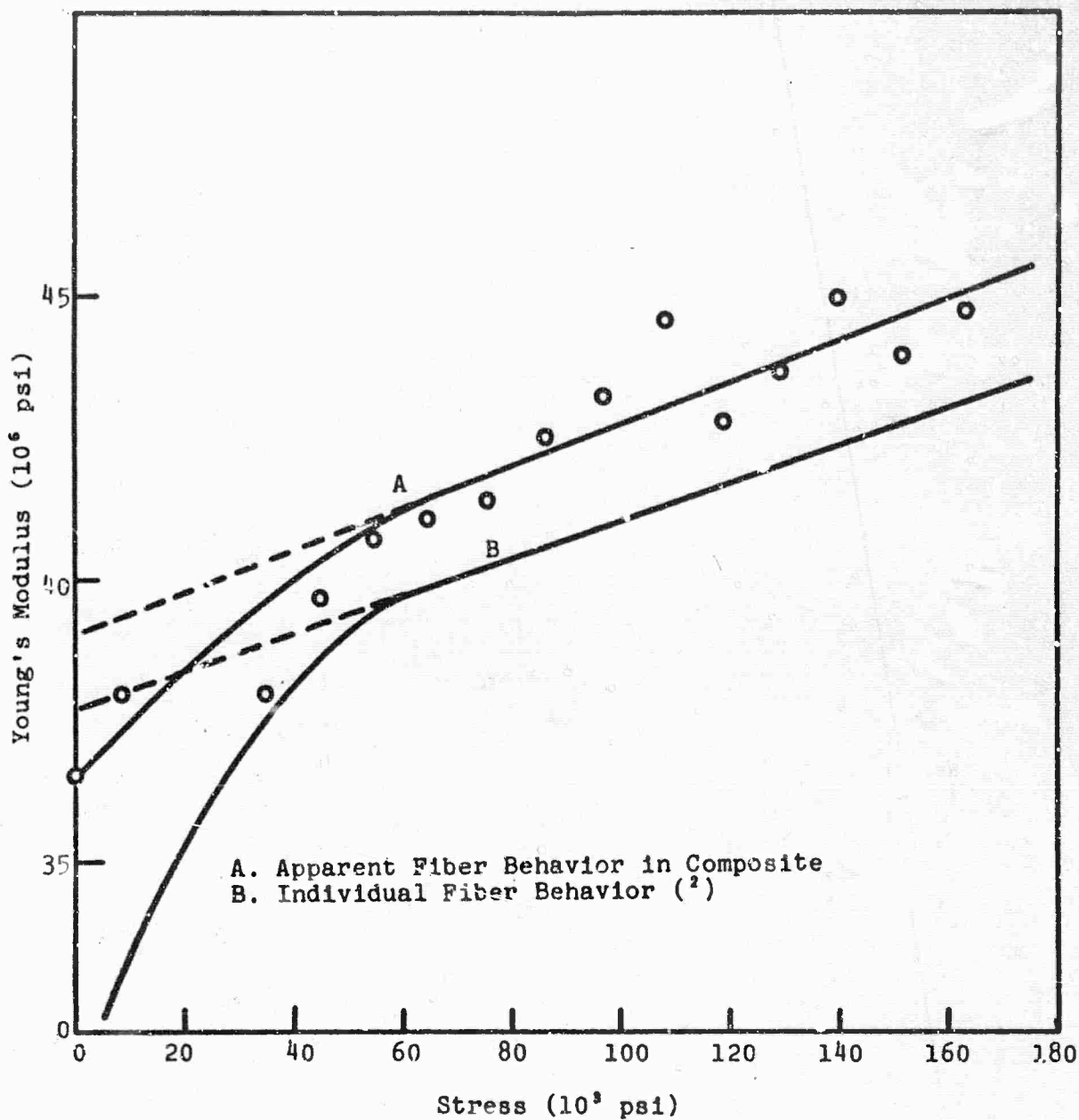
N-22038

Figure 21. Stress-Strain Curves of Unidirectional Off-Axis Test Specimens.



N-22037

Figure 22. Effect of Specimen Gauge Width on Stress-Strain Behavior of 90° Specimens.

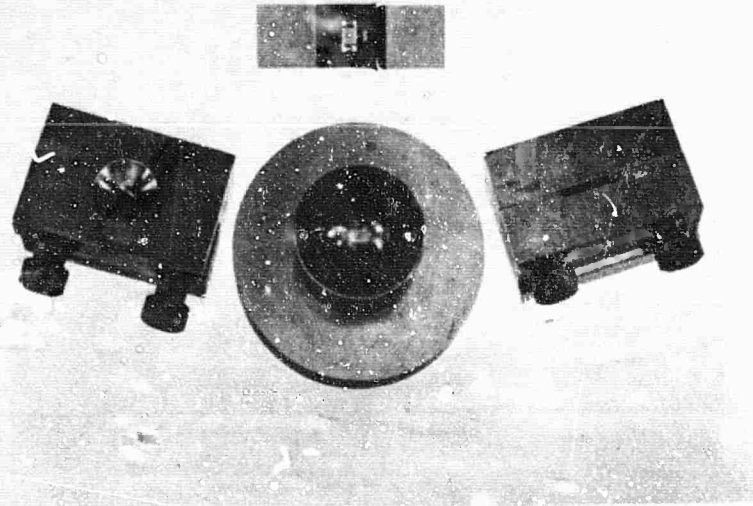


N-21830

Figure 23. Relationship Between Young's Modulus of Graphite Fibers and Applied Stress.

2. Compression Stress-Strain Behavior of Unidirectional Composites

A compression test was made on a unidirectional, straight-sided specimen having dimensions of 0.068 x 0.500 x 1.5 inches. Nickel tabs were soldered on the ends of the specimen for gripping purposes and to prevent "brooming." The gauge section was 0.500 inch square. A photograph of the test fixture and specimen are shown in Figure 24. The specimen was fitted precisely in the grip slots prior to aligning in the Instron test instrument. The latter was facilitated by the aid of two strain gages and the ball and socket feature which is evident in the photograph. The two strain gages were monitored separately during the compression test and indicated that bending was absent.



N-21983

Figure 24. Compression Specimen and Test Fixture.

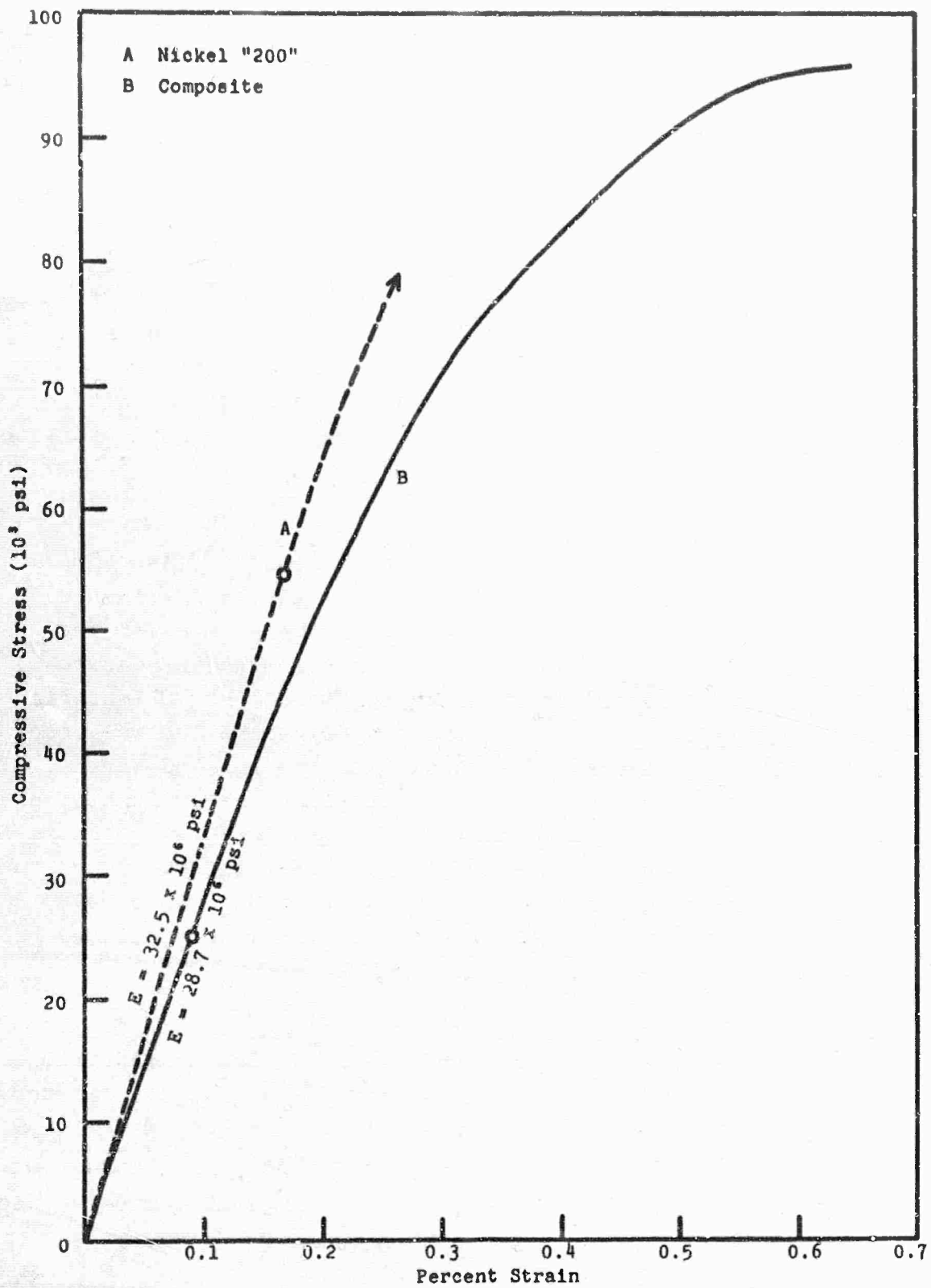
The compression stress-strain curve for nickel "200" and for a composite specimen is shown in Figure 25. The composite modulus is 28.7×10^6 psi or appreciably less than the tensile modulus of 32.2×10^6 psi. The elastic limit is noted by the circle at 25,000 psi in Figure 25. Failure in compression occurred at 95,000 psi. On the assumption that "rule-of-mixtures" prevail, the fiber modulus corresponds to 27×10^6 psi. The initial modulus in tension and compression is generally similar in graphite-fiber, resin-matrix systems but a distinct difference is observed for this metal matrix composite. The low elastic modulus for the fiber in compression might be a continuation of the trend depicted in Figure 23. Yielding of the matrix in compression is more subtle than was observed when tensile stresses were applied.

3. Poisson Ratios

Longitudinal and transverse strains were measured simultaneously in unidirectional composites as the specimens were stressed in tension. Specimens with fibers parallel and perpendicular to the applied load were used for these measurements. Data for a composite with longitudinal fiber orientation are shown in Figure 26; similar stress-strain behavior was noted in composites with fibers perpendicular to the applied stress. The increasing tangent modulus and yield point are evident in both stress-strain curves. The major Poisson's ratio, ν_{12} , which is the ratio of the transverse to longitudinal strain, was found to be 0.29. The Poisson's ratio ν_{21} was determined to be 0.049. Both values were discussed previously in connection with predicted values shown in Figure 19.

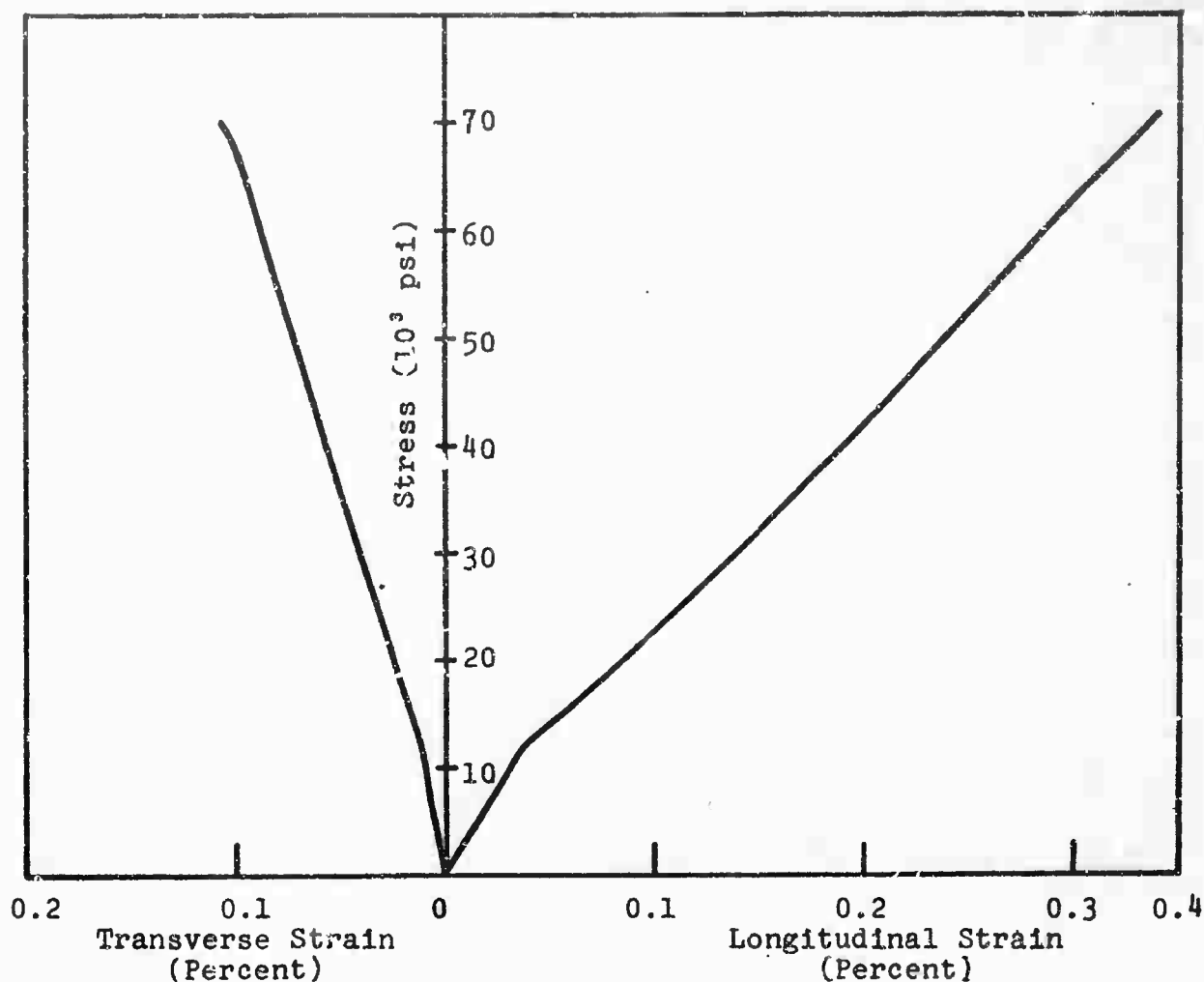
4. Strain Cycling

The deformation of a composite as it is subjected to cycles of loading and unloading is an important design parameter, for if the procedure is repeated sufficiently, the culmination will be failure by fatigue. Recently Mehan⁽³¹⁾ observed a "ratcheting" effect (progressive length increase) in an Al_2O_3/Al composite when sufficiently high stress limits were employed in the cycles.



N-22036

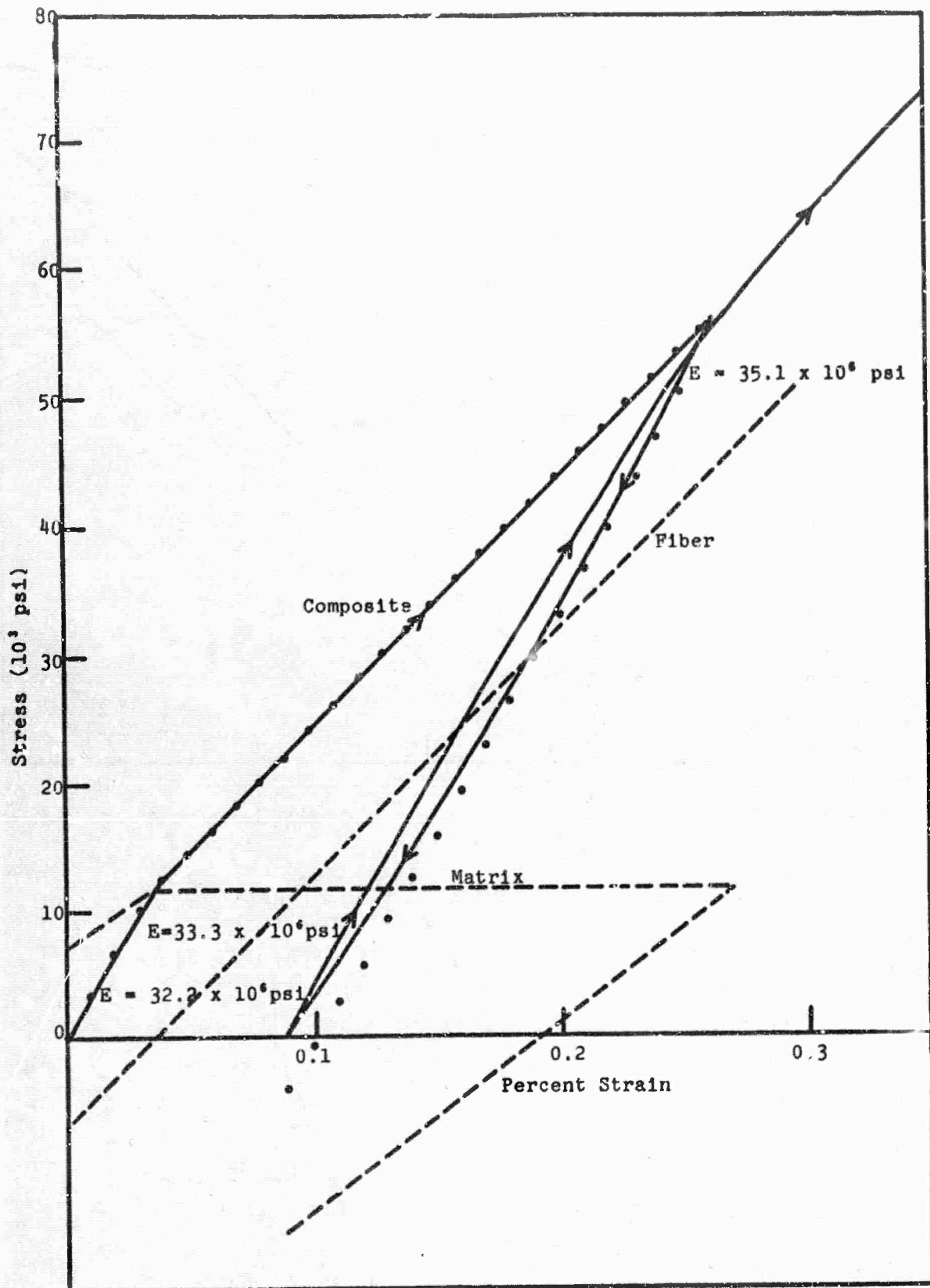
Figure 25. Stress-Strain Behavior of Nickel and Graphite-Fiber, Nickel-Matrix Composite in Compression.



N-21831

Figure 26. Stress-Strain Curves for Unidirectional Composite.

Deformation processes such as these are not completely understood. However, the basic stages of deformation encountered during limited cycles of loading and unloading when the composite contains constituents that are elastically incompatible has been appropriately described by McDanel.⁽³²⁾ A single cycle experiment similar to McDanel is shown in Figure 27. The solid curve indicates that the specimen was stressed to 55,000 psi, unloaded to essentially zero stress and reloaded until failure occurred at 77,000 psi. Failure was out of the gauge area for this and four other comparable three-inch long specimens at an average stress of 77,000 psi.



N-22035

Figure 27. Cyclic Behavior of Constituents and Composite.

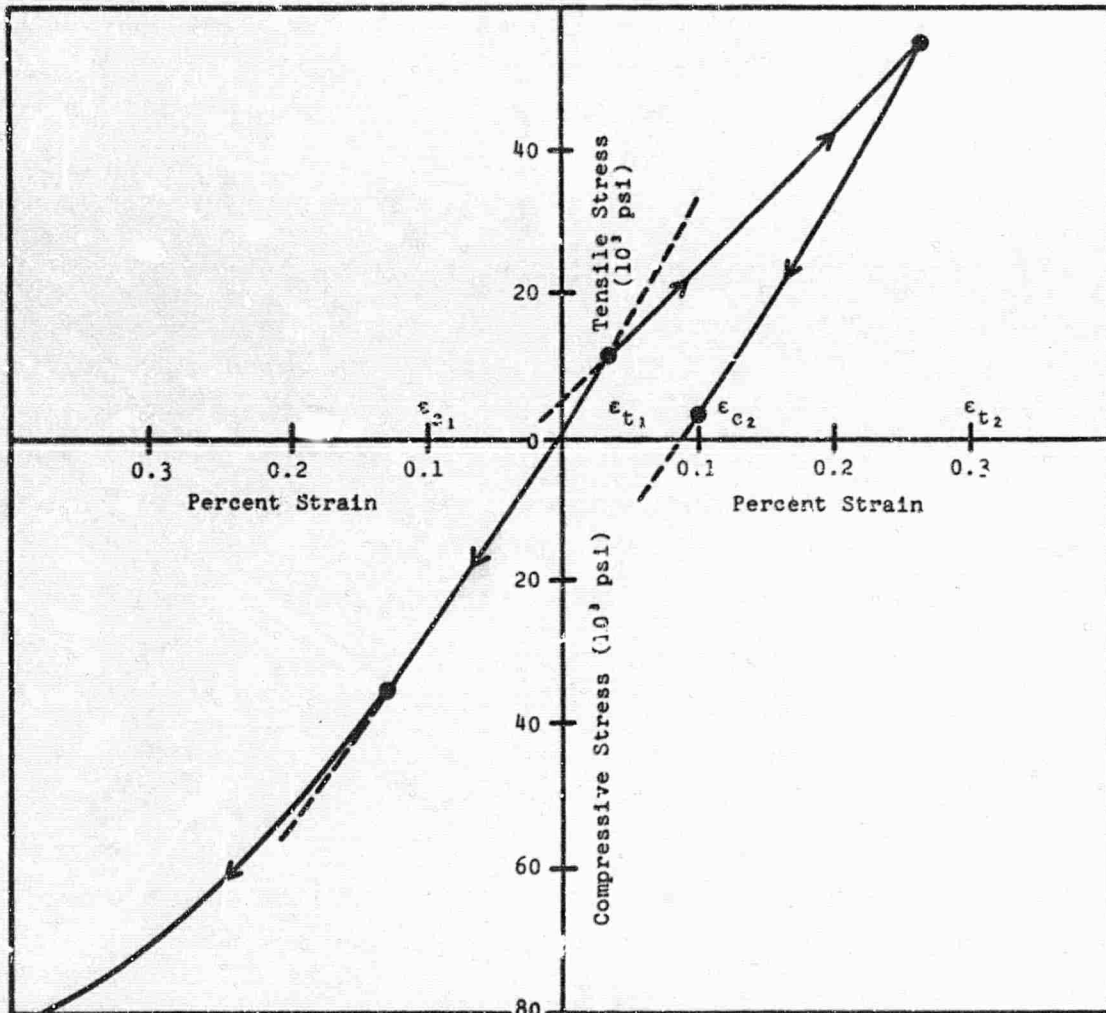
According to Figure 27, when the applied stress exceeds 12,000 psi, the yield strength is exceeded and plastic deformation of the nickel takes place. Because of plastic deformation, the stress-strain curve is not retraced when the stress is reduced from 55,000 psi. Permanent deformation corresponds to 0.09 percent. When the load is released at 55,000 psi, the initial contraction is elastic as evidenced by a slope that is similar to the initial elastic modulus. As the unloading continues, a change in slope is evident in the curve which has been associated with a secondary elastic behavior. This feature is not clear in Figure 27 for the tangent modulus is still much greater than 19×10^6 psi indicated for E_s in Section V D-1. In this secondary portion of the unloading curve, the fibers cause plastic deformation of the matrix in compression. Reloading of the composite again is elastic in behavior but then the matrix deforms plastically under the tensile forces, the prevailing condition before unloading was initiated.

The generalized constituent behavior according to the preceding discussion is depicted in Figure 27 as the dashed curves. The load values, σV , which apply are based on a volume fraction, V , of 50 percent. The result of summing the two constituent curves according to the "rule-of-mixtures" is the dotted stress-strain curve. It is evident that the summation agrees well with the measured stress-strain curve through the loading and unloading cycle. The subtle differences which are present are due to fiber content (46 instead of 50 percent) and overly simplified versions of matrix and fiber stress-strain curves.

A low axial thermal expansion of the fiber and high thermal expansion of the matrix creates tensile stresses in the matrix and compressive stresses in the fiber on cooling from the fabrication temperature. An approximation of residual stresses resulting from the mismatch in thermal expansion is possible on the basis of the following expression:

$$\sigma_0 = \left(\frac{\epsilon_t + \epsilon_c}{2} - \epsilon_t \right) E_m.$$

The above expression is valid only to the extent that the matrix, in the absence of reinforcing fibers, has a yield strength which is similar in either tension or compression. "Break away" points are identified in Figure 28 which are believed to be associated with the transition from elastic to plastic deformation of the matrix. On the basis of the identified tensile (ϵ_t) and compression (ϵ_c) strains in Figure 23, the residual stress, σ_0 , is determined to be 14,000 psi. The residual stresses depicted in Figure 27 for the constituents are based on the 14,000 psi value.



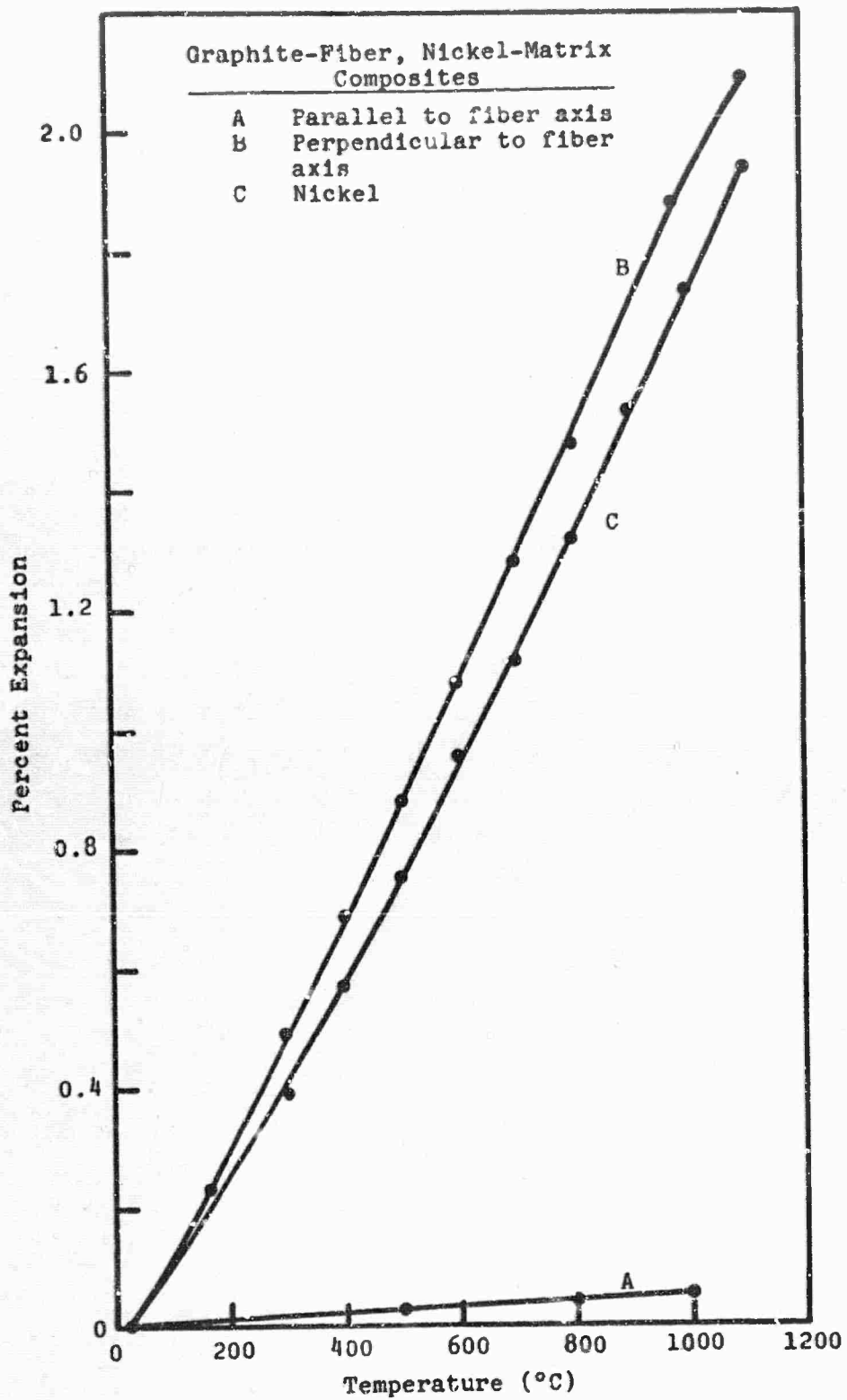
N-22034

Figure 28. Tension-Compression "Breakaway" Points in Unidirectional Composite.

E. Thermal Expansion of Graphite-Fiber, Nickel-Matrix Composite

The linear thermal expansion of unidirectional graphite fiber nickel-matrix composites was determined between room temperature and approximately 1050°C. The composite was measured in the longitudinal and transverse directions. Specimens used for this study had dimensions of 3 x 1/2 x 1/16 inch and contained 46 volume percent fibers. The specimens were heated in a graphite tube furnace in a helium atmosphere to prevent oxidation. Expansion and contraction were monitored with precision micrometer telescopes. The thermal expansion of nickel was also measured and found to agree favorably with published results.⁽³³⁾

The thermal expansion of the composite parallel and perpendicular to the fiber axis and for pure nickel is shown in Figure 29. Between 25° and 1000°C, the unidirectional composite is characterized by expansion coefficients of $0.5 \times 10^{-6}/^{\circ}\text{C}$ and $20 \times 10^{-6}/^{\circ}\text{C}$ in the longitudinal and transverse directions, respectively. In the same temperature interval, nickel has an expansion coefficient of $17 \times 10^{-6}/^{\circ}\text{C}$. These results show that the composite expansion is highly anisotropic and is controlled by the thermal behavior of the graphite fiber. Although the "Thornel" yarn is polycrystalline, the crystallites are preferentially aligned with their "a" axes parallel to the longitudinal axis of the fiber; the crystallite "c" axes are perpendicular to the fiber axis. The thermal expansion coefficient of single crystal graphite⁽³⁴⁾ in the "c" direction varies from $27 \times 10^{-6}/^{\circ}\text{C}$ at room temperature to approximately $30 \times 10^{-6}/^{\circ}\text{C}$ at 1000°C. The "a" axis expansion coefficient is much less than the "c" axis expansivity; for example, between 0° and 150°C, $\alpha = -1.5 \times 10^{-6}/^{\circ}\text{C}$; at approximately 400°C, $\alpha = 0$; and between 600° and 800°C, $\alpha = 0.9 \times 10^{-6}/^{\circ}\text{C}$. The longitudinal expansion of "Thornel" graphite fibers was found to be essentially the same as the "a" direction expansion of single crystal graphite.⁽³⁵⁾ Although the thermal expansion perpendicular to the fiber axis has not been measured, it is presumed to be similar to the "c" axis of graphite.



N-21209

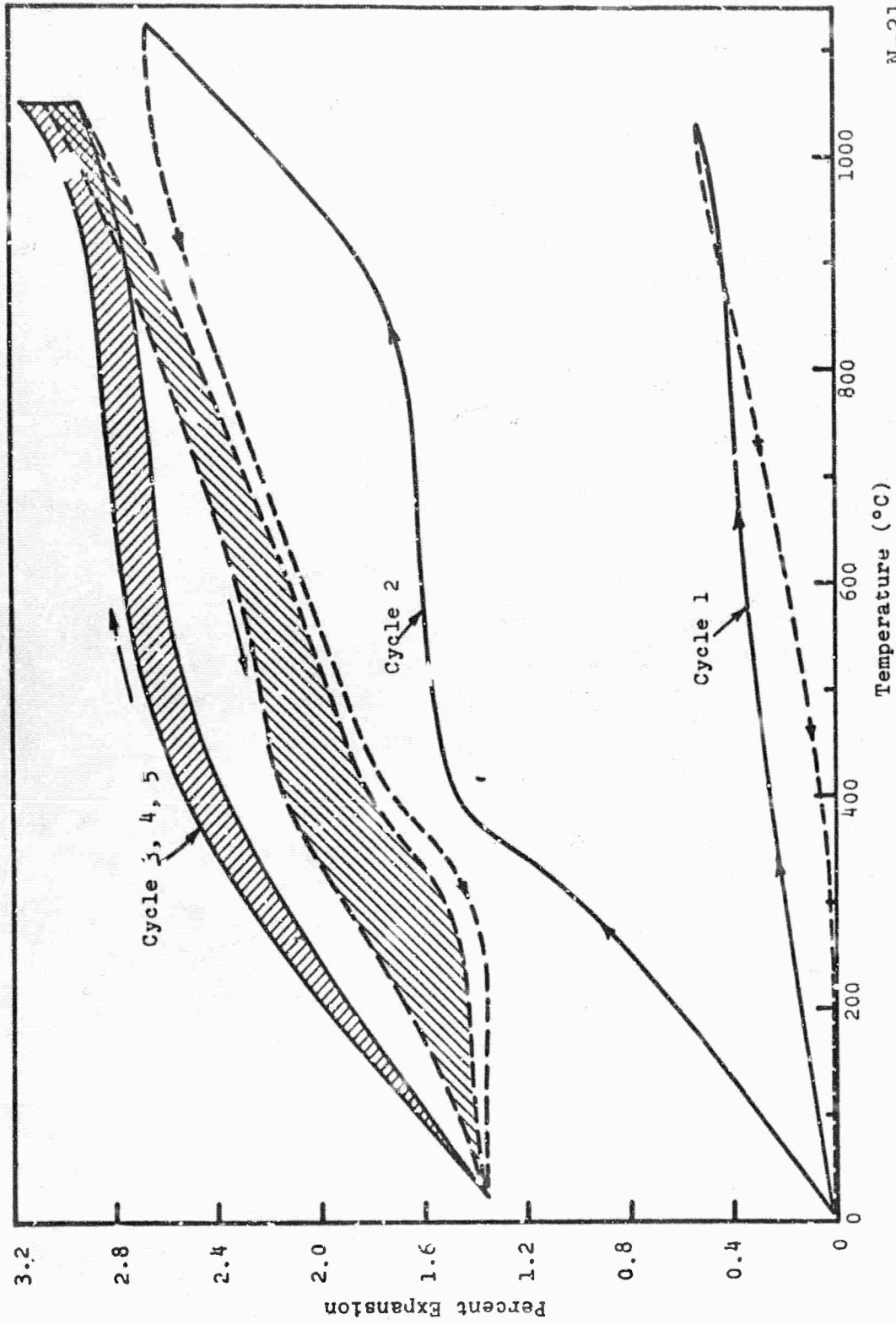
Figure 29. Linear Thermal Expansion of Nickel and of Graphite-Fiber, Nickel-Matrix Composite.

The data in Figure 30 show the cyclic thermal expansion behavior of graphite-fiber, nickel-matrix composites parallel to the fiber axis. Factors responsible for the differences between the first and second cycles are not understood at this time, but an alteration in the residual stresses is one possibility. The second-through-fifth cycles are similar except for the large expansion commencing at approximately 850°C in the second cycle. The total expansion recorded above 850°C in this instance also corresponds to the permanent elongation recorded at room temperature; the bulk density was found to be lower as a result of this dimensional change.

The longitudinal thermal expansion predicted for a 46-volume percent fiber composite through the use of the rule-of-mixtures and strain compatibility⁽³⁶⁾ is $7 \times 10^{-6}/^{\circ}\text{C}$. Figure 31 shows that all experimental values are less than the predicted $7 \times 10^{-6}/^{\circ}\text{C}$. Thermal expansion of the composite is controlled by the fibers to a greater extent than that predicted by the rule-of-mixtures. Between 500° and 900°C, for instance, the fiber and composite have similar expansion coefficients. One possible reason for the low expansion in this temperature range is that the nickel compression yield strength has been exceeded and the nickel is, therefore, deforming plastically. This effect could be caused by stresses resulting from the fiber-matrix expansion mismatch. The temperature at which the nickel yield strength is exceeded in the various cycles might correspond to the reversal in coefficients at low temperatures (see Figure 31).

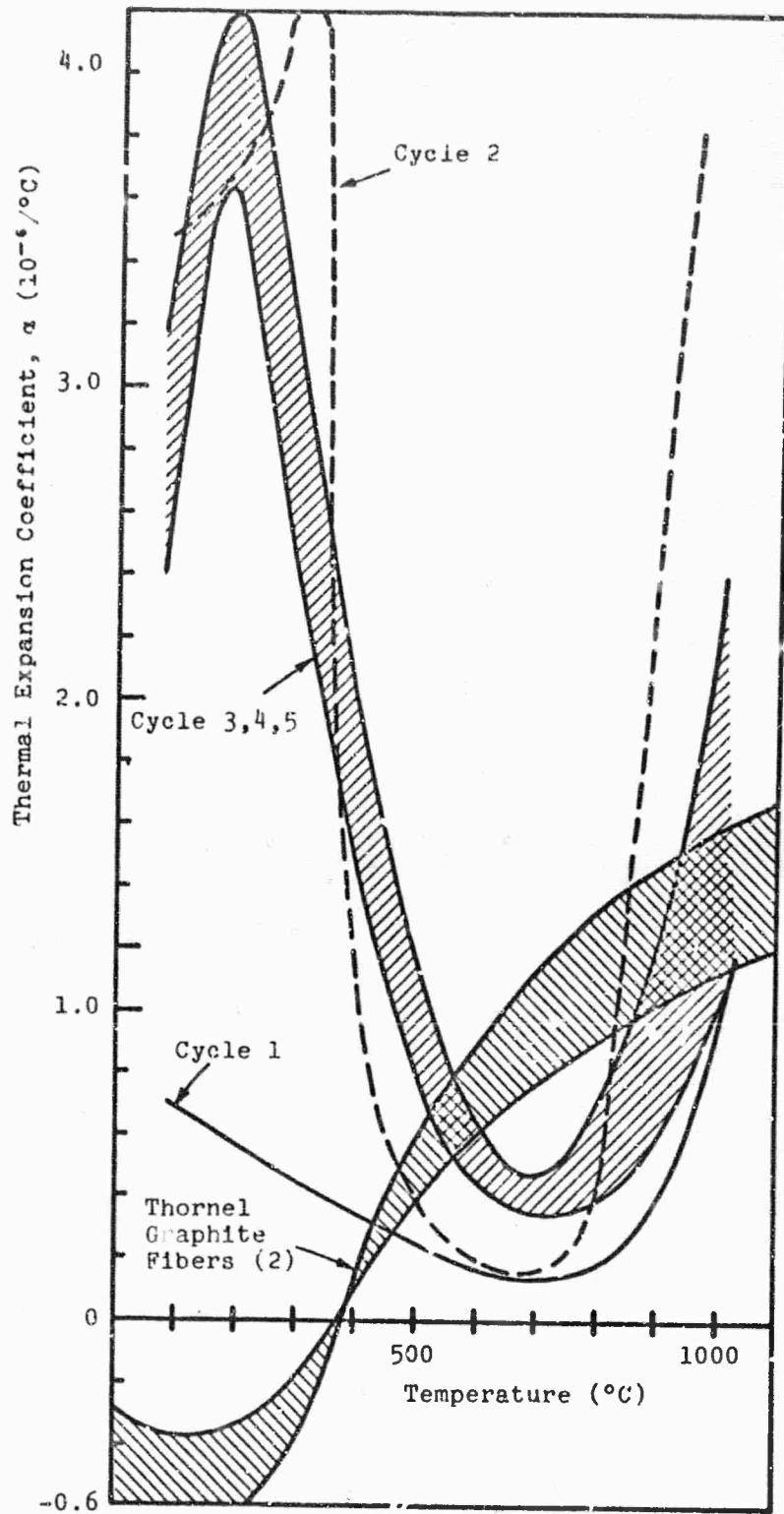
The temperature at which plastic deformation occurs in the matrix can be estimated from the following expression:

$$\Delta T = \frac{\epsilon_m \left(1 + \frac{A_m E_m}{A_f E_f} \right)}{(\alpha_m - \alpha_f)}$$



N-21208

Figure 30. Effect of Thermal Cycling on Longitudinal Expansion of Graphite-Fiber, Nickel-Matrix Composite.



N-21207

Figure 31. Temperature and Cyclic Dependence of Composite Longitudinal Thermal Expansion Coefficient and of Axial Thermal Expansion Coefficient of "Thornel" Graphite Fibers.

The value used for the strain, ϵ_m , is the same as noted for the breakaway point on the compression curve in Figure 28, i.e., 1300 μ in. The result for ΔT is 170°C when matrix modulus (E_m) and fiber modulus (E_f) values are assumed to be 30×10^6 psi and 36.5×10^6 psi, respectively. Thermal expansion coefficients used for the matrix (α_m) and fiber (α_f) were $15.2 \times 10^{-6}/^\circ\text{C}$ and 0, respectively. The predicted temperature at which plastic deformation of the matrix would occur is 195°C, a value that corresponds with the reversal in thermal expansion coefficient for cycles 3, 4, 5 in Figure 31.

A hysteresis effect is evident in the last three cycles. The cooling curve has a coefficient of approximately $1.8 \times 10^{-6}/^\circ\text{C}$ in the 300° to 900°C range; this value differs from the coefficients determined on the first two heating cycles. The expansion contraction loop is closed and retraceable.

Between 25° and 1050°C, the linear expansion of the composite perpendicular to the fiber axis is $20 \times 10^{-6}/^\circ\text{C}$. This value was also determined from second-cycle measurements. A permanent expansion was recorded after the second cycle, similar in magnitude to that for the deformation resulting from the longitudinal expansion cited in Figure 30. The transverse expansion coefficient of $20 \times 10^{-6}/^\circ\text{C}$ is intermediate between the value for pure nickel and that for the "c" axis expansion of graphite.

F. Fabrication and Properties of Uniaxial and Orthogonal Plates

Uniaxial and orthogonal plates (1 1/2-inch square) having 3-, 5-, and 7-ply configurations were fabricated in the manner described previously in Section III D of the Third Annual Report.⁽³⁾ The plies were uniformly thick and parallel in each plate specimen. The plates were sectioned into conventional specimens measuring 1/8 x 1/16 x 1 inch. The specimens with orientations of 0°, 45° and 90° were analyzed by sonic techniques to determine Young's modulus and then tested in tension to obtain the static modulus, stress-strain behavior, and ultimate tensile strength.

Before relating these data to uniaxial properties, it was necessary to clarify the poor results reported for the uniaxial properties in Section III D of the Third Annual Report.⁽²⁾ The plates from which the earlier test specimens were cut represented the first efforts at fabricating flat shapes. Two factors in the hot-pressing operation were suspected as being responsible for the poor properties. First, there was concern about fiber damage resulting from poor load distribution during pressing; and second, a poor vacuum was noted in the first runs. During the present study, two plates were fabricated under good (10^{-5} torr) vacuum conditions. One of these plates was pressed between two foils of nickel (0.005 inch thick) under the supposition that at 1050°C nickel would plastically deform and assist in distributing the load uniformly to the specimen, thus minimizing fiber breakage. An average tensile strength and Young's modulus of 84,300 psi and 33.4×10^6 psi, respectively, were obtained on specimens fabricated in this manner. Specimens from a second plate pressed without the nickel foils had average strength and modulus values of 81,400 psi and 33.3×10^6 psi, respectively. Both new plates represent substantial improvements over the results reported in the Third Annual Report,⁽³⁾ i.e., $\sigma_{\text{ult}} = 65,600$ psi and $E = 31.9 \times 10^6$ psi. The increased property values appear to be mainly the result of improved vacuum conditions employed during hot pressing.

The data in Figure 32 represent tensile strength values obtained at various test angles for uniaxial and orthogonal laminates, with the curves drawn to represent the best fit to the experimental data. Tensile strength of the 45° specimens is essentially independent of ply configuration.

The ultimate tensile strength in the 0° and 90° directions is also represented in Figure 33. The curves for the strength of composites containing odd number of plies were computed from

$$\sigma_{0^{\circ}} = k \frac{x+1}{2x} \sigma_t$$

$$\sigma_{90^\circ} = k \frac{x-1}{2x} \sigma_t$$

where x is the number of plies, and k is a proportionality constant used to convert from theoretical average strength (σ_t) to measured average values:

$$k\sigma_t = \frac{1}{2N} \sum_{n=1}^N [\sigma_{0^\circ}(n) + \sigma_{90^\circ}(n)].$$

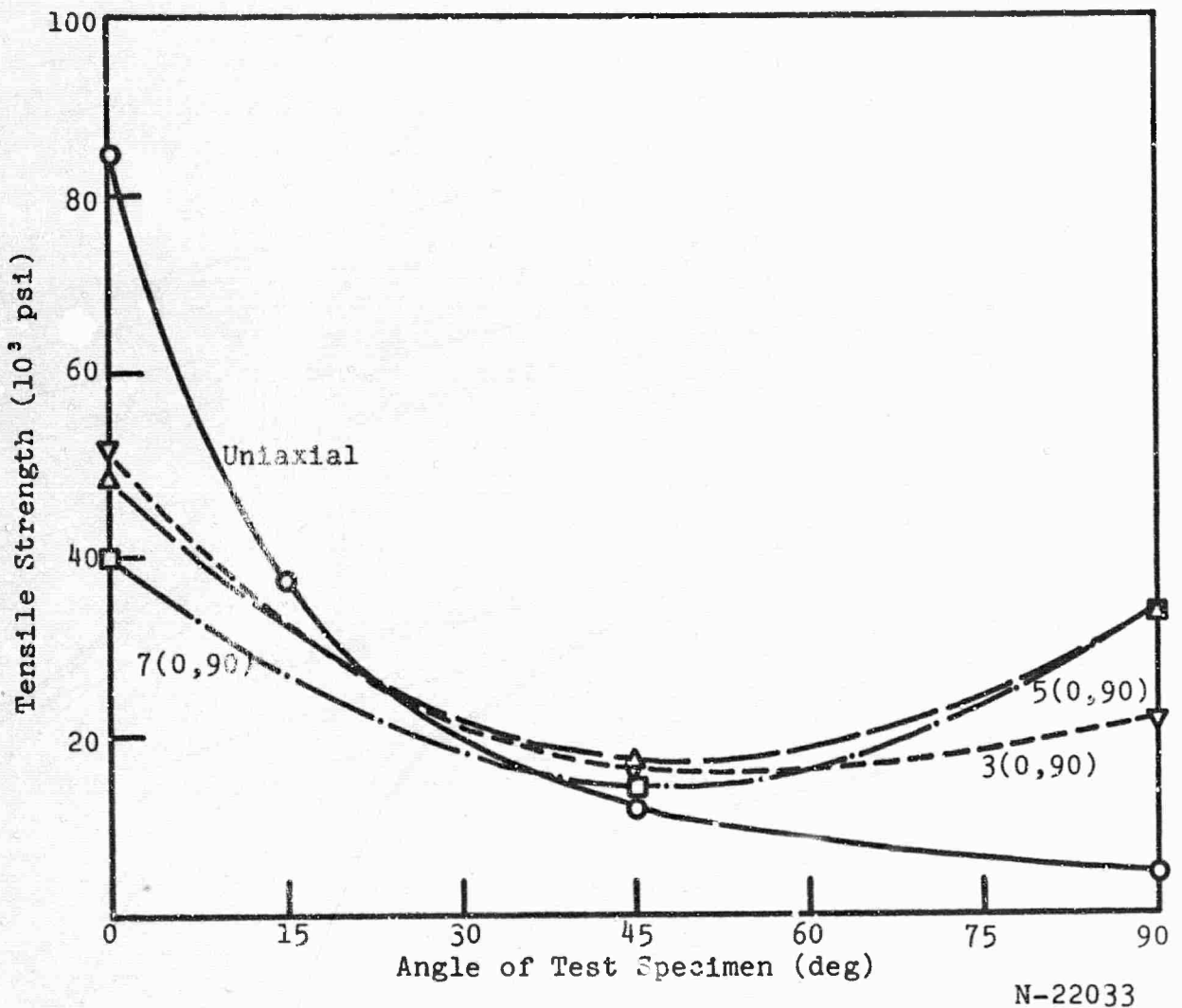
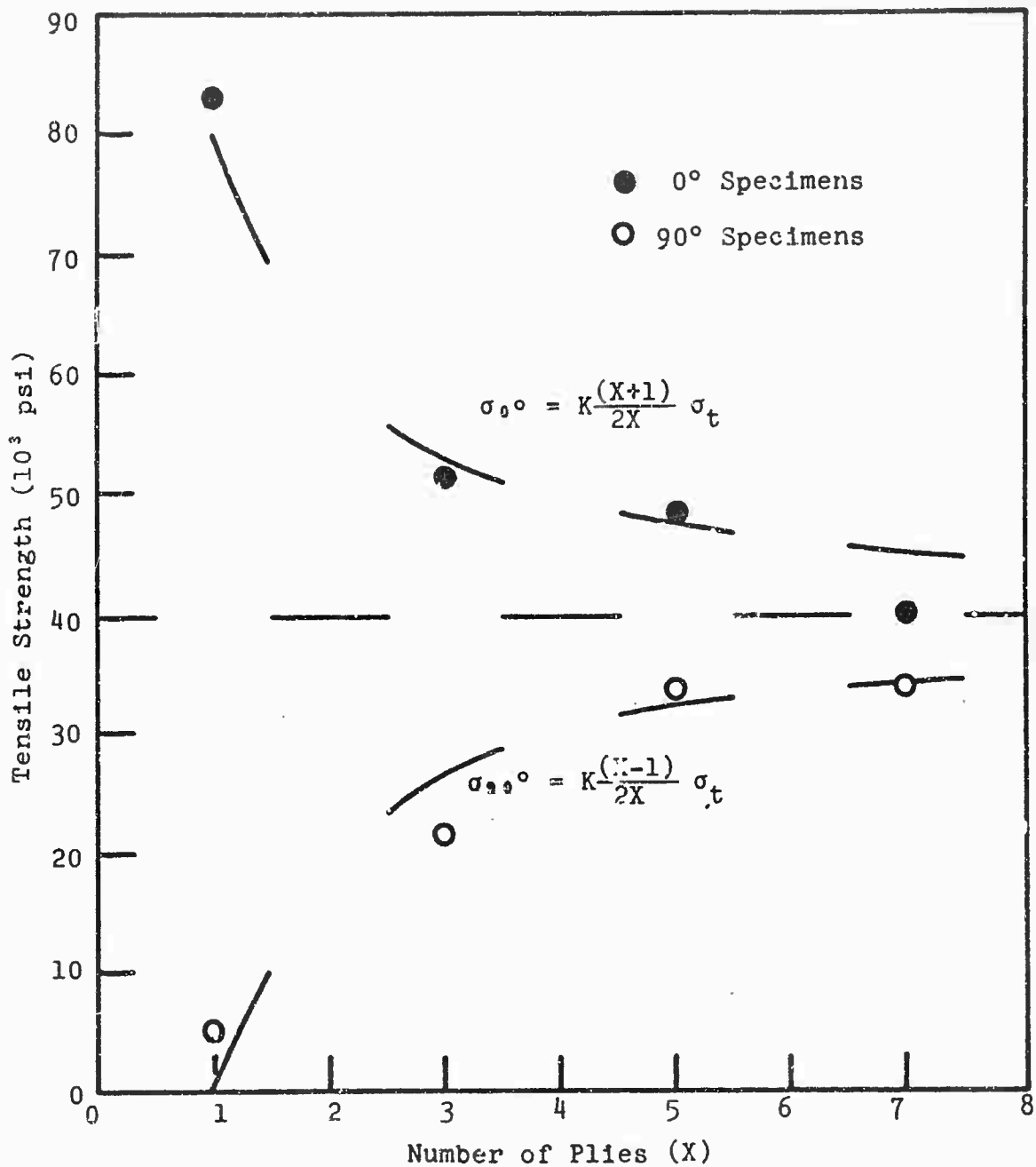


Figure 32. Variation in Tensile Strength of Uniaxial and Orthogonal Composites with Test Angle.



N-21832

Figure 33. Normalized Ultimate Tensile Strengths versus Number of Plies for Orthogonal Laminates.

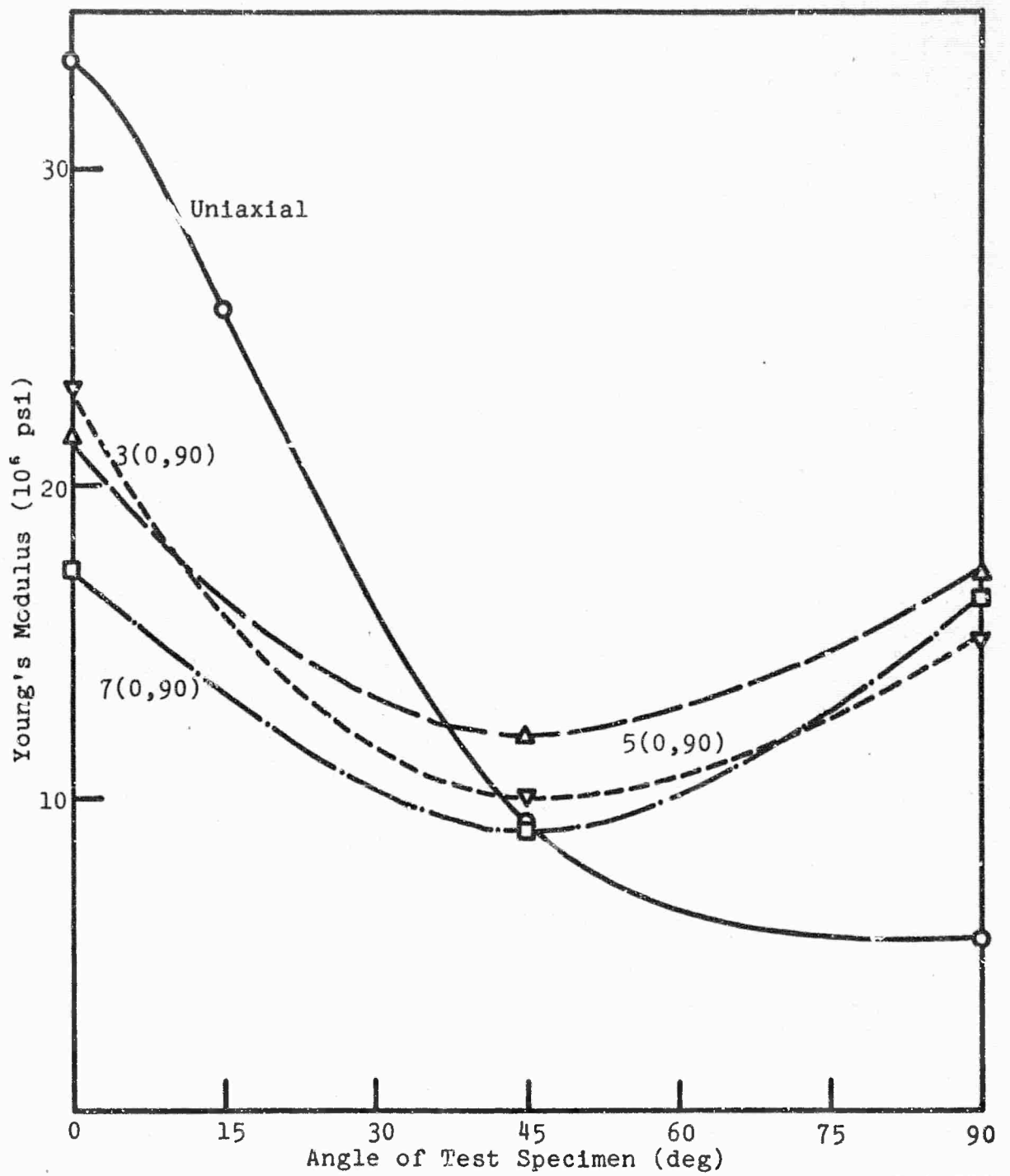
The theoretical longitudinal strength determined by the rule-of-mixtures is 135,000 psi. Assuming that the transverse strength is zero, then the theoretical average strength (σ_t) is one-half the longitudinal strength, or 67,500 psi. The measured average tensile strength for the four different ply configurations is 39,500 psi. This strength is also the asymptotic value indicated in Figure 33. Therefore, the value for k is 39,500 psi/67,500 psi or 0.6. The experimental data conform reasonably well to the predicted values. The Second Annual Report,⁽²⁾ Sections VI and VIII, provides additional details on the above relationships and also shows results for graphite-fiber, resin composites.

The Young's modulus for various ply configurations and specimen orientations was determined by sonic and static methods. Data obtained by the latter method are probably more reliable because assumptions are required in the sonic modulus calculations relevant to laminates. Experimental results based on static measurements are depicted in Figure 34. Data for uniaxial specimens are included for comparison purposes. The curves are drawn to pass through all experimental points. The trend in modulus with ply number is not in the expected order when the test angle is 90°. At a test angle of 45°, the configurations have a common Young's modulus of approximately 10×10^6 psi. The relationship between experimental and predicted moduli in the 0° and 90° directions for orthogonal laminates is shown in Figure 35. Values for E_{0° and E_{90° as a function of the number of plies were calculated in a manner similar to that used for the tensile strength. The expressions used for determining the two moduli are:

$$E_{0^\circ} = k \left(\frac{x+1}{2x} E_1 + \frac{x-1}{2x} E_2 \right)$$

$$E_{90^\circ} = k \left(\frac{x-1}{2x} E_1 + \frac{x+1}{2x} E_2 \right) .$$

Theoretical values of 39.1×10^6 psi and 11.1×10^6 psi were used for the longitudinal (E_1) and transverse (E_2) moduli, respectively.



N-22032

Figure 34. Variation in Young's Modulus of Uniaxial and Orthogonal Composites with Test Angle.

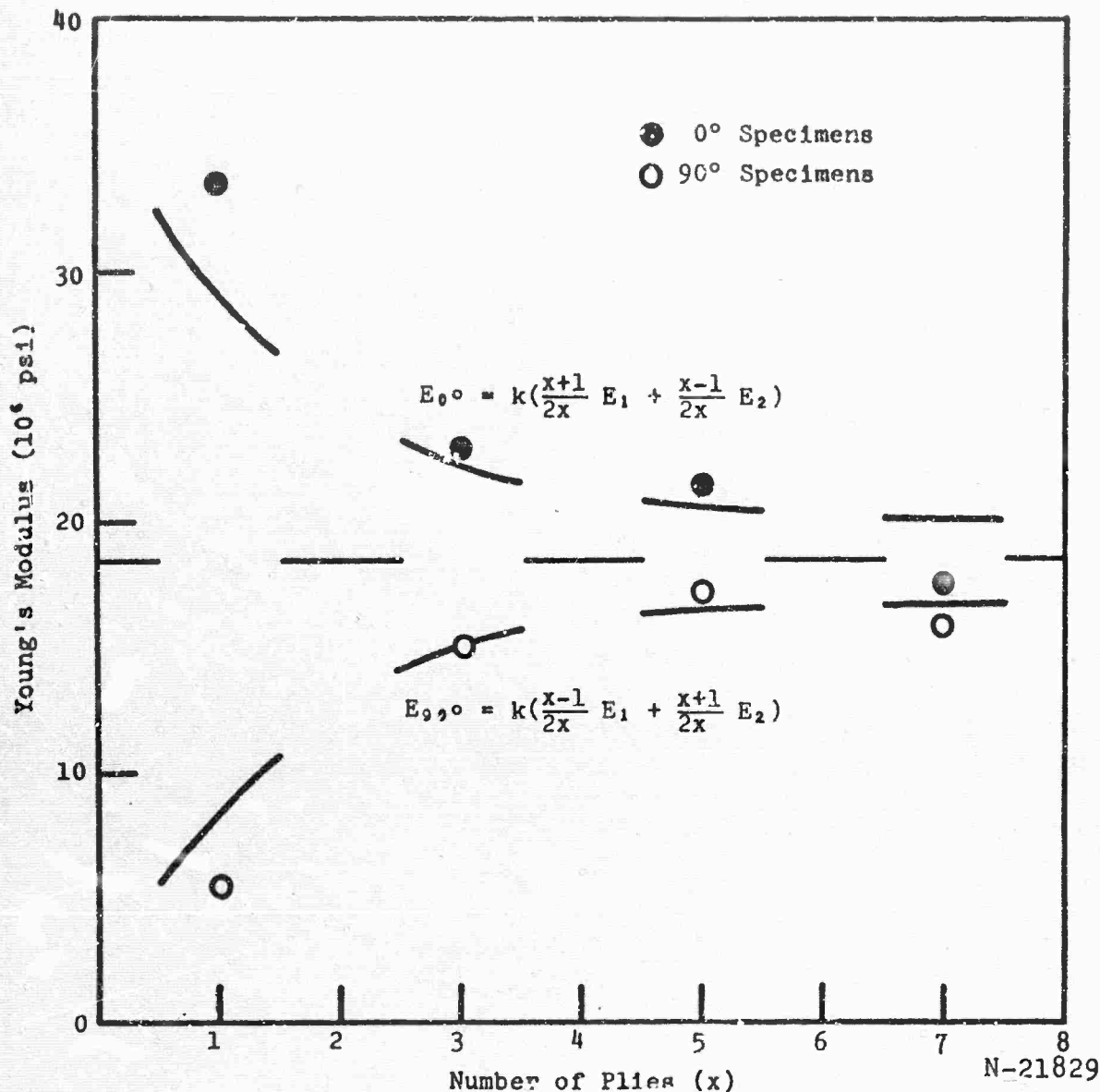


Figure 35. Normalized Young's Modulus Versus Number of Plies for Orthogonal Laminates.

These values were calculated using Whitney's ⁽²⁸⁾ micromechanics model; fiber moduli of $E_L = 50 \times 10^6$ psi and $E_T = 1 \times 10^6$ psi were assumed. The proportionality constant k was determined to be 0.73 and is the ratio of the experimental average value to the theoretical average value $(E_1 + E_2)/2$:

$$k (E_1 + E_2)/2 = \frac{1}{2N} \sum_{n=1}^N [E_{0^\circ}(n) + E_{90^\circ}(n)] .$$

The asymptote or experimental average value of the two moduli is 19.5×10^6 psi and is independent of the number of plies. The porosity, or delaminations, described in Section III D of the Third Annual Report⁽³⁾ evidently does not significantly influence the Young's modulus of orthogonal laminates. Agreement between experimental and predicted values was found to be poorer when a lower theoretical longitudinal modulus (e.g., 33.5×10^6 psi) was employed. However, the best correlation with experimental results was obtained when E_1 and E_2 were both assumed to be lower (e.g., 33.5×10^6 and 5.5×10^6 psi, respectively). The latter values were experimentally derived from unidirectional composites.

Stress-strain curves were obtained on 0° , 45° , and 90° specimens cut from 3-, 5-, and 7-ply laminates. Although the stress-strain data shown in Figure 36 are for 5-ply specimens, the data are also typical for the other configurations. The strain at failure for all 0° and 90° specimens is approximately 0.4 percent, the same value as observed in virtually all unidirectional graphite-fiber, nickel-matrix composites. A yield point and, in almost all cases, an increasing tangent modulus are evident in the stress-strain curves. Elongation before failure in the 45° specimens is much greater than that which occurs for the 0° and 90° orientations. Contribution of the transverse plies to the composite stress-strain behavior is negligible, as evidenced by the similarity between dashed and solid curves in Figure 36. The dashed curves represent a predicted contribution of longitudinal plies to the stress-strain behavior. The longitudinal contribution is based on a rule-of-mixtures approach in conjunction with the stress-strain characteristics of a unidirectional composite (Curve B in Figure 36).

Engineering properties were also obtained on the remaining 45° specimens with 3-, 5-, and 7-ply configurations.

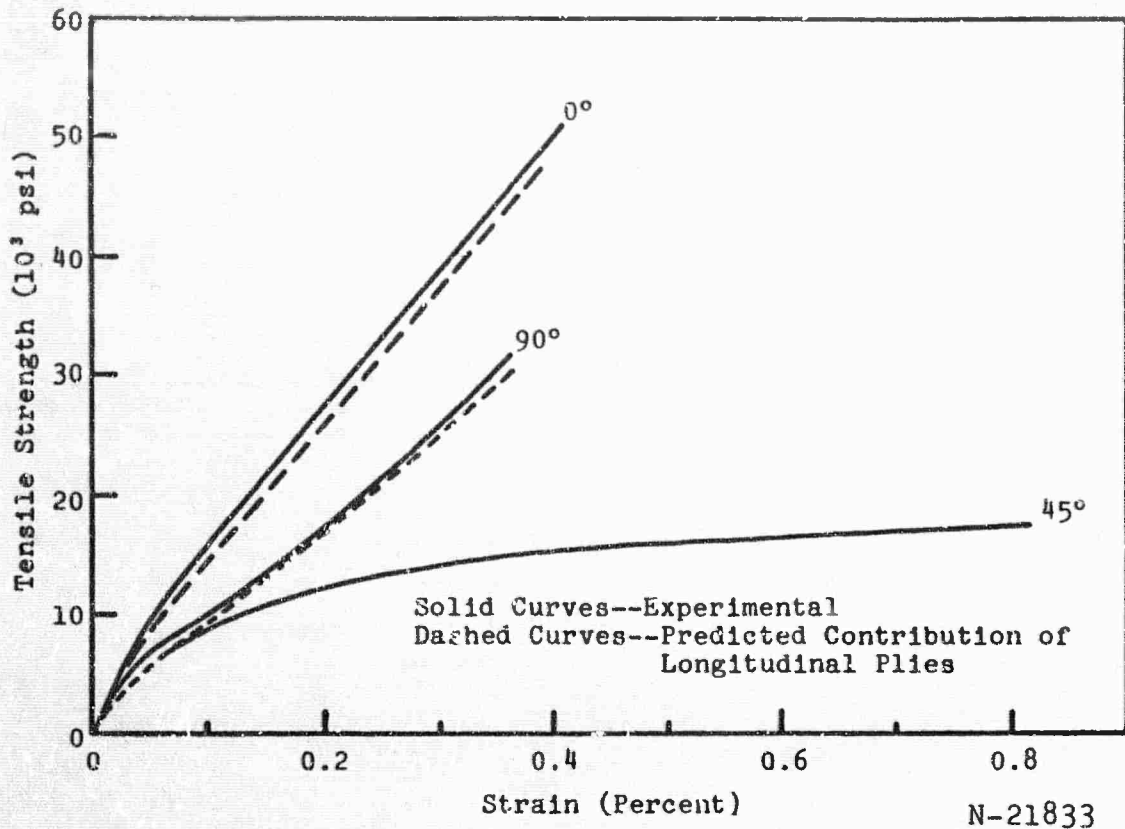


Figure 36. Stress-Strain Curves for 5-Ply Orthogonal Specimens with Different Orientations.

The values for E , determined by static methods, did not vary significantly with ply lay-up. The average value for the three different ply patterns is 10.4×10^6 psi. The average tensile strength corresponds to 15,600 psi.

In order to achieve greater fabrication flexibility in terms of size and configuration of laminates, studies of the fabrication of thin tape (≈ 0.010 inch thick) were undertaken. These short sections of tape will serve as basic units which may be stacked in a prescribed manner and diffusion bonded. A problem which arose during the fabrication of suitable tape was the adherence between the mold surface and tape which took place after hot-pressing. Numerous mold liners were evaluated to overcome this problem. Boron nitride (Union Carbide Corporation Grade HD 0092)

proved to be superior for this purpose, and tape up to 1-1/2 inches square were fabricated successfully. When attempts to fabricate 3-inch square tape were made, some delamination occurred parallel to the fibers; the cause of this delamination has not been ascertained. The nickel was not embrittled after having been hot pressed in contact with boron nitride. The tape made by the above process will be used to fabricate laminates for study before scale-up is considered.

G. Fabrication Studies and Tensile Testing of Unidirectional Composite

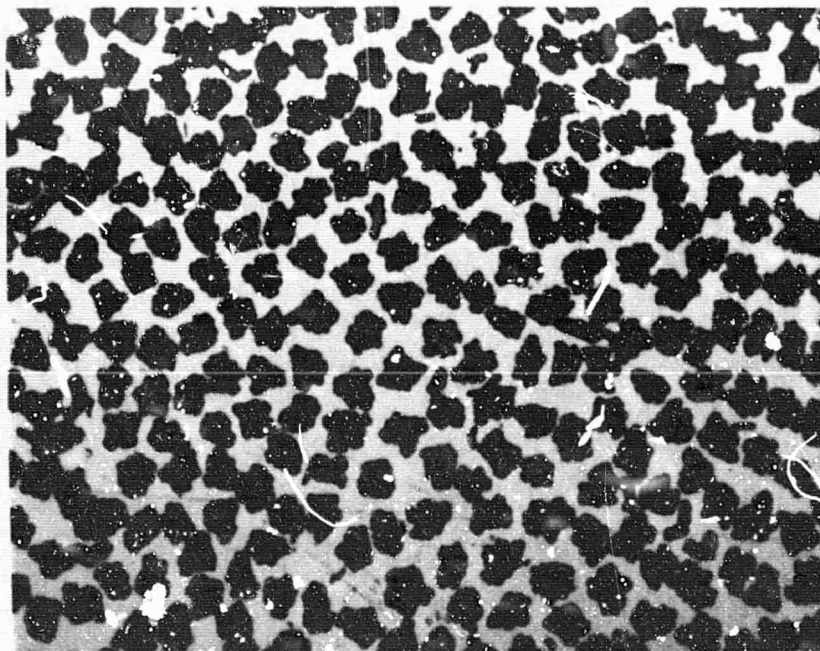
1. Effect of 1250°C Forming Temperature on Composite Properties

In previous fabrication studies, data were reported for hot pressing temperatures up to 1125°C.⁽³⁾ Current work was extended to include 1250°C as the fabrication temperature; the pressure and time corresponded to 3500 psi and one hour, respectively. Pyrolytic graphite foils were used to line certain regions of the graphite mold. Extensive bonding of the composite to the mold occurred where the foils were not employed. The average ultimate tensile strength, Young's modulus, and shear modulus for six specimens corresponded to 89,400 psi, 33.6×10^6 psi, and 5.03×10^6 psi, respectively. The scatter in values was generally less than was encountered when other fabrication parameters were varied. Studies of the composite microstructure revealed a subtle change in the fiber morphology. This change is evident in Figure 37 as the reduction in radii of curvature of the "fluted" areas in the fiber cross-section. The region of the composite bordering the tensile fracture edge has a greater population of single and multiple fiber breaks than was evidenced in earlier studies (see Figure 38). The broken fibers suggest that they were stressed to their ultimate strength prior to

failure of the composite. The stress at which this occurred, according to

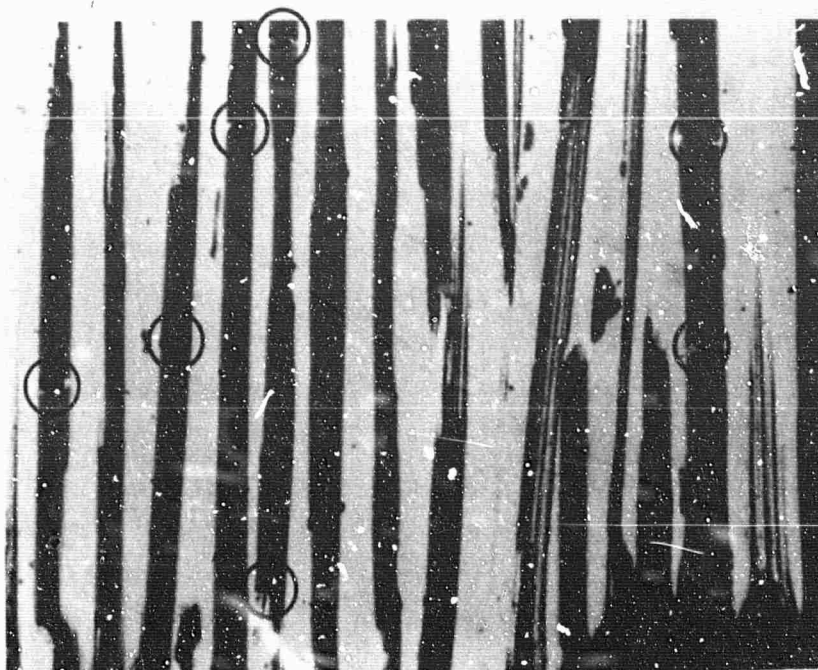
$$\sigma = E\epsilon,$$

is 150,000 psi. This value is based on a fiber modulus, E of 38×10^6 psi and strain at failure ϵ of the composite at 4000 μ inches. This fiber strength is slightly less than average results of 175,000 psi measured on fibers extracted from composites (see Section III of the Third Annual Report.⁽³⁾)



N-22128
429-1-0-4

Figure 37. Microstructure of Graphite-Fiber, Nickel-Matrix Composite Fabricated at 1250°C. Magnification 750X.



N-22127
429-1-0-1

Figure 38. Fracture Edge of Graphite-Fiber, Nickel-Matrix Composite Tensile Specimen. Magnification 750X.

2. Effect of Specimen Gauge Width on Transverse Property Measurements

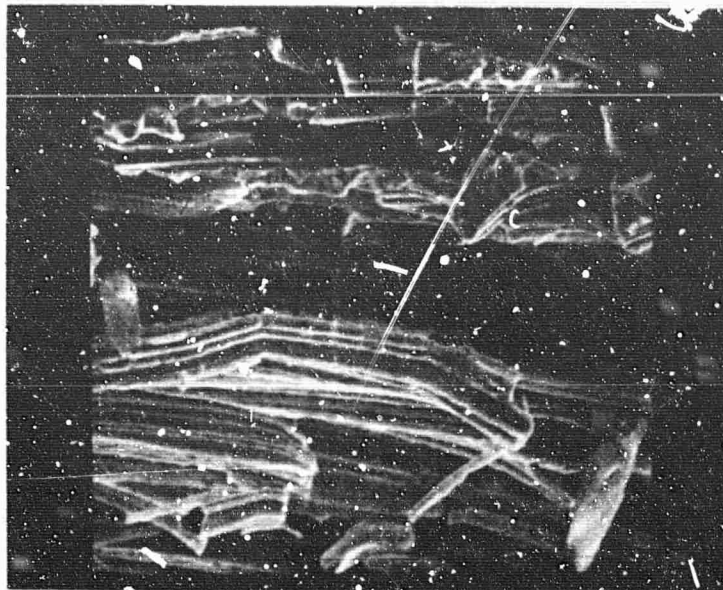
The transverse strength value reported previously (³) was based on tests made on straight-sided specimens with gauge dimensions of 1/16 x 1/8 inches. Studies conducted on graphite-fiber, resin-matrix composites(²) indicated that the transverse strength was dependent on the gauge dimensions. For the present study, the tensile strength and Young's modulus were determined on straight-sided specimens which were 1/16-inch thick but the widths were 1/8, 1/4, and 1/2 inch. The Young's modulus was determined from stress-strain curves. Typical stress-strain curves for 1/8 and 1/4 inch wide specimens were shown previously in Figure 22. The 1/2 inch wide specimens provided results similar to that depicted for the 1/4 inch gauge width. The Young's modulus (6.1×10^6 psi) for the widest specimens was slightly greater than the 1/8 inch gauge width (5.7×10^6 psi).

The tensile strength, as noted in Figure 22, is higher for the wider specimens (5800 psi) than was obtained for the narrowest gauge width (4000 psi). The fracture mechanism is complex because several processes are involved. A fracture edge as shown in Figure 39 suggests that "peeling" of fiber bundles precedes fracture of the fibers in bending. A feature of the composite which probably contributes to the "peeling" and low transverse strength is the poor fiber-matrix bond. Figure 40 shows nickel clearly removed from large areas of fiber after tensile failure. The fiber flute impressions are clearly evident in the matrix (lighter areas). Within these impressions are periodic arrays of dark spots which have not been identified. The spots might be porosity, graphite from the fiber surface, or irregularities on the fiber surface. A saw-tooth condition is evident on the fiber flutes but the frequency of the ridges do not coincide with the impressions left in the matrix. Additional microscopic study is needed before these fractures are clarified completely.



N-22088
428-1-510

Figure 39. Fracture Edge of Graphite-Fiber, Nickel-Matrix Composite with Transverse Fiber Orientation.



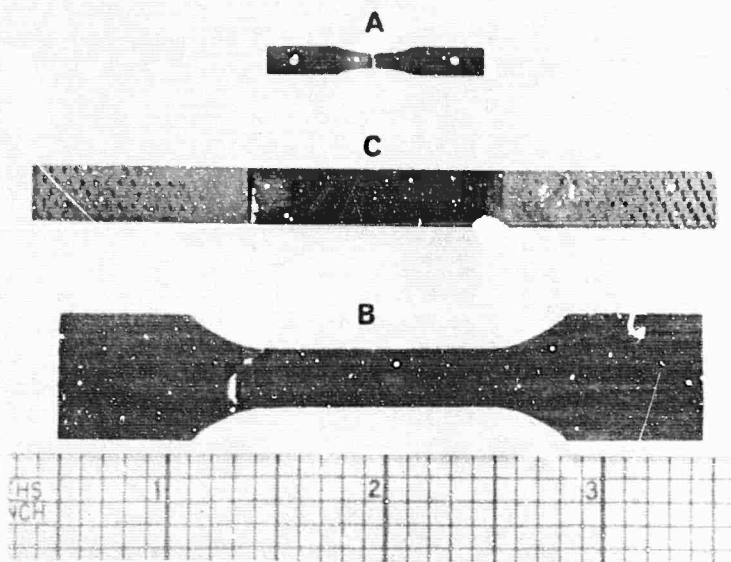
N-22089
428-1-511

Figure 40. Fiber-Matrix Debonding in a Tensile Specimen with Transverse Fiber Orientation.

3. Tensile Coupon Configurations

The majority of tensile testing during this program was on the smallest specimen (A) shown in Figure 41. This size was used extensively because the nickel plated yarn supply and hot pressing facilities were limited. Both conditions have since been rectified thereby providing an opportunity to study larger specimens. As a prelude to this change it seemed advisable to establish a correlation between specimen size and certain properties such as tensile strength. Failures in the small specimens were generally confined to the reduced gauge section as shown in the photograph of Figure 41. A series of five three-inch specimens, "dog boned" in the manner identified by specimen "C" in Figure 41 consistently failed in the radius as if due to stress concentrations. The use of larger radii of curvature did not improve the failure mode. The average stress at which failure

occurred for the five specimens was 77,000 psi. Ten small specimens salvaged from the material removed from "C" were ground in the form of specimen "A". The average tensile strength of ten small specimens was 82,700 psi. Finally, specimen "B" resembles the IITRI configuration which is receiving great attention in the testing of composites. The tapered tabs on the end are annealed nickel which were soldered to the composite. Three specimens of this type were tested and each failed in the tab area as shown in Figure 41. The average failure stress was 75,000 psi. Stress-strain curves from the IITRI specimens showed yield strengths of approximately 6000 psi or one-half that which is evident in Figure 20. Failures in the large specimens might be premature, and until gauge area failures are obtained, the correlation of strength data between small and large specimens will be questionable.



N-21984

Figure 41. Tensile Specimen Configurations.

REFERENCES

1. Union Carbide Corporation, Carbon Products Division, in Association with Case Western Reserve University and Bell Aerosystems Company, a Textron Company, Integrated Research on Carbon Composite Materials, AFML-TR-66-310 Part I (October 1966) (AF 33(615)-3110, Air Force Materials Laboratory, Wright-Patterson Air Force Base, Ohio).
2. Union Carbide Corporation, Carbon Products Division, in Association with Case Western Reserve University and Bell Aerosystems Company, a Textron Company, Integrated Research on Carbon Composite Materials, AFML-TR-66-310 Part II (December 1967) (AF 33(615)-3110, Air Force Materials Laboratory, Wright-Patterson Air Force Base, Ohio).
3. Union Carbide Corporation, Carbon Products Division, in Association with Case Western Reserve University and Bell Aerosystems Company, a Textron Company, Integrated Research on Carbon Composite Materials, AFML-TR-66-310 Part III (January 1969) (AF 33(615)-3110, Air Force Materials Laboratory, Wright-Patterson Air Force Base, Ohio).
4. J. D. Kovtsky, D. G. Walton, and E. Baer, J. Poly. Sci., D-2, 4 611(1966).
5. L. S. D. Glasser, F. P. Glasser, and H. F. W. Taylor, Quarterly Reviews 16:3^b3 (1962).
6. H. Morawetz, S. Z. Jakabhazy, J. B. Lando, and J. Shafer, Proc. Nat. Acad. of Sciences 49(6):789 (1963).
7. F. L. Hirshfeld and F. M. J. Schmidt, J. Polymer Sci. 2(A): 2181 (1964).
8. H. Morawetz, Pure and Appl. Chem. 12(1-4):201 (1966).
9. J. Willems and I. Willems, Experientia 13:465 (1957).
10. E. W. Fischer, Kolloid-Zeitschrift 159:108 (1958).
11. J. A. Koutsky, A. G. Walton, and E. Baer, J. Polymer Sci. 4(A-2):611 (1966).
12. J. Willems, Disc. Farady Soc. 25:111 (1958).
13. J. P. Hirth, and G. M. Pound, "Progress in Materials Science," Vol. 11, Macmillan, New York (1967).
14. C. J. Brown, Acta Cryst. 21:185 (1966).

REFERENCES, (Cont'd.)

16. H. Zahn, H. Dietrich, and F. Schmidt, *Acta Cryst.* 10:477 (1957).
17. B. Post, G. Bodor, and A. Bednowitz, *Acta Cryst.* 23:482 (1967).
18. P. H. Hermanns, *Rec. Trav. Chim.* 72:798 (1953).
19. I. Rothe and M. Rothe, *Chem. Ber.* 88:284 (1955).
20. J. L. Koenig and M. C. Agboatwalla, *J. Macromol. Sci-Phys.*, B2(3):391 (1968).
21. C. J. Brown, A. Hill, and P. V. Youle, *Nature* 177:128 (1956).
22. P. D. Frayer, J. L. Koenig, and J. B. Lando, "Infrared Studies of Chain Folding in Polymers IV Polyhexamethylene Adipamide and its Cyclic Oligomers," T.R. No. 111, Case Western Reserve University, November 19, 1968.
23. R. W. Coughlin, F. S. Ezra, and R. N. Tan, *J. Colloid and Interface Sci.* 28 (314):386 (1968).
24. W. Ruland, C. Herinckx, and R. Perret, *Nature* 220:63 (1968).
25. F. Tuinstra, (private communication).
26. W. Ruland, (private communication).
27. M. Rothe, *J. Polymer Sci.*, 30, 227 (1958).
28. J. M. Whitney, "Elastic Moduli of Composite Materials Reinforced with Orthotropic Filaments," Technical Report AFML-TR-65-411, January 1966.
29. Z. Hashin, and B. W. Rosen, "The Elastic Moduli of Fiber Reinforced Materials," *Journal of Applied Mechanics*, Vol. 31, 1-9, March 1964.
30. G. J. Curtis, J. M. Milne, W. N. Reynolds, "Non-Hookean Behavior of Strong Carbon Fibers," *Nature*, Vol. 220, 1024-1025, 1968.
31. R. L. Mehan, R. Jakas, "Behavior Study of Sapphire Wool Aluminum and Aluminum Alloy Composites," Technical Report AFML-TR-69-62, January 1969.

REFERENCES, (Cont'd.)

32. D. L. McDanel, R. W. Jech, and J. W. Weeton, "Analysis of Stress-Strain Behavior of Tungsten-Fiber-Reinforced Copper Composites," Trans. Metal. Soc. AIME, Vol. 233, 636-642, 1965.
33. T. Lyman, Metals Handbook, 18th ed., Vol. 1, American Society for Metals, 1961.
34. J. B. Nelson and D. P. Reilly, "The Thermal Expansion of Graphite from 15°C to 800°C: Part 1. Experimental," Phys. Soc. Proc. 57, 477-486, 1945.
35. R. Bacon, "High Strength-High Modulus Carbon Fibers," AFML-TR-66-334, Part II, December 1967.
36. L. Greszczuk, "Thermoplastic Considerations for Filamentary Structures," Proc. 20th Tech. Conf. SPI Reinforced Plastics Division, Section 5-C, Chicago, Illinois, February 1965.

UNCLASSIFIED

Security Classification

DOCUMENT CONTROL DATA - R & D

(Security classification of title, body of abstract and indexing annotation must be entered when the overall report is classified)

1. ORIGINATING ACTIVITY (Corporate author) Union Carbide Corporation Case Western Reserve University Bell Aerosystems Company		2a. REPORT SECURITY CLASSIFICATION Unclassified	
		2b. GROUP	
3. REPORT TITLE INTEGRATED RESEARCH ON CARBON COMPOSITE MATERIALS - Volume I (of three Volumes) Materials Research			
4. DESCRIPTIVE NOTES (Type of report and inclusive dates) Summary Technical Report July 1968 to June 1969			
5. AUTHOR(S) (First name, middle initial, last name) Union Carbide Corporation, Carbon Products Division, in Association with Case Western Reserve University and Bell Aerosystems Company, a Textron Company			
6. REPORT DATE September 1969	7a. TOTAL NO. OF PAGES 99	7b. NO. OF REFS 36	
8a. CONTRACT OR GRANT NO. AF 33(615)-3110	8b. ORIGINATOR'S REPORT NUMBER(S)		
b. PROJECT NO. ARPA Order No. 719			
c. Program Code 6D10	8c. OTHER REPORT NO(S) (Any other numbers that may be assigned this report) AFML-TR-66-310, Part IV		
10. DISTRIBUTION STATEMENT This document is subject to special export controls and each transmittal to foreign governments or foreign nationals may be made only with prior approval of the Nonmetallic Materials Division, MAN, Air Force Materials Laboratory, Wright-Patterson Air Force Base, Ohio 45433.			
11. SUPPLEMENTARY NOTES		12. SPONSORING MILITARY ACTIVITY Air Force Systems Command Air Force Materials Laboratory Wright-Patterson AFB, Ohio	
13. ABSTRACT The surface characteristics of various carbon and graphite fibers and the interfacial region between fibers and resin in composites were investigated by using electron microscopy, electron diffraction and Raman spectroscopy. The latter technique permits differentiation between graphite fibers of different origin. Graphite fiber composites were prepared by <i>in situ</i> polymerization on nylon 6. This technique improves the wetting of the fibers and yields void-free composites. Oriented crystallization of the monomers of nylon 6 and nylon 66 on graphite fibers and subsequent solid state reaction yielded dimers and trimers, respectively, instead of the usual polymers, thus showing a strong and specific effect of surface interactions. Sophisticated vacuum microbalance equipment has been constructed to study the surface characteristics of graphite fibers by gas adsorption. Work on graphite-fiber, nickel-matrix composites was concerned with improvements in the electrodeposition process, the fabrication of larger test specimens, the fabrication of thin foils which can be further processed into samples of more complicated configurations, and the evaluation of composite properties. The latter included measurements of the elastic properties, stress-strain curves and composite thermal expansion.			

UNCLASSIFIED

Security Classification

14. KEY WORDS	LINK A		LINK B		LINK C	
	ROLE	WT	ROLE	WT	ROLE	WT
Carbon Graphite Fibers Graphite Fibers Composites Plastic Matrix Metal Matrix Properties Analysis Synthesis Mechanical Properties						

DD FORM 1473 (BACK)
1 NOV 65
S/N 0101-807-8021

UNCLASSIFIED

Security Classification

A-41409